

Foliation boudinage

Dissertation zur Erlangung des Grades
„Doktor der Naturwissenschaften“
im Promotionfach Geologie/Paläontologie

am Fachbereich Chemie, Pharmazie und Geowissenschaften
der Johannes Gutenberg-Universität Mainz

Arzu Arslan
geboren in Salihli

Mainz, 2007

Erklärung

Ich versichere hiermit, die vorliegende Arbeit selbstständig und nur unter Verwendung der angegebenen Quellen und Hilfsmittel verfasst zu haben.

Mainz, Dezember 2007

Abstract

In this thesis foliation boudinage and related structures have been studied based on field observations and numerical modeling. Foliation boudinage occurs in foliated rocks independent of lithology contrast. The developing structures are called ‘Foliation boudinage structures (FBSs)’ and show evidence for both ductile and brittle deformation. They are recognized in rocks by perturbations in monotonous foliation adjacent to a central discontinuity, mostly filled with vein material.

Foliation boudinage structures have been studied in the Çine Massif in SW-Turkey and the Furka Pass-Urseren Zone in central Switzerland. Four common types have been distinguished in the field, named after vein geometries in their boudin necks in sections normal to the boudin axis: lozenge-, crescent-, X- and double crescent- type FBSs. Lozenge-type FBSs are symmetric and characterized by lozenge-shaped veins in their boudin neck with two cusps facing opposite sides. A symmetrical pair of flanking folds occurs on the two sides of the vein. Crescent-type FBSs are asymmetric with a single smoothly curved vein in the boudin neck, with vein contacts facing to one side. X- and double crescent- type FBSs are asymmetric. The geometry of the neck veins resembles that of cusped-lobate structures. The geometry of flanking structures is related to the shape of the veins. The veins are mostly filled with massive quartz in large single crystals, commonly associated with tourmaline, feldspar and biotite and in some cases with chlorite. The dominance of large faceted single quartz crystals and spherulitic chlorite in the veins suggest that the minerals grew into open fluid-filled space. FLAC experiments show that fracture propagation during ductile deformation strongly influences the geometry of developing veins. The cusps of the veins are better developed in the case of propagating fractures. The shape of the boudin neck veins in foliation boudinage depends on the initial orientation and shape of the fracture, the propagation behaviour of the fracture, the geometry of bulk flow, and the stage at which mineral filling takes place.

A two dimensional discrete element model was used to study the progressive development of foliation boudinage structures and the behavior of visco-elastic material deformed under pure shear conditions. Discrete elements are defined by particles that are connected by visco-elastic springs. Springs can break. A number of simulations was

performed to investigate the effect of material properties (Young's modulus, viscosity and breaking strength) and anisotropy on the developing structures. The models show the development of boudinage in single layers, multilayers and in anisotropic materials with random mica distribution. During progressive deformation different types of fractures develop from mode I, mode II to the combination of both. Voids develop along extension fractures, at intersections of conjugate shear fractures and in small pull-apart structures along shear fractures. These patterns look similar to the natural examples. Fractures are more localized in the models where the elastic constants are low and the competence contrast is high between the layers. They propagate through layers where the constants are high and the competence contrast is relatively low. Flow localize around these fractures and voids. The patterns similar to symmetric boudinage structures and extensional neck veins (e.g. lozenge type) more commonly develop in the models with lower elastic constants and anisotropy. The patterns similar to asymmetric foliation boudinage structures (e.g. X-type) develop associated with shear fractures in the models where elastic constants and anisotropy of the materials are relatively high. In these models boudin neck veins form commonly at pull-aparts along the shear fractures and at the intersection of fractures.

Zusammenfassung

In dieser Arbeit wurden Foliationsboudins und dazugehörige Strukturen untersucht, basierend auf Geländebeobachtungen und numerischer Modellierung. Foliationsboudins kommen in foliierten Gesteinen vor, unabhängig von der Lithologie. Die sich entwickelnden Foliationsstrukturen (foliation boudinage structures, FBS) zeigen sowohl Hinweise auf spröde als auch auf duktile Deformation. Sie sind in gleichmäßig foliierten Gesteinen als Störungen erkennbar. Angrenzend an eine zentrale Diskontinuität sind diese in der Regel mit Adermaterial gefüllt.

Derartige Foliationsstrukturen wurden im Cinemassiv (SW-Türkei) sowie in der Furkapass-Urserenzone (Zentralschweiz) untersucht. Insgesamt wurden vier unterschiedliche, häufig auftretende Typen von Foliationsboudins im Gelände charakterisiert. Diese werden nach der Adergeometrie in den Boudineinschnürungen in Schnitten normal zur Boudinachse benannt und als Rauten-, Sichel-, X- oder Doppelsichel-FBS bezeichnet.

Rauten-FBS sind symmetrisch und durch rautenförmige Adern in den Boudineinschnürungen mit zwei zu verschiedenen Seiten gewandten Spitzen charakterisiert. Ein symmetrisches Paar flankierender Falten kommt auf beiden Seiten einer Ader vor. Sichel-FBS sind symmetrisch mit einer einzelnen leicht gebogenen Ader an der Boudineinschnürung. X- und Doppelsichel-FBS sind asymmetrisch. Die Geometrie der Einschnürungsadern ähnelt denen von kuspato-lobaten Strukturen. Die Geometrie der flankierenden Strukturen ist an die Form der Adern gekoppelt.

Die Adern sind in der Regel mit massigem Quarz gefüllt, häufig assoziiert mit Turmalin, Feldspat, Biotit und in einigen Fällen Chlorit. Die Dominanz von großen variantenreichen einzelnen Quarzkristallen und spherulitischem Chlorit in den Adern legt nahe, dass die Minerale in offenen fluidgefüllten Raum hineingewachsen sind. FLAC-Experimente zeigen, dass Bruchausbreitung während duktiler Deformation die Geometrie der sich entwickelnden Adern stark beeinflusst. Die Spitzen der Adern sind bei sich ausbreitenden Brüchen deutlicher entwickelt.

Die Form der Einschnürungsadern in Foliationsboudins hängt von der anfänglichen Orientierung und Form des Bruches, dem Ausbreitungsverhalten des Bruches, der Geometrie der Gesamtbewegung und dem Zeitpunkt der einsetzenden Mineralfüllung ab. Ein

zweidimensionales diskrete Elemente Modell wurde zur Untersuchung der fortschreitenden Entwicklung von Foliationsboudins sowie dem Verhalten von viskoplastischem Material, deformiert unter reiner Scherung, angewendet. Diskrete Elemente sind durch Partikel definiert, die durch viskoelastische Federn verbunden sind, welche unterbrochen werden können. Eine Reihe von Simulationen wurde durchgeführt um den Einfluß von Materialeigenschaften (Young's Modul, Viskosität und Bruchfestigkeit) und Anisotropie auf die sich entwickelnden Strukturen zu untersuchen. Die Modelle zeigen die Entwicklung von Boudins in einzelnen Lagen, in multiplen Lagen und in anisotropem Material mit zufälliger Glimmerverteilung. Verschiedene Bruchtypen entwickeln sich während fortschreitender Deformation von mode I und mode II zur Kombination aus beiden. Es entwickeln sich Lücken entlang von Extensionsbrüchen am Schnittpunkt zusammenlaufender Scherbrüche sowie in kleinen „pull-apart“-Strukturen entlang von Scherbrüchen. Diese Muster entsprechen den Beobachtungen an natürlichen Proben. In den Modellen sind Brüche mehrheitlich dort zu finden wo die Elastizitätskonstanten niedrig und der Kompetenzkontrast zwischen den einzelnen Lagen hoch ist. Sie breiten sich durch Lagen aus in denen die Konstanten hoch und der Kompetenzkontrast relativ niedrig ist. Bewegung kann um diese Brüche und Lücken lokalisiert werden. Die Muster, die symmetrischen Boudinstrukturen und Extensionseinschnürungen entsprechen (z.B. Rautentyp) entwickeln sich weitgehend in den Modellen mit niedrigeren Elastizitätskonstanten und geringer Anisotropie. Im Gegensatz dazu entwickeln sich Muster, die asymmetrischen Boudintypen (z.B. X-Typ) entsprechen eher in Modellen mit relativ hohen Elastizitätskonstanten und hoher Anisotropie. In diesen Modellen bilden sich Einschnürungsadern üblicherweise an „pull-apart“-Strukturen entlang der Scherbrüche und an den Schnittpunkten der Brüche.

Özet

Bu tezde foliyasyon budinajı ve yakın ilişkili yapılar temel olarak arazi çalışmaları ve bilgisayar ortamında yapılan deneylere dayanarak araştırılmaktadır. Foliyasyon budinajı foliyasyonlu kayalarda herhangi bir litolojiye bağlı olmaksızın gelişmektedir. 'Foliyasyon budinaj yapıları (FBSs)' olarak adlandırılan yapılar hem sünümlü hem de kırılğan deformasyon ile ilgili bilgi taşımaktadır. Bu yapılar kayalarda tekdüze bulunan foliyasyon düzlemlerinin varolan bir süreksizlik yapısı çevresinde sapmaya uğramasıyla tanınır. Süreksizlik düzlemleri çoğunlukla mineral içeren damarlar şeklinde bulunmaktadır.

Foliyasyon budinaj yapıları Çine masifinde (GB-Türkiye) ve Furka Pass-Urseren zonunda (İsviçre) çalışılmıştır. Arazide 4 ana tip ayrılmış olup adlamaları yapıların merkezinde bulunan mineral taşıyan damarların geometrilerine göre budin eksenlerine normal kesitlerde yapılmıştır. Bunlar lozenge (baklava ya da eskenar dörtgen şekilli)-, crescent (ay şekilli)-, X (çapraz-makas şekilli)- ve double crescent (çift ay şekilli)- foliyasyon budinaj yapılarıdır. Eskenar dörtgen şekilli (lozenge) foliyasyon budinaj yapıları bakımsızdır (symmetric) ve merkezlerinde bulunan damarlar zıt yönlere bakan keskin açıyla kıvrılmış iki uca (cusp) sahiptir. Bu damarların duvarlarında kayadaki foliyasyon simetrik kenar kıvrımları (flanking folds) yapmaktadır. Ay şekilli (crescent) foliyasyon budinaj yapıları bakımsızdır (asymmetric) ve merkezlerinde heriki duvarı da tek yöne bakan yumusak açıyla bükülmüş tek bir damar vardır. Çapraz (X) ve çift ay (double crescent) şekilli foliyasyon budinaj yapıları da bakımsızdır (asymmetric) ve merkezde bulunan damarları alev-lob yapılarına (cusped-lobate structures) benzemektedir. Kenar kıvrımlarının biçimleri doğrudan damarların şekilleriyle ilişkilidir. Budin damarları çoğunlukla büyük tek kristalli som kuvars ile birlikte turmalin, feldisfar ve biyotit ve bazen klorit içermektedir. Damarlarda kristal yüzeyleri iyi gelişmiş tek kristaller şeklinde bulunan kuvars ve küçük, yuvarlak şekilli (spherulitic) kloritler bu minerallerin sıvı-akışkan dolu boşluklarda büyüdüğünü göstermektedir. Bilgisayar ortamında yapılan FLAC (Fast Lagrangian Analysis of Continua) deneyleri sünümlü deformasyon ile eşzamanlı ilerleyerek büyüyen kırıkların gelişen damar geometrileri üzerindeki etkisini göstermektedir. Duraylı kırıkların (stable fractures) aksine sünümlü deformasyon sırasında ilerleyerek gelişen kırıklar keskin açıyla bükülen damarların oluşumunu sağlamaktadır.

Foliyasyon budinajında budin merkezindeki damarların biçimleri kırıkların ilksel yönelimleri ve geometrilerine, kırıkların ilerleyip ilerlememesine, hacimsel akmanın/deformasyonun (bulk flow) geometrisine ve mineral dolgusunun hangi asamada gerçekleştiğine bağlıdır.

Foliyasyon budinaj yapılarının gelişimi ve viskoelastik maddelerin tam makaslama altındaki deformasyon (pure shear deformation) davranışları bilgisayar ortamında iki boyutlu süreksiz element deneyleriyle (discrete element model) araştırılmıştır. Süreksiz elementler viskoelastik yaylarla bağlanmış parçacıklardan oluşmaktadır. Bu bağlar kopabilme özelliğine sahiptir. Madde özellikleri (Young modülü, viskozite ve kırılma dayanımı) ve anizotropinin gelişen yapılar üzerindeki etkisini araştırmak için bir seri deney yapılmıştır. Modeller tek tabakalarda, çoklu ardalanan tabakalarda ve mika minerallerinin rastgele dağılımını içeren anizotropik kayalarda budinaj yapılarının gelişimini göstermektedir. Deneylerde ilerleyen deformasyon sırasında mod I, mod II ve herikisinin birlikte bulunduğu farklı kırık tiplerinin gelişimi gözlenmiştir. Bosluklar açılma kırıkları, esli kırıkların arakesitleri ve makaslama kırıkları boyunca gelişen çekme yapıları (pull-apart) boyunca oluşmuştur. Modellerde gözlenen bu yapılar doğal örneklerle yakın benzerlik sunmaktadır. Kırıklar, elastik katsayıları düşük ve tabakalar arasındaki dayanımlılık oranının yüksek olduğu modellerde daha lokalize olmaktadır. Tabakalar arasındaki dayanımlılık oranının nisbeten düşük olduğu modellerde kırıklar tabakalar boyunca ilerlemiştir. Akma/deformasyon, bu kırıklar ve boşluklar çevresinde lokalize olmaktadır. Simetrik budinaj yapılarına ve merkezlerinde bulunan açılma damarlarına benzer (örneğin lozenge tipi) geometriler elastik katsayıların ve anizotropinin düşük olduğu modellerde yaygın olarak gelişmiştir. Asimetrik budinaj yapılarına benzer (örneğin X-tipi) geometriler elastik katsayıların ve anizotropinin nisbeten yüksek olduğu modellerde yaygın olarak gelişmiştir. Bu modellerde budin merkezindeki damarlar genellikle makaslama kırıkları boyunca çekme-açılma damarları olarak ve kırık arakesitlerinde gelişmiştir.

Contents

Abstract	vi
Zusammenfassung	viii
Özet	x
Contents	xii
Preface	1
Chapter 1. Foliation boudinage	4
Abstract	4
1.1. Introduction	5
1.2. Study areas	7
1.2.1. Geology of the Çine submassif	7
1.2.2. Geology of the Furka Pass-Urseren Zone	9
1.3. Foliation boudinage structures (FBSs)	11
1.3.1. Foliation boudinage structures (FBSs) in the Çine submassif	11
1.3.1.1. Variations in geometry of FBSs in the Çine Massif	17
1.3.1.2. Vein material	18
1.3.2. FBSs in Furka Pass-Urseren Zone	20
1.4. Numerical modelling	23
1.5. Development of foliation boudinage structures (FBSs)	27
1.5.1. Development of the main types of FBSs	28
1.5.2. Development of other varieties of structures in the Selimiye shear zone ...	29
1.6. Conclusions	32
Acknowledgements	32
Chapter 2. Numerical modelling of foliation boudinage	33
Abstract	33
2.1. Introduction	34
2.2. The numerical model	36
2.3. Results	39
2.3.1. Layer boudinage	39
2.3.2. Multilayer boudinage	43
2.3.3. Foliation boudinage	55
2.4. Conclusions	66
Chapter 3. General conclusions	67
Appendix	69
1. FLAC	69
2. Explanations for the movies, CD-ROM	72
References	73
Lebenslauf	

Preface

Boudinage is a segmentation of a volume of rock due to extension. In most cases, a planar body of relatively high viscosity in a less viscous matrix undergoes boudinage. Examples are sandstone layering in slate, or a granitic dyke in a metasediment. Foliation boudinage is different since it is not associated with particular lithology but forms in strongly foliated parts of a rock mass. Foliation boudinage structures (FBSs) occur at several metamorphic conditions, from greenschist to granulite facies. Their geometry can be symmetric or asymmetric, both in sections parallel and normal to the lineation. They show evidence for both ductile and brittle deformation. Boudinage of layers is relatively well understood. However, formation of boudinage structures in homogeneous anisotropic rocks is still not fully understood. Their study is important to understand rock deformation, rheology and strain localization. Therefore the aim of this thesis is to investigate the initiation and evolution of foliation boudinage and related structures and their formation mechanisms based on field observations and on numerical modelling.

In the first chapter different types of foliation boudinage structures (FBSs) are described. A classification is made for the main types based on detailed outcrop-scaled mapping of the 3D-geometry of all available type of boudins mainly in the Çine Massif, Turkey and in the Furka Pass-Urseren Zone, Switzerland. The Çine Massif is part of the Menderes Metamorphic Core Complex (MMCC) in western Turkey and consists of rocks of Proterozoic to Mesozoic age, mainly gneisses and augen gneisses, which represent mylonitised granitoid foliation, and metasedimentary micaschists. All these rocks contain a single subhorizontal foliation. This foliation apparently developed in several stages in different orogenic phases at upper amphibolite to greenschist facies conditions. The Çine Massif is unique because the gneisses and schists contain a large number of foliation boudinage structures. Several generations of FBSs apparently developed under decreasing metamorphic conditions so that different FBS types can be found. Besides the large density of boudins, the well-exposed outcrops with horizontal orientation of the foliations allow studying the structures in three-dimensional shape. The boudin necks are mostly filled with massive quartz in large single crystals, commonly associated with tourmaline, feldspar and biotite and in

some cases with chlorite spherulites. The second study area, the Furka Pass-Urseren Zone between the Aar- and Gotthard Massifs is a narrow zone in the Infra-Helvetic Complex in Central Switzerland. The massifs, mainly late Variscan granites and old crystalline rocks together with narrow zones of Carboniferous sediments and volcanics, form the pre-Mesozoic basement of the Helvetic nappes. They represent updomed basement nappes separated by their Mesozoic sedimentary cover and by the basal Glarus thrust from the overlying Helvetic nappes. In the southern Aar Massif, Alpine overprint was strong and the basement and cover rocks were affected by ductile deformation under greenschist facies metamorphism and further to the south in the Gotthard Massif reached amphibolite facies metamorphism. Foliation boudinage structures occur in the mylonitic rocks of the massif with an approximately NE-SW striking and vertical to steeply dipping penetrative foliation. The aggregate and grain lineations are mostly vertical or steeply plunging. Both structures formed in anastomosing shear zones with a vertical displacement component.

FLAC experiments were performed to study the effect of fracture propagation on necking during ductile deformation. Fractures are predefined in the model. Fracture propagation is modelled by removing elements at fracture tips from a finite difference mesh. A series of experiments was performed for a range of kinematic vorticity numbers from pure shear to simple shear in several combinations with different initial fracture orientations. Symmetric and asymmetric neck veins with flanking structures similar to the natural structures developed in the models.

In the second chapter a two-dimensional discrete element method has been used to study the progressive development of foliation boudinage structures and the behavior of visco-elastic material deformed under pure shear conditions. The effect of material properties and anisotropy on the developing structures was investigated in a range of simulations with a single layer, multilayers with different elastic properties and a random distribution of “micas”, rows of horizontally aligned elements with the same elastic properties. The models show the initiation of fractures and evolution of single layer, multilayer and foliation boudinage in homogeneous anisotropic materials with random mica distribution.

Published parts

-Chapter 1: Arslan, A., Passchier, C.W., Koehn, D., 2007 (*in press*). Foliation boudinage. Journal of Structural Geology, doi:10.1016/j.jsg.2007.11.004

-Chapter 2: Arslan, A., Koehn, D., Passchier, C.W., (*in prep for publ*). Numerical modelling of foliation boudinage. Journal of the Geological Society of London, Special Issue.

Conference Abstracts

-Arslan, A., Koehn, D., Passchier, C.W., 2007. Foliation boudinage: natural examples and numerical modeling. DRT Milano.

-Arslan, A., Passchier, C., Koehn, D., 2006. Foliation boudinage. TSG Manchester.

-Arslan, A., Koehn, D., Passchier, C.W., 2005. Numerical modelling of foliation boudinage. DRT Zürich.

-Arslan, A., Passchier, C., Koehn, D., 2005. Foliation boudinage. DRT Zürich.

Chapter 1

Foliation boudinage

Abstract

Foliation boudinage is a form of boudinage that develops in foliated rocks independent of lithology contrast. This paper describes foliation boudins from the Çine Massif in SW-Turkey and the Furka Pass-Urseren Zone in central Switzerland. Four common types of foliation boudin structures can be distinguished in the field, named after vein geometries in their boudin necks in sections normal to the boudin axis: lozenge-, crescent-, X- and double crescent- type. The boudin necks are mostly filled with massive quartz in large single crystals, commonly associated with tourmaline, feldspar and biotite and in some cases with chlorite spherulites. The presence of blocky crystals and chlorite spherulites suggest that these veins formed as open, fluid filled cavities during the initiation and development of foliation boudin structures, even in ductilely deforming gneiss at a depth of mid-crustal levels (7-10 kbar). The presence of cavities allowed the formation of closed fishmouth structures that are typical for many foliation boudins. The geometry of foliation boudin structures mainly depends on initial fracture orientation, propagation of the fracture during further deformation, and flow type in the wall rock.

1.1. Introduction

Boudinage is a common phenomenon in layered rocks, where layers of a specific lithology are disrupted into elongate fragments. Such separation can develop by planar fracturing into rectangular fragments (torn boudins) or by necking and tapering into elongate depressions and swells known as drawn boudins (Goscombe et al., 2004: fig. 1). Where the boudins are separated by fractures or vein material, the separation zones are known as boudin necks. In some types of torn boudins, and in all drawn boudins, the layers are deflected into the boudin neck in a characteristic geometry (Goscombe et al., 2004: fig. 1). In some cases, the deflection can be so strong that the upper and lower contact of a layer touches in the boudin neck. If this occurs by infolding of the original fracture, the developing structure is known as a “fishmouth boudin” where the deformed fracture forms the “mouth” of the “fish” (Goscombe et al., 2004: fig. 1). Boudin necks normally occur in a series of similar structures along a layer with regular spacing, separating the layer into “boudins”. This type of layer-restricted boudinage is thought to result from differences in rheology between a relatively stiff layer and a viscous matrix, where the stiff layer ruptures or necks normal to the extension direction in the rock (e.g. Ramberg, 1955; Strömgård, 1973; Lloyd and Ferguson, 1981; Lloyd et al., 1982; Ramsay and Huber, 1983).

Besides this usual type of boudinage, similar structures are observed in foliated rocks that do not have layering. Many strongly foliated rocks show veins at a high angle to the foliation plane with a deflection of the foliation into the veins similar to that of boudin necks in layering (Fig. 1.1). Because of this similarity and the apparent link to foliated rocks, this type of structure is known as “foliation boudinage” (Hambrey and Milnes, 1975; Platt and Vissers, 1980). There is a continuum in “layeredness” between foliation boudinage through multi-layer boudinage of successively thicker planes to true layer-boudinage (Goscombe et al., 2004).

In layer-boudinage, boudin blocks can be easily defined as distinct elongate fragments of the competent layer. Foliation boudinage occurs at isolated sites in foliated rocks, and is not generally related to any apparent rheologically contrasting layer (Fig. 1.1). As a result, the prominent elements of foliation boudinage are not the boudins, but the neck regions. In this paper we will therefore mostly avoid the term “foliation boudin” and either use the term “foliation boudinage” for the process or “foliation boudinage structure (FBS)” for the structure in the necks.

Foliation boudinage was first analysed by Cobbold et al. (1971), who studied the behaviour of homogeneous, anisotropic rocks during layer normal compression and suggested

that internal instabilities lead to the development of boudin-like structures. They referred to these as “internal boudinage”. The term “foliation boudinage” was first used by Hambrey and Milnes (1975) to describe boudin-like structures in glacier ice, which shows a strong planar anisotropy or foliation. Platt and Vissers (1980) described the phenomenon in homogeneous rock masses that are strongly anisotropic. Aerden (1991) stressed the economic importance of foliation boudinage since it commonly controls ore bodies. A number of studies have shown that foliation boudinage structures (FBSs) can also be used as shear sense indicators (e.g. Platt and Vissers, 1980; Hanmer, 1986; Lacassin, 1988; Swanson, 1992; Grasemann and Stüwe, 2001; Goscombe and Passchier, 2003; Grasemann et al., 2003). Analogue modelling by Druguet and Carreras (2006) presents the important role of rheological change through melt crystallization during deformation.



Fig. 1.1. Foliation boudinage structure (FBS) in augen gneiss, the Çine Massif, southwestern Turkey. The geometry of the boudin neck is a typical fishmouth. Vein fill is massive quartz. Location: Asmaköy (37°43'33N; 28°26'42E).

In this paper, we describe and classify different types of foliation boudinage structures from the Çine Massif, SW Turkey and the Furka Pass-Urseren Zone, Central Switzerland, where FBSs are particularly common. We have chosen to investigate structures from two areas with different tectonic regime, protolith and metamorphic grade in order to see if our observations have general validity. Our aim is to investigate if and how the geometry of FBS is dependent on foliation strength, rock type, flow regime and other parameters. Formation mechanisms of FBSs are discussed based on field observations and on numerical modelling.

1.2. Study areas

1.2.1. *Geology of the Çine submassif*

The Çine submassif is part of the Menderes Metamorphic Core Complex (MMCC) in western Turkey (Fig. 1.2). The MMCC consists of a core of tectonic units known as the Menderes nappes (Ring et al., 1999) of mainly orthogneiss and micaschist of Neoproterozoic to Palaeozoic age tectonically overlain by a number of other thrust sheets. The highest units are the İzmir-Ankara zone of Neotethys in the north (Sengör and Yılmaz, 1981) and the Lycian nappes of the Taurides in the south (Graciansky, 1968; Bernoulli et al., 1974), which consist of dominantly Permo-Mesozoic passive margin successions and ophiolitic mélangé. The underlying Dilek nappe and Selçuk melange (Güngör, 1998 and the references therein) have been correlated to the Cycladic blueschist unit (Candan et al., 1997; Ring et al., 1999; Gessner, 2000) and consist of a Mesozoic platform sequence with emery- and rudist- bearing marbles and overlying metaolistostromes. The Menderes nappes are, from highest to lowest structural level, the Selimiye, Çine, Bozdag and Bayındır nappes (Fig. 1.2a). The nappes were emplaced during the Late Cretaceous to Tertiary and later underwent Tertiary to recent regional extensional deformation. This extension by vertical shortening and N-S horizontal extension in the nappes, caused development of foliations, lineations, boudins and related structures, and later formed the E-W trending grabens which dissect the region into three sub-massifs: from north to south the Gördes, Ödemis and Çine submassifs. This study focuses on the Çine submassif, and specifically on the structures in mylonitised granitoid and metasedimentary rocks of the Çine nappe (Fig. 1.2).

Gessner et al. (2001) divided granitic rocks of the Çine nappe into older orthogneiss and younger meta-granites that have yielded Neoproterozoic to Cambrian ages (Kröner and Sengör, 1990; Hetzel and Reischmann, 1996; Loos and Reischmann, 1999; Gessner et al., 2004). However, a Tertiary age has also been suggested for gneissic granites along the southern margin of the Çine submassif due to an intrusive contact with Mesozoic micaschist (Bozkurt, 2004; Erdogan and Güngör, 2004).

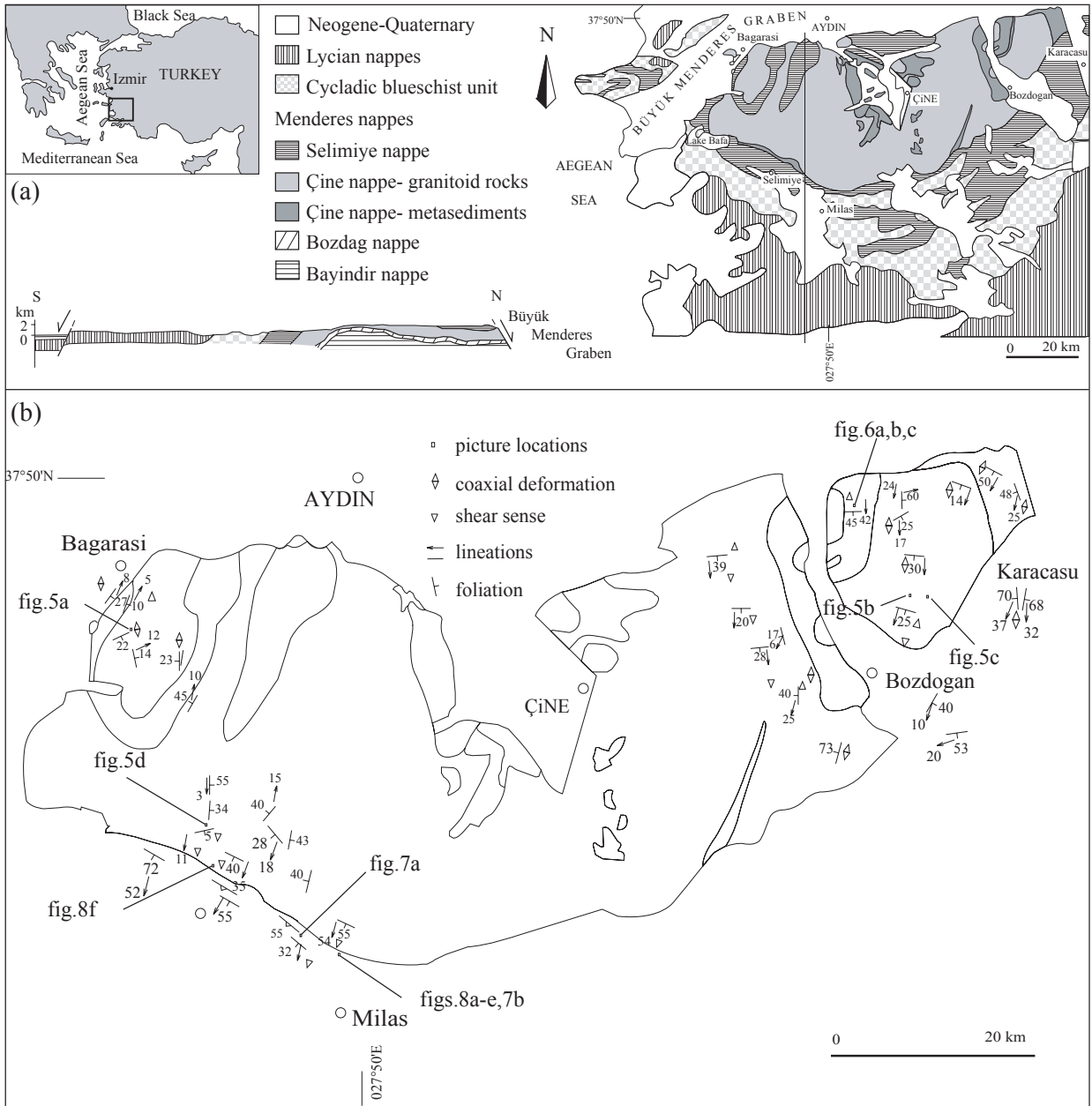


Fig. 1.2. Location of the study area in SW Turkey. **(a)** Simplified geological map and cross-section after Candan and Dora (1997) and Gessner et al. (2001). **(b)** Measurements of foliation and lineation in gneiss where foliation boudinage structures have been investigated. Locations of figures in the text shown.

Although the contact relations between the units, the age of metamorphism and deformation are still subject to discussion, there is general consensus on an early top-to-N/NE shear sense in orthogneiss and metasedimentary rocks of the Çine nappe during amphibolite facies metamorphism, overprinted by top-to-South shear sense during greenschist facies metamorphism (Gessner et al., 2001; Régnier et al., 2003, 2007; Bozkurt and Satır, 2000;

Bozkurt, 2007; Bozkurt et al., 2006). Régnier et al. (2003) recorded maximum P-T conditions of about 7 kbar and >550 °C for the metasedimentary rocks of the Çine nappe underneath the Selimiye shear zone and 8-11 kbar and 600-650 °C in the north for the same rocks. Similar P-T conditions of 8-10 kbar and 600-640 °C were also reported for the metasedimentary enclaves in the orthogneiss in the western Çine Massif by Régnier et al. (2007). The metamorphic conditions in the orthogneiss were defined by the fabrics which seem to have formed above 500°C (Gessner et al., 2001). Variable shear sense in the orthogneiss, with top-to-the-North in the north and top-to-the-South in the south and with local coaxial deformation, was attributed to strain partitioning by Régnier et al. (2007).

Foliation boudinage structures are common in both orthogneiss and micaschist of the Çine nappe. The orthogneiss is granodioritic in composition and contains cm-scale feldspar augen surrounded by a biotite foliation. The foliation is subhorizontal in the central part of the Çine submassif and aggregate lineations are well developed and generally N-S trending but gradually become steeper to the south, especially along the southern margin in the Selimiye shear zone (Fig. 1.2b). The micaschist is a biotite-garnet micaschist with indications of retrogression in the form of chlorite veins. Alteration of garnet and biotite to chlorite is common.

1.2.2. Geology of the Furka Pass-Urseren Zone

The Furka Pass-Urseren Zone between the Aar- and Gotthard Massifs is a narrow zone in the Infra-Helvetic Complex, north of the Lepontine Metamorphic Dome and the Periadriatic Line and north-northeast of the Simplon Fault Zone, in Central Switzerland (Fig. 1.3). The massifs, mainly late Variscan granites and old crystalline rocks together with narrow zones of Carboniferous sediments and volcanics, form the pre-Mesozoic basement of the Helvetic nappes and are the northernmost exposures of the external crystalline massifs. They represent updomed basement nappes separated by their Mesozoic sedimentary cover and by the basal Glarus thrust from the overlying Helvetic nappes (Milnes and Pfiffner, 1977). The basement has partially been reworked by the Variscan and Alpine orogenesis. The pre-Alpine evolution, including Variscan, Ordovician and Precambrian events, has been reported in detail by many workers (e.g. Albrecht et al., 1991; Albrecht, 1994; Schaltegger, 1994; Schaltegger and Gebauer, 1999; von Raumer et al., 1999; and references therein). In the southern Aar Massif, Alpine overprint was strong and

the basement and cover rocks were affected by ductile deformation under greenschist facies metamorphism with P/T conditions of 300–450 °C and 3–4.5 kbar increasing from north to south and further south in the Gotthard Massif reaching amphibolite facies (Marquer and Burkhard, 1992; Frey and Mahlmann, 1999). The geometry of this heterogeneous deformation shows anastomosing patterns of shear zones corresponding to a bulk vertical stretching. For the southern Aar Massif 450 °C and 4.4 kbar conditions are constrained by fluid inclusion data from fissure quartz (Frey and Mahlmann, 1999).

We studied foliation boudinage structures in the mylonitic gneisses and metasediments of the Furka Pass-Urseren Zone that have an approximately NE-SW striking and vertical to steeply dipping regional penetrative foliation (Figs. 1.3a, b). The aggregate and grain lineations are mostly vertical or steeply plunging. Both structures formed in anastomosing shear zones with a vertical displacement component. However in some narrow shear zones evidence for a strike-slip component of motion is found.

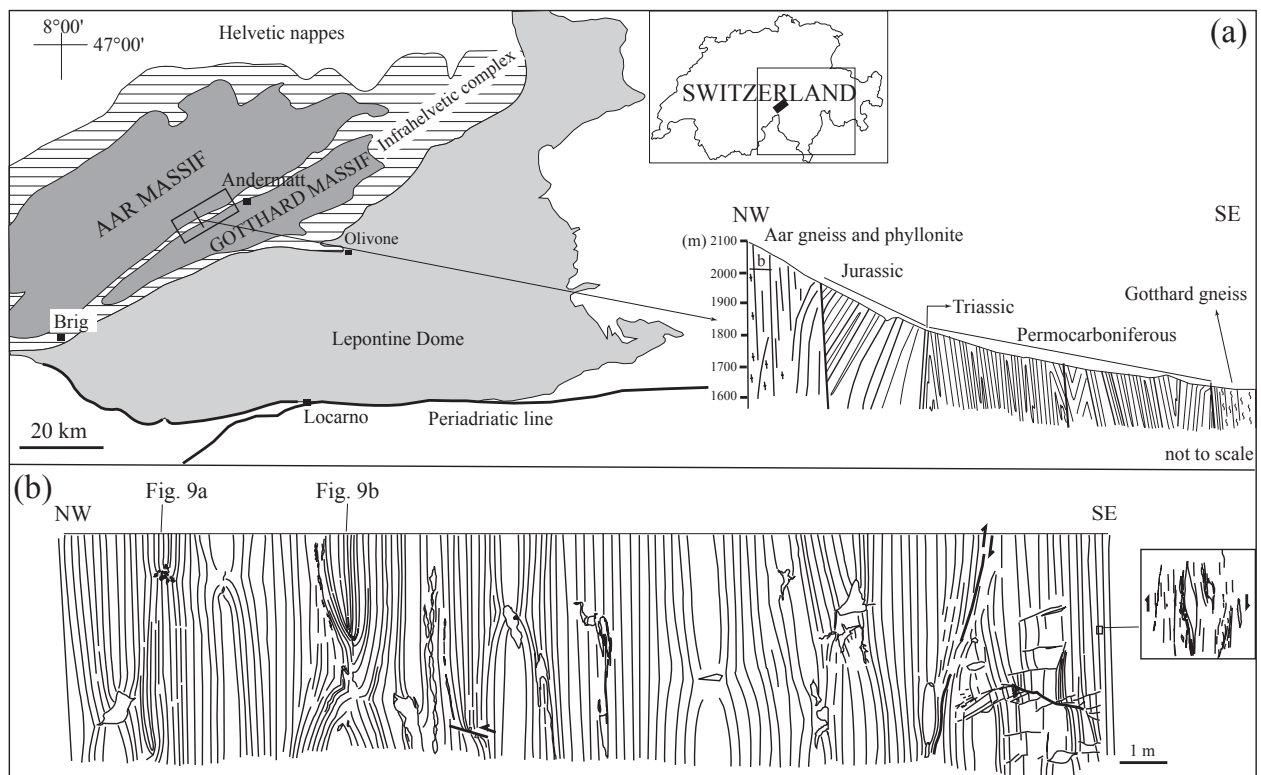


Fig. 1.3. (a) Location of the area in Switzerland where foliation boudinage structures were studied. Simplified geological map and cross-section modified after Lebit (1989). (b) Sketches of FBSs along a short road-cut section opposite the Belvedere Hotel, Furka Pass.

1.3. Foliation boudinage structures (FBSs)

1.3.1. Foliation boudinage structures (FBSs) in the Çine submassif

Foliation boudinage structures (FBSs) are isolated structures in rocks recognized by perturbations in the monotonous foliation adjacent to a central discontinuity, mostly filled with vein material. The planar foliation and straight lineation in the far-field wall rock is deflected close to the central discontinuity, and the typical shape of a foliation boudinage structure as described below is defined by the deflection pattern of the foliation, and the shape of the central veins. The deflection pattern close to a central vein is a category of flanking folds (Passchier, 2001). Boudin neck veins are normally structures with an elongate, commonly curved disc-shaped geometry; the longest axis (L_b) is parallel to the foliation and typically normal to the aggregate lineation (L) in the rock and the shorter axis normal or oblique to the foliation (Fig. 1.4).

We have applied and in some cases adapted the boudin terminology of Goscombe and Passchier (2003) to describe the geometry of FBSs (Fig. 1.4). Since most of the FBSs in the studied area have mineral-filled boudin neck veins, an inter-boudin surface (S_{ib} ; Goscombe and Passchier, 2003) is defined as an imaginary median surface passing through the centre of the neck vein. Symmetry of FBSs can be easily recognised when these interboudin surfaces (S_{ib}) are drawn. The angle θ between S_{ib} and the main foliation is between 50° and 90° changing with different FBS types.

Since there is no boudinaged single competent layer, a boudin exterior S_b is defined here as a foliation plane that starts at the vein tips, extends away from the vein and becomes parallel to the external, far-field foliation (f_e); f_e is the main penetrative foliation in the host rock and is not affected by perturbations around the vein. The foliation affected by perturbations adjacent to the vein, described in Passchier (2001) as internal host element (HE_i), is here referred to as the internal foliation (f_i). The deflection of the foliation, measured as an angle β , is the deviation of the internal foliation from its external, f_e orientation (Figs. 1.4 and 1.5e). There is a gradual transition between f_i and f_e .

A large number of foliation boudinage structures were analysed in the Çine Massif, ranging in size from cm- to m- scale. Both symmetric and asymmetric types of FBSs are

common. Symmetrical FBSs at the northwestern margin of the Çine Massif were first mentioned by Gessner et al. (2001) and Régnier et al. (2003) as amphibolite facies structures. Boudin neck veins strike approximately E-W relative to N-S oriented aggregate lineations. The axial planes of boudin veins crosscut the regional foliation at steep angles.

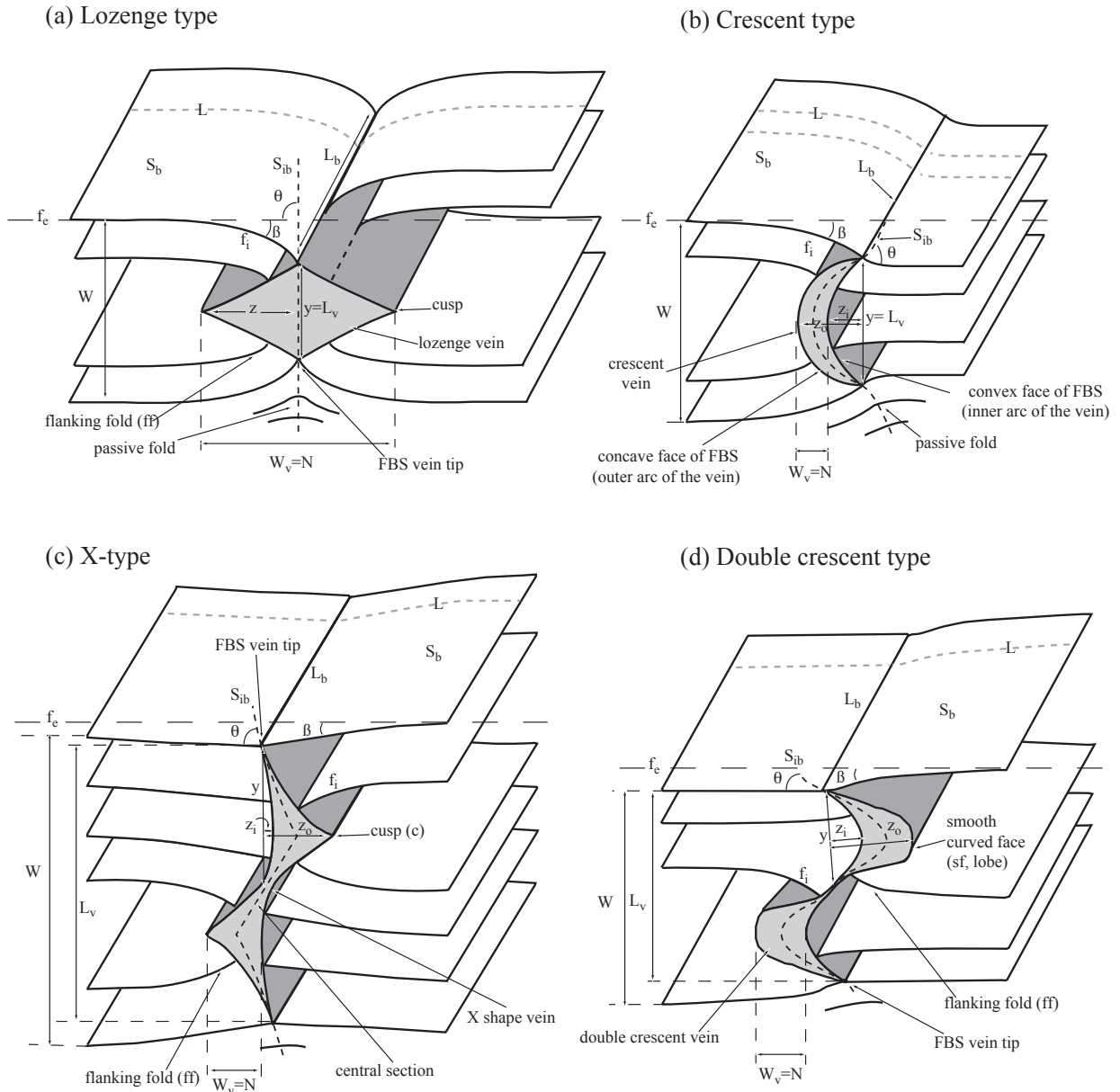


Fig. 1.4. Geometry of foliation boudinage structures (FBSs). (a) Lozenge type. (b) Crescent type. (c) X-type. (d) Double crescent type. See text for explanation.

On sections parallel to the aggregate lineation and normal to the foliation in the rocks, both symmetric and asymmetric types of FBSs occur and several hundred were investigated in the Çine Massif (Fig. 1.5). We classified the common types of foliation boudinage structures into four categories; lozenge-, crescent-, X- and double crescent- type FBSs (Figs. 1.4 and 1.5). These categories are easily distinguished in the field and are named after vein geometries in the boudin necks in cross-sections normal to the foliation and parallel to the aggregate lineation.

Lozenge- and X- type FBSs have sharp, angular vein geometries whereas crescent- and double crescent- type FBSs have smooth, curved vein geometries (Figs. 1.4, 1.5 and 1.6). The curve of the FBS neck vein reflects the geometry of FBS faces and these faces can be concave and convex/concave with respect to the boudin interior. The curve of the FBS faces can be defined by a ratio z/y (Goscombe et al., 2004) where z is a maximum normal deviation of the FBS face out of or into the FBS interior from a straight line connecting the edges of the FBS face at the vein tips. y is a measure of the length between the vein tips passing through the centre of the vein (Fig. 1.4). In the case of X- and double crescent- types, y is measured from the vein tip to the centre of the structure instead, since both are paired structures. z is measured for both inner and outer arc/curve as z_i and z_o respectively. The inner arc can be straight if the deviation z of that face is zero, or curved. The maturity of the curvature through progressive deformation can be defined by this ratio as it decreases and approaches zero when the geometry reaches that of a closed fishmouth.

Lozenge-type FBSs are symmetric and characterized by lozenge-shaped veins in their boudin neck with two cusps facing opposite sides (Figs. 1.4a and 1.5a). A straight S_{ib} passing through the tips of the neck vein divides the structure into two symmetric parts and is at a high angle ($\theta = 90^\circ$) to the external foliation f_e . The sharp, strongly curved vein faces also reflect the boudin face geometries known as fishmouth structures. The length/width (L_v/W_v) ratios of the boudin neck veins are low. They are known as short-type FBSs. Foliation boudin exteriors, S_b , are straight and parallel to each other on both sides except close to the neck vein.

In lozenge-type FBS, a symmetrical pair of flanking folds occurs on the two sides of the vein. The shape of these folds can be measured along single foliation planes and through the cross-section in different foliation planes. The angle β increases towards the vein cusps and decreases to the vein tips (Figs. 1.4a and 1.5a). The maximum value of β is reached near the cusp, while at the cusp it is zero in a symmetric structure. Contours for these angles can be drawn to define the exact shape of the folds (e.g. Fig. 1.5e). At the end of the vein tips (top and bottom) the

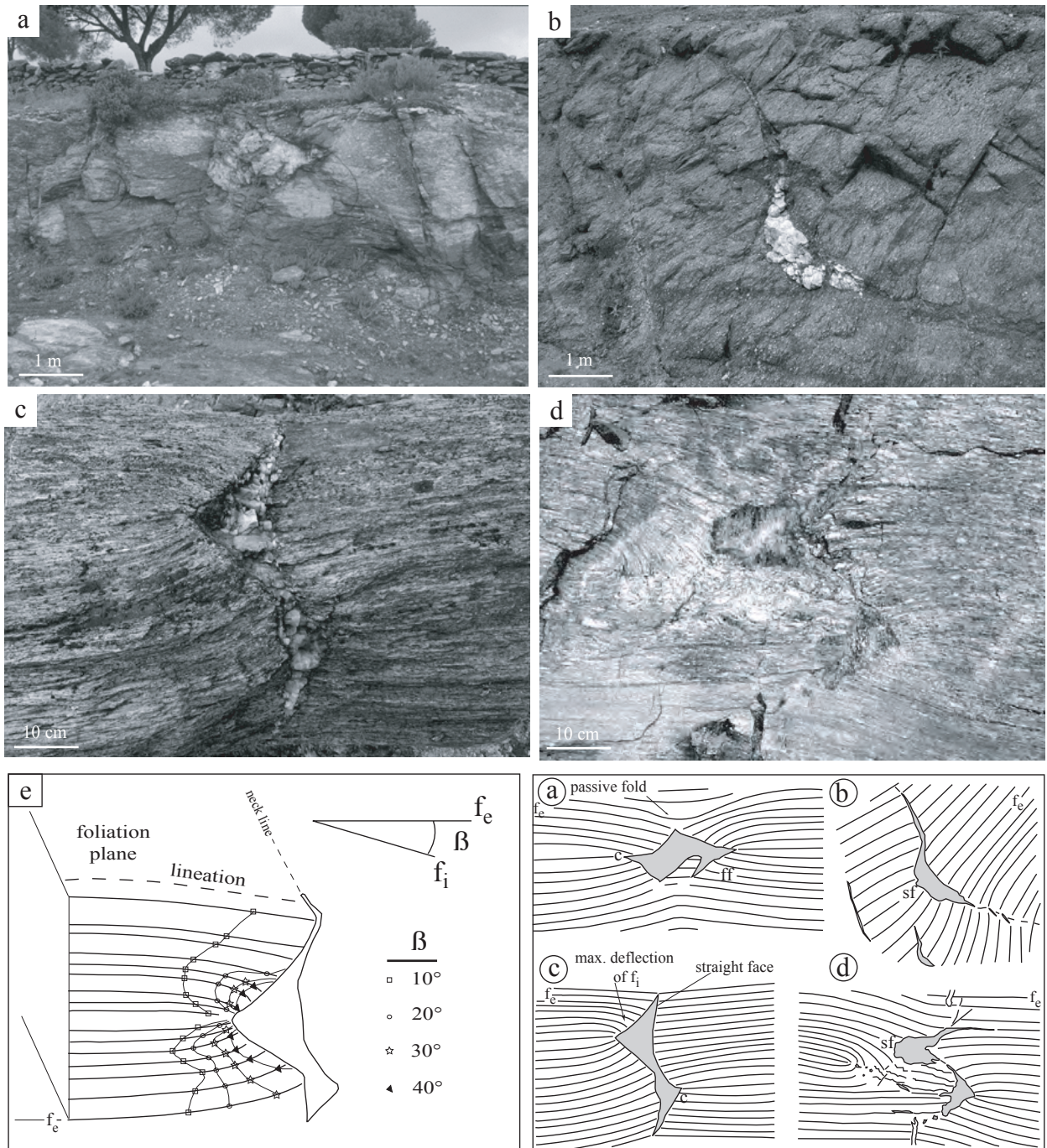


Fig. 1.5. Photographs and sketches of FBSs from the Çine Massif. All views are in cross section normal to the boudin axis. **(a)** m-scale lozenge type FBS in orthogneiss, northwestern Çine Massif ($37^\circ40'32\text{N}$; $27^\circ33'98\text{E}$). Two symmetric cusps face in opposite direction and the foliation is deflected towards the central vein. **(b)** m-scale asymmetric crescent type FBS in orthogneiss, northeastern Çine Massif ($37^\circ42'14\text{N}$; $28^\circ26'63\text{E}$). Curved vein walls face the same direction. **(c)** X-type FBS in orthogneiss. Maximum deflection of foliation around veins is around cusps and the deflection angle decreases to the tips of the vein. On the opposite straight side of the vein foliation is at a high angle to the vein wall. Vein fill is biotite, quartz and feldspar ($37^\circ42'36\text{N}$; $28^\circ27'69\text{E}$). **(d)** cm-scale double crescent type FBS in orthogneiss, southern Çine Massif ($37^\circ29'88\text{N}$; $27^\circ38'74\text{E}$). This type has asymmetric double curved faces. **(e)** Contours connecting the same β angles measured along the foliation planes showing the deflection of foliation around cusp. Locations are shown on Fig. 2b.

foliation is passively folded. The degree of the curvature of these passive folds decreases away from the vein tips and becomes parallel to the straight foliation in the far field (Figs. 1.4a and 1.5e). Passive folds are common in other types of FBSs as well.

Crescent-type FBSs are asymmetric with a single smoothly curved vein in the boudin neck, with curving vein contacts facing to one side (Figs. 1.4b and 1.5b). S_{ib} is curved but close to the vein tips it is at a high angle or is normal to the foliation. FBS neck veins have high length/width ratios. Two ratios are measured to define the curve of the FBS faces for the asymmetric types: z_o/y for the outer arc of the vein and z_i/y for the inner arc. z_o is the maximum normal distance from the outer arc of the vein to the straight line connecting the vein tips while z_i is the maximum normal distance from the inner arc of the vein to this line. The length y is measured between the vein tips. Foliation bends into the outer arc of the vein and bends slightly out along the inner part.

X- and double crescent- type FBSs are asymmetric (Figs. 1.4c, d and 1.5c, d). These structures are similar to the dilational forked-gash asymmetric boudins and sigmoidal-type asymmetric boudins in layers, as described by Goscombe et al. (2004). The geometry of the neck veins resembles that of cusped-lobate structures. FBS neck veins have high length/width ratios and are long FBS types. X-type FBSs have veins in the boudin necks with two cusps facing opposite sides similar to the lozenge-type, but here cusps are not opposite each other. S_{ib} is sharp with central and outer sections, X- or Z- shaped and in the central section at a high angle to the foliation (Figs. 1.4c, 1.5c and 1.6a, c). Asymmetric flanking structures are present at the “cusped” faces of the veins and the foliation is at a high angle to the contact on the opposite straight (Fig. 1.6a) or slightly curved (Figs. 1.5c, 1.6c) faces. On the side of the cusps, the deviation of the foliation (β) increases from 0° close to the vein tips to 40° near the cusps. The maximum deviation angles are found near cusps. The cusps commonly develop into fishmouth structures (Fig. 1.6b). On the opposite, slightly curved faces β does not deviate much from zero.

The most regular double crescent- and X- type FBSs are in fact two linked, stacked symmetric half-boudin structures with opposite polarity (Fig. 1.4), but we prefer to refer to the entire structure as “asymmetric” in our classification.

For the X- and double crescent- types the curve of the FBS faces are measured as two ratios (z_o/y and z_i/y) as for crescent types. y is a measure of length between the vein tip and the vein centre along the straight line connecting vein tips (Figs. 1.4c, d). Double crescent-type FBSs have double curved veins with lobes in the neck facing opposite sides (Figs. 1.4d and 1.5d). S_{ib} is

smooth and sigmoidal. In the central part of the vein S_{ib} is at a higher angle to the foliation than at the tips. Fishmouth structures can be found associated with all types of FBSs and form an end stage in the tightening of these structures.

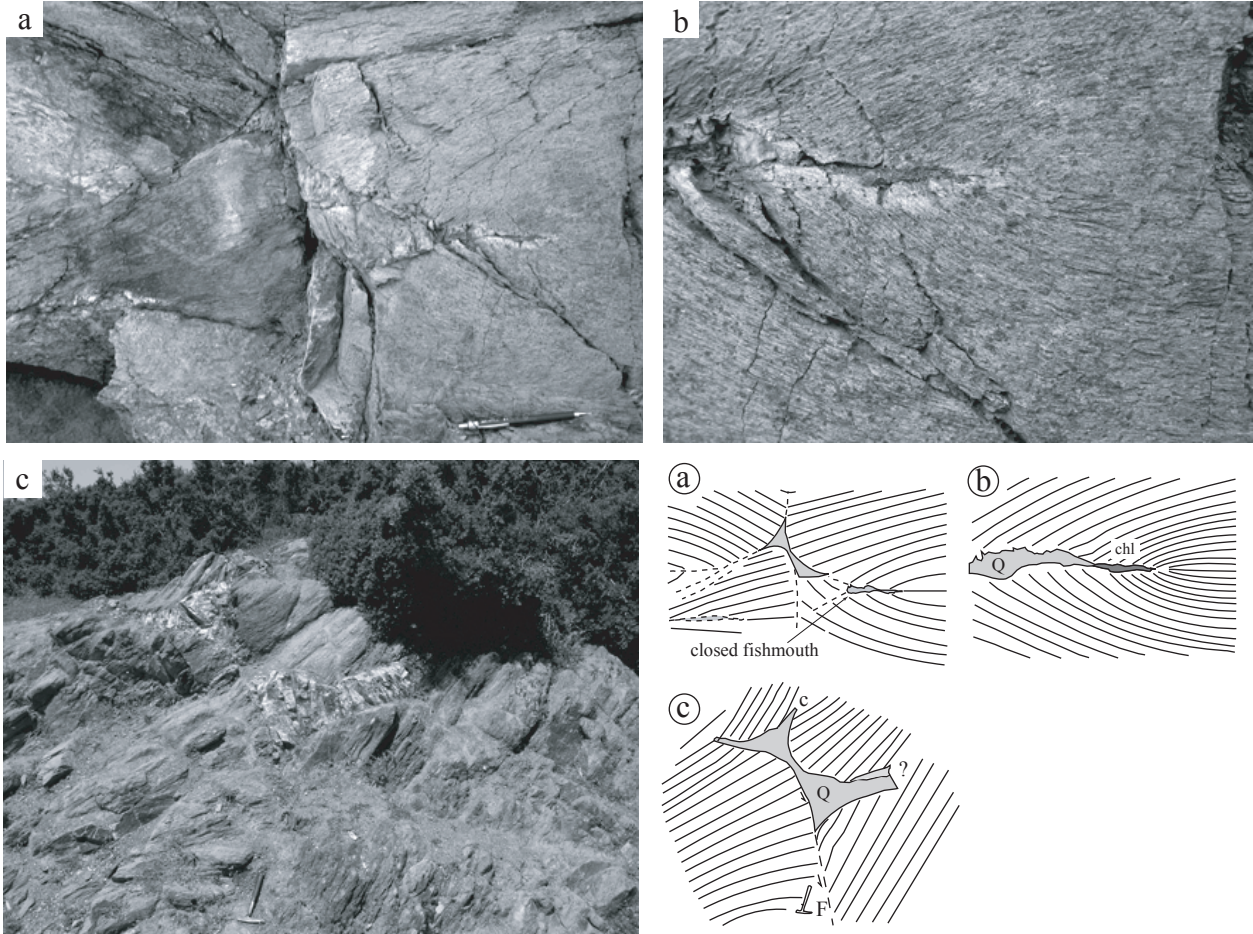


Fig. 1.6. Complex X-shaped FBSs from the northeastern Çine Massif **(a)** X-type FBS with closed fishmouth structure at the end of the cusps in metasediments of the Çine nappe (Location: 37°47'37N; 28°22'44E). **(b)** Detail of closed fishmouth structure in (a). Note the alteration rim around the vein. **(c)** m-scale X-type FBS in metasediments, northeastern Çine Massif (Location: 37°47'37N; 28°22'71E). Note the asymmetric cusps and necking of foliation around the cusps. On the opposite sides from the cusps, where the vein wall is straight, foliation is at a high angle to the vein wall.

The geometries described above are visible in cross-section parallel to the lamination in the rock, but the 3D shape of the FBS is not cylindrical. On foliation surfaces, FBSs occur mostly with one of two shapes; lens shaped and triangular shaped veins (Fig. 1.7). Both foliation and lamination bend symmetrically in on two sides of the lens shaped veins (Fig. 1.7a). They belong to the symmetric FBS types described above. Around the triangular veins the lamination is straight

and at a high angle to the vein contact on the straight face of the vein and on the opposite cusped side it is deflected (pinched in) in accord with the curved side of the vein but again at a high angle to the vein wall (Fig. 1.7b). Triangular veins belong to the asymmetric FBS types described in cross-sections. The curve of the cusp can be sharp, angular (e.g. X-type) or smooth (e.g. crescent- and double crescent- types) depending on the asymmetric FBS type. In the Çine Massif, FBS veins have a length-width ratio on the foliation surface of at least three and usually more.

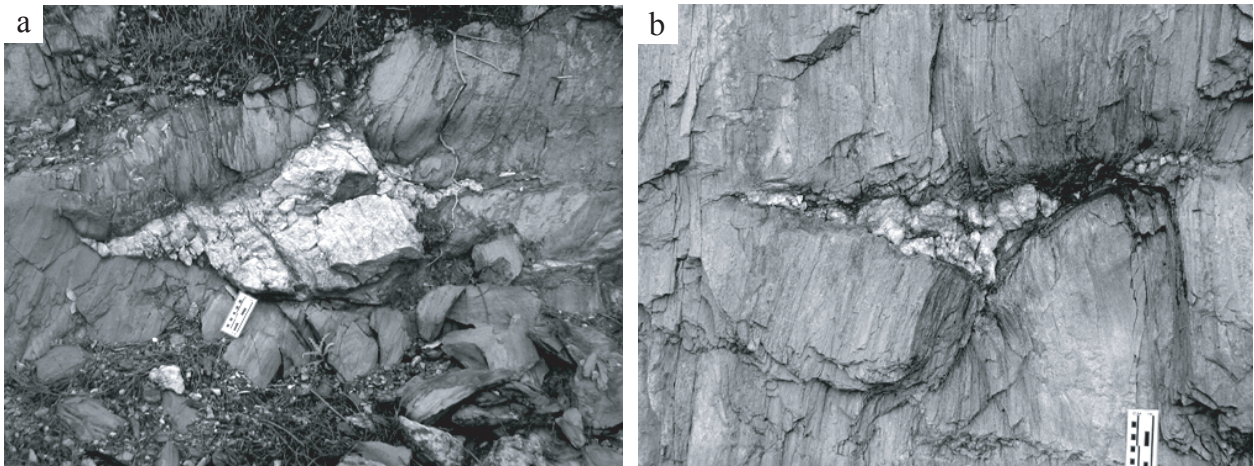


Fig. 1.7. Photographs of FBSs in cross-section looking down on the foliation plane. The aggregate lineation on foliation plane bends in towards the vein. **(a)** Symmetric FBS with a lens shaped vein in the neck (Location: 37°23'66N; 27°45'06E). **(b)** Asymmetric FBS with a triangular vein in the neck (Location: 37°22'68N; 27°47'73E). Scale in the photographs is 10 cm long. Locations are shown on Fig. 2b.

1.3.1.1. Variations in geometry of FBSs in the Çine Massif

In strongly mylonitic rocks of the Selimiye shear zone in the southern Çine Massif, a number of interesting asymmetric types of boudinage structures have been found (Fig. 1.8). These local structures are small veins (Fig. 1.8a) in quartz micaschist and micaschist of the shear zone, which mainly developed in shearbands. In sections normal to the foliation and parallel to the aggregate lineation, these asymmetric types have lozenge-shaped and triangular quartz plugs in the neck region of FBSs and they differ in some aspects from the main common types mentioned above (Fig. 1.8). We therefore prefer to place them in another category.

Asymmetric lozenge-type FBSs have flanking folds on two opposite sides of the vein walls that are at a relatively high angle to the main foliation in the host rock. The foliation presents a shearband geometry on the other two sides of the vein, where the vein walls lie at lower angles to the main foliation (Fig. 1.8b).

Relatively common are isolated triangular vein geometries (Figs. 1.8c-f), similar to those observed in X-type FBSs, but not occurring in pairs. These triangular veins show remarkable variety in their angular relations with the adjacent foliation in the host rock. Some types present asymmetric flanking folds on different faces of the triangle (Figs. 1.8c, d). In these types one face of the triangle is at a high angle or orthogonal to the main foliation in the host rock whereas the other two faces are oblique to the foliation. Such veins can be wing cracks, where fractures form and open at the tip of a fault (Fig. 1.8c), or cusped triangular veins that have one folded fracture wall (Fig. 1.8d). In the other types of FBSs with triangular neck veins (Figs. 1.8e, f), the foliation is symmetrically arranged on two sides of the vein. In such symmetrical triangular veins two faces of the triangular neck vein are oblique to the foliation and the angle between these two faces is acute. The other face of the triangle is parallel or at very low angle to the foliation.

Some FBSs in the Çine Massif are associated with a quartz layer in the central part of the boudin structure. These are not classical lithology-defined boudins, since the deflection of the foliation extends far beyond the width of the central quartz layer. However, the central quartz layer predates formation of the FBS and may play a role in localisation of boudinage in these structures.

1.3.1.2. Vein material

The boudin neck veins of FBSs in the Çine Massif are mostly filled with massive quartz in large single crystals and with spherulitic chlorite aggregates. Tourmaline, feldspar and biotite are also present in some veins in the studied areas. The veins can contain up to several cubic meters of quartz (Fig. 1.5). However, some FBSs have very little or no vein material in their cores, especially those that have a closed “fishmouth” shape (Goscombe et al., 2004). Such FBS can be easily confused with isoclinal folds. Minerals in the veins are never fibrous or elongate in shape, but always coarse grained, equidimensional and blocky (Fig. 1.10a). This habit of the grains is an original feature of vein filling, and not due to deformation or recrystallisation; quartz

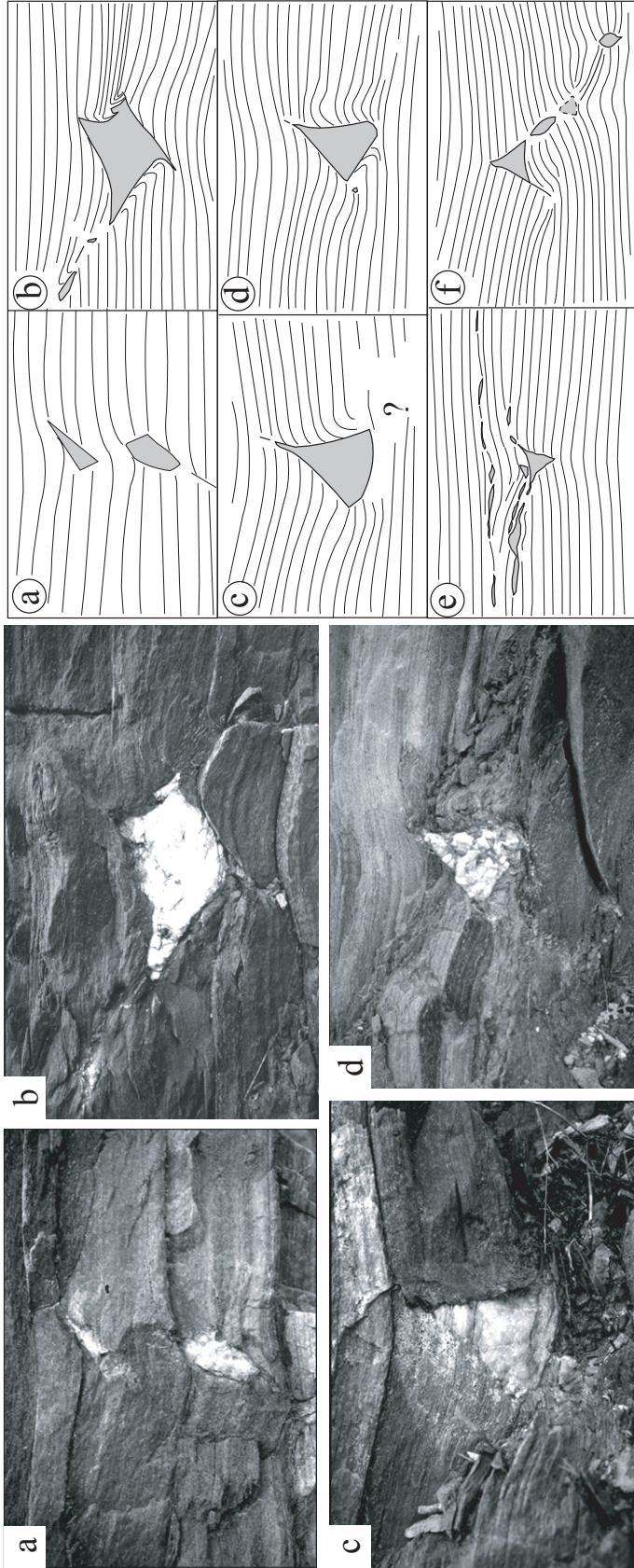


Fig. 1.8. Various types of FBSs with triangular veins from mylonitised quartz mica schist in the Selimiye shear zone, southern Çine Massif. **(a)** Small veins in a shearband. **(b)** Asymmetric lozenge-shaped vein with flanking folds on opposite sides of the vein walls that are at an angle to the main foliation in the host rock. On the upper left and the lower right sides of the vein foliation is deflected as in a shearband. **(c)** Triangular vein with asymmetric flanking folds, probably a type of wing crack. **(d)** Cusped triangular vein with flanking folds on both sides with small interlimb angles. **(e)** Triangular vein with fishmouth structure on the left side of the vein (Location of outcrop for a, b, c, d, e: 37°22'74N; 27°47'82E). **(f)** Several triangular and lens-shaped veins in a shearzone with bending and passive amplification of foliation around and at the tips of the veins (Location of outcrop: 37°28'61N; 27°35'19E). Locations are shown on Fig. 2b. The development of these variations of FBSs are explained in Fig. 14.

in the veins is weakly deformed with some undulose extinction. Many veins contain faceted large quartz crystals that face a central void in the boudin necks.

In some outcrops in the gneisses (e.g. in the northeasternmost Çine Massif) spaced mode I fractures cut the pervasive foliation, and are easily recognized by red-brown iron oxides. These mode I fractures are mainly filled with chlorite and range in length from mm- to m- scale and are up to several mm wide. Wider fractures are mostly filled with massive quartz. In some cases biotite concentrations or stacks in the host rock are found at vein margins. Garnets in the host rock were altered to chlorite close to the veins.

Growth of minerals in narrow veins that open slowly leads to the formation of elongate or fibrous crystals (Bons, 2001; Hilgers et al., 2001). If veins open more rapidly than crystal growth, blocky crystals develop with faceted crystal faces according to their mineral-specific crystal morphology (Spry, 1969; Passchier and Trouw, 2005). The best examples of fibrous veins are found in low to medium grade rocks, while massive quartzo-feldspathic veins that must have filled tensile fractures are common at higher metamorphic grades (Ethridge et al., 1984). Extension fractures filled with minerals reflect the pressure-temperature conditions of their host rock.

The dominance of large faceted single quartz crystals and spherulitic chlorite in the veins in the FBSs of the Çine Massif suggest that the minerals did not grow by slow opening but grew into open fluid-filled space with a fluid pressure exceeding the minimum principal stress by at least the tensile strength of the rock. These fluid-filled voids must have been present for a substantial period of time during the later stages of deformation in the Massif, while the FBSs developed; there was time to allow first ductile deformation and infolding of fracture walls followed by vein filling, since the vein material is not deformed.

1.3.2. FBSs in Furka Pass-Urseren Zone

In order to test the general validity of our observations in gneiss and micaschist of the Çine Massif, we also studied FBSs in the Furka Pass-Urseren area of the central Alps.

In the Furka Pass-Urseren area a great number of FBSs occur, both symmetric and asymmetric (Fig. 1.3b). In general, the same types of FBSs are observed as in the Çine Massif. Closed fishmouth type lozenge-shaped FBSs dominate, many of which are asymmetric with flanking folds on one side (Fig. 1.9). The FBS neck veins are smaller than those of the Çine

Massif, up to several tens of centimetres long. The associated neck veins are mostly lens shaped. They are filled with coarse massive quartz, feldspar and spherulitic chlorite aggregates (Figs. 1.9 and 1.10b). Chlorite aggregates are not only found as vein fill but also occur along the edge of veins in the wall rock (Fig. 1.10b). Alteration rims in the host rock around boudin neck veins are common. They are easily recognized by a difference in colour with the host rock (Fig. 1.9a), while their width depends on vein size.

On the foliation surface, FBS neck veins are lens-shaped with a high length-width ratio that exceeds 4. The local aggregate lineation is mostly at a high angle to the vein wall. However some late veins with lineation oblique to the vein wall are also found. In some outcrops, a crenulation is visible on micaceous foliation planes slightly oblique to the vein axes.

On planes normal to the foliation and parallel to the aggregate lineation FBS neck veins lie both highly oblique (Fig. 1.9a) and parallel to the foliation (Fig. 1.9b). They are present as a single vein or trains of several irregular lens-shape veins. Flanking folds adjacent to veins with axes parallel to the boudin axes (e.g. Fig. 1.9c) show interlimb angles changing from open to completely closed (Fig. 1.9). Gentle, open flanking folds are observed at FBSs where boudin neck veins are at a high angle to the foliation and are mostly associated with symmetric FBSs (Fig. 1.9a). Small interlimb angles of flanking folds, mostly less than 30° where fold limbs became almost parallel to each other and to the vein wall, are observed with veins parallel or at low angle to the foliation and near asymmetric FBSs (Figs. 1.9b-e). In some cases flanking folds are cut by minor fractures or small veins at a high angle to the FBS neck, probably formed as accommodation fractures in response to a high angle of rotation of the vein (Fig. 1.9e). The curvature of the flanking folds is strongest on one side of the FBS neck region (Figs. 1.9b-e). On the opposite side of the vein the foliation is parallel or at a low angle to the vein wall. Although rare, foliation boudins separated by two veins have been found in the Urseren area (Fig. 1.9d). Mode I and/or conjugate mineral-filled fractures with high aspect ratio are also observed at high angles to the foliation but these are probably late, based on cross-cutting relations seen in outcrop. In some outcrops FBSs are cut along the neck region and displaced by cm to m-scale faults or shearzones that lie at an angle to the main foliation in the host rock (Fig. 1.3b).

The rocks of the Çine nappe contain a subhorizontal foliation and lineation developed at upper amphibolite to greenschist facies conditions, while the rocks in the Furka Pass-Urseren zone present vertical to subvertical foliation and lineation formed under greenschist facies. The closed fishmouth type lozenge-shaped FBSs, which dominate here (Figs. 1.9b, c) are thought to

be the end-stages in development of more open asymmetric lozenge-type veins by a process similar to that in the Çine Massif.

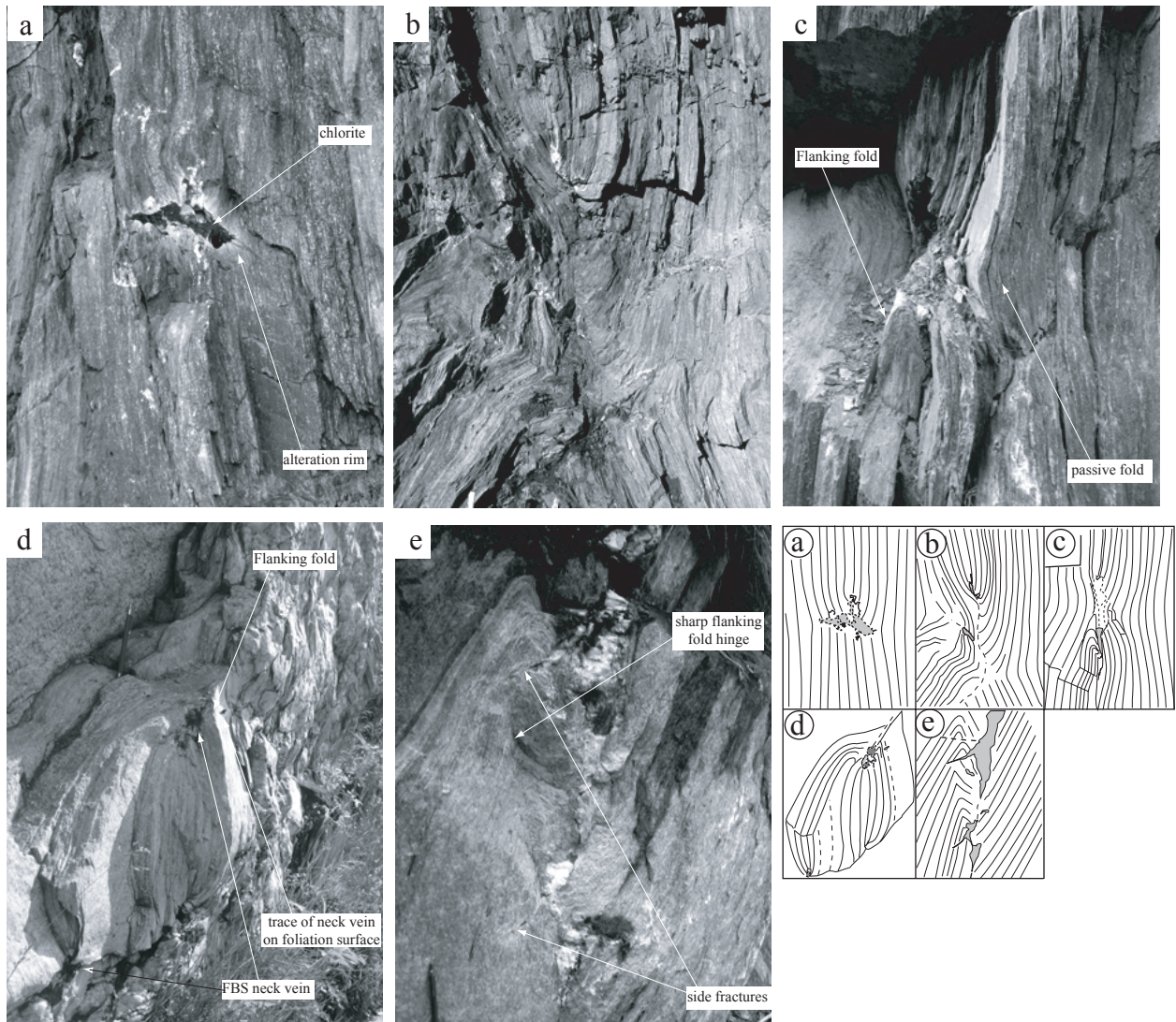


Fig. 1.9. Photographs and sketches of FBSs from the Furka Pass-Urseren Zone. All views are in cross-section normal to the FBS axis. **(a)** Symmetric FBS with alteration rim around a chlorite-quartz vein in mylonitic gneiss. **(b)** Asymmetric FBS with small quartz, feldspar, chlorite veins in boudin necks (Location of outcrop for pictures a, b: 46°34'65N; 08°23'32E also indicated in Fig. 3b). **(c)** Asymmetric FBS, a neck vein lies parallel to the foliation and to the axial plane of a flanking fold with small interlimb angle in quartz sericite schist. The open fold is due to passive amplification of foliation at the vein tip. **(d)** Boudin block between two neck veins filled with quartz, albite, chlorite and mica (Location: 46°37'17N; 08°33'21E). **(e)** Central vein structure in a FBS neck pinched into several small lens shaped veins. To the left of the veins are tight flanking folds with sharp hinges. Flanking folds are cut and slightly displaced by the small subsidiary fractures to the FBS neck (Location: 46°37'11N; 08°33'05E).

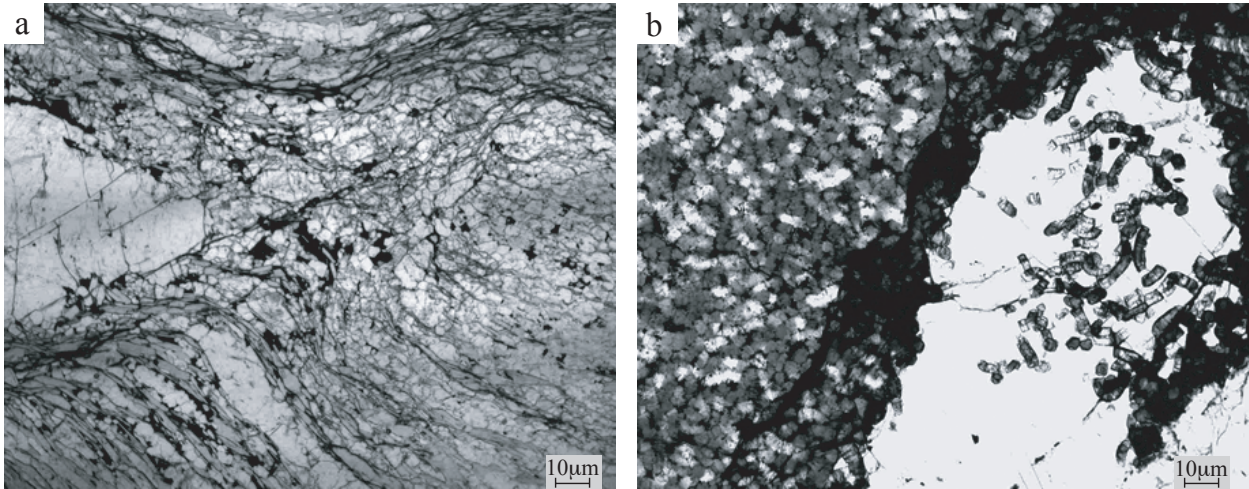


Fig. 1.10. Photomicrographs of FBS neck regions. **(a)** Fishmouth FBS. In the central part of the picture necking of the foliation in the host rock is visible close to the vein. The V-shaped vein in the FBS neck consists of massive blocky quartz. At the lower contact of the vein, micas (biotite+muscovite) bend in towards the vein as in a shearband (Sample location: Labranda road, Çine Massif; 37°22'98N; 27°47'79E). **(b)** Spherulitic chlorite aggregates at the edge of and inside a feldspar filled neck vein. (Sample location: Belvedere, Furka Pass; 46°34'56N; 08°23'39E).

1.4. Numerical modelling

In order to explain the geometry of the developing foliation boudinage structures, we carried out simple numerical experiments using FLAC (Itasca Consulting Group, Inc., 1999) described in Passchier and Druguet (2002). FLAC is a 2D explicit finite difference model and is based on 4-node quadrilateral meshes.

In all numerical experiments we used a grid size of 60x42 elements in x - and y -coordinates respectively. The exact location of each element and each node in the grid, in which all variables are stored, is defined by a pair of x -, y - coordinates. Fractures were modelled by removing elements and replacing them by a void within a finite difference mesh (Figs. 1.11 and 1.12). Experiments were run for a range of kinematic vorticity numbers from pure shear to simple shear in several combinations with different initial fracture orientations (Figs. 1.11 and 1.12), θ varying between 30° and 150°. Here, only the most important results are shown. We adopted a visco-elastic (Maxwell) substance model in numerical simulations. Kinematics of flow in the models was defined as a function of the bulk-stretching rate, which was set at $1e-10 \text{ s}^{-1}$, and the kinematic vorticity number (W_k), ranging between 0 (pure shear) and 1 (simple shear). The maximum creep time was set to 8e8 s. Material properties were set as follows: bulk modulus = $2e10 \text{ Pa}$, shear modulus = $1.2e10 \text{ Pa}$, viscosity = $1e19 \text{ Pa s}$ and Poisson's ratio = 0.25.

The experiments were run for 6500 to 12500 steps. Elements were removed from the mesh at each 1000 (Figs. 1.11b, c) or 500 steps (Fig. 1.12) to mimic fracture propagation. We examined fracture growth and deformation for experiments run at different rates and the processes in individual experiments at each stage. The plots in Figures 1.11 and 1.12 are shown at the same deformation steps for each experiment. Aspect ratios of initial fractures were defined as 21:1 for a stationary fracture (Fig. 1.11a) and 2:1 in fracture growth experiments (Figs. 1.11b, c and 1.12) as the ratio of a number of elements removed in vertical (y) direction to the elements removed in horizontal (x) direction. Models assume an initial fracture that can remain open during the deformation. We simulated fracture growth by alternating deformation steps with steps where we allowed removal of grid elements at the tip of the initial fracture. Although the method to simulate a fracture is rather simple and without feedback between fracture shape, stress intensity and fracturing, it gives interesting results.

One important observation is that if an open fracture precedes ductile deformation in the rock and is fixed in length and the surrounding material is deformed in pure shear, the fracture opens to an elliptical and even circular shape (Fig. 1.11a). Only if we allow fractures to grow laterally during ductile deformation of the wall rock, a typical lozenge shape forms and the walls of the vein start to buckle towards a fishmouth shape (Figs. 1.11b and c). The rounded, lens-shaped opening that occurs for non-propagating fractures was never observed in natural FBSs. Short veins with slightly convex shape are common in nature, also in the Çine and Furka areas, and these may in some cases represent incipient FBSs. From our field observations and the FLAC experiments it seems, however, that fractures must grow laterally during opening to give the typical lozenge shape that is characteristic for many FBSs.

The initial orientation of the fracture is important in defining the resulting geometries through progressive deformation. Figure 1.12a shows an example of the development of asymmetric FBS in which an initial oblique fracture ($\theta = 60^\circ$) propagates and is deformed under pure shear conditions. During progressive deformation, rotation of and slip along the fracture leads to opening of an asymmetric vein and development of flanking structures in the adjacent grid. Similar asymmetric FBSs are also developed in simple shear (Fig. 1.12b). However, angular relations between the adjacent grid and the vein are slightly different from those in Figure 1.12a. The simple shear experiment was carried out with a vertical initial fracture. The asymmetry could

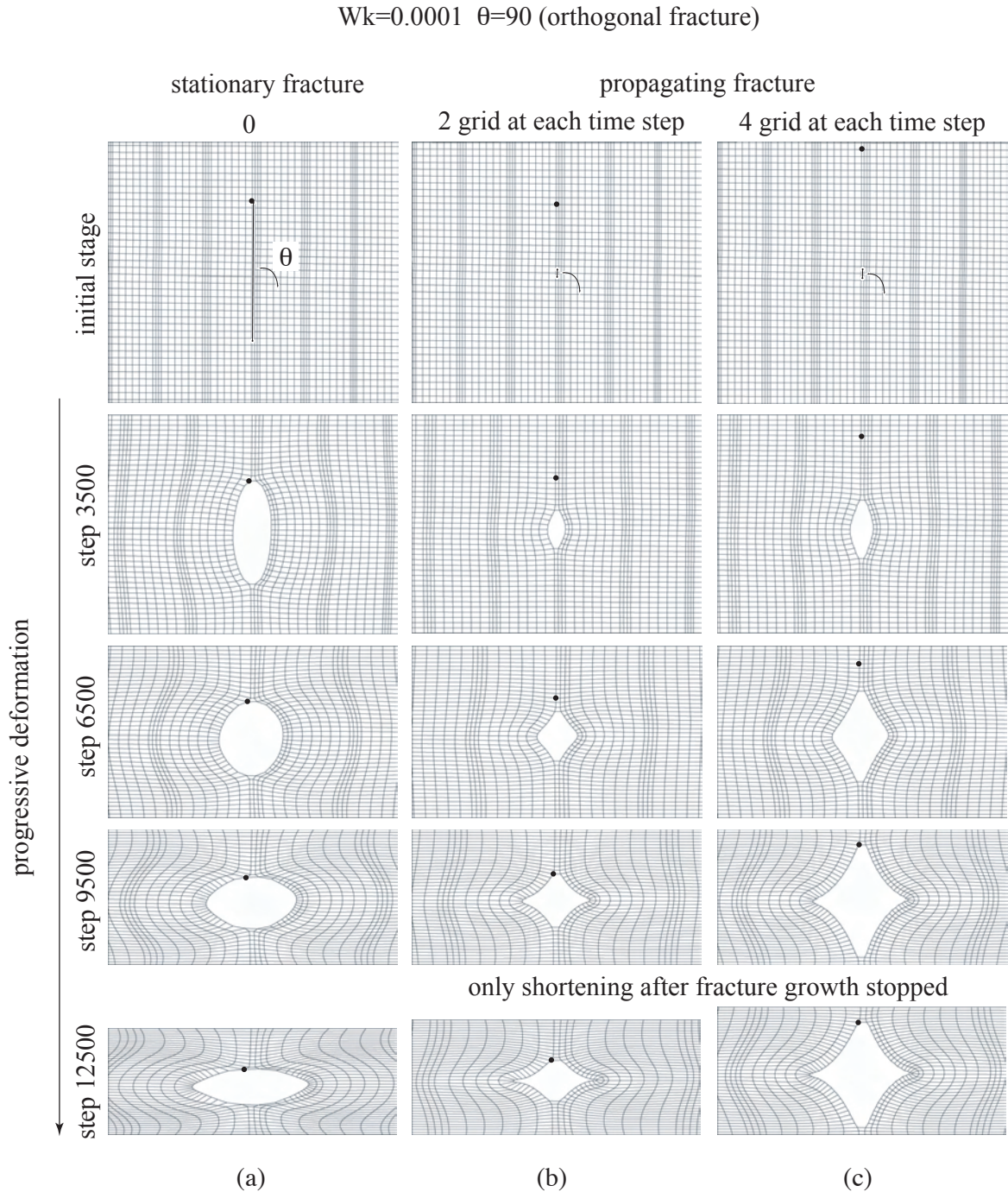


Fig. 1.11. Results of FLAC experiments showing the effect of different fracture propagation speeds on necking and vein geometry during ductile flow. Only the central part of the grid in the models is shown. In the models grids were deformed under pure shear conditions and $\theta = 90^\circ$. θ is an angle between the initial fracture and the horizontal grid-foliation. Initial geometry is shown in the first row, results of deformation experiments in the following rows. **(a)** Absence of fracture growth during deformation leads to elliptical veins with strong ductile deformation at the fracture tips. **(b, c)** Fracture propagation during deformation leads to veins with a lozenge shape similar to those observed in most foliation boudinage structures. The last row (at step 12500) shows the structures at stages where further deformation has accumulated after fracture growth was stopped. With slow fracture propagation, cusps are more pronounced and lozenge geometries more angular. A small black dot is fixed on one node in the grid to show the displacement throughout the progressive deformation in the experiments. See also the simulations in Appendix 1.

be expected to be even greater with an inclined initial fracture parallel to the instantaneous shortening direction of simple shear. In FLAC it is not possible to model this geometry because vein walls can overlap since non-connected elements in the model do not register each other.

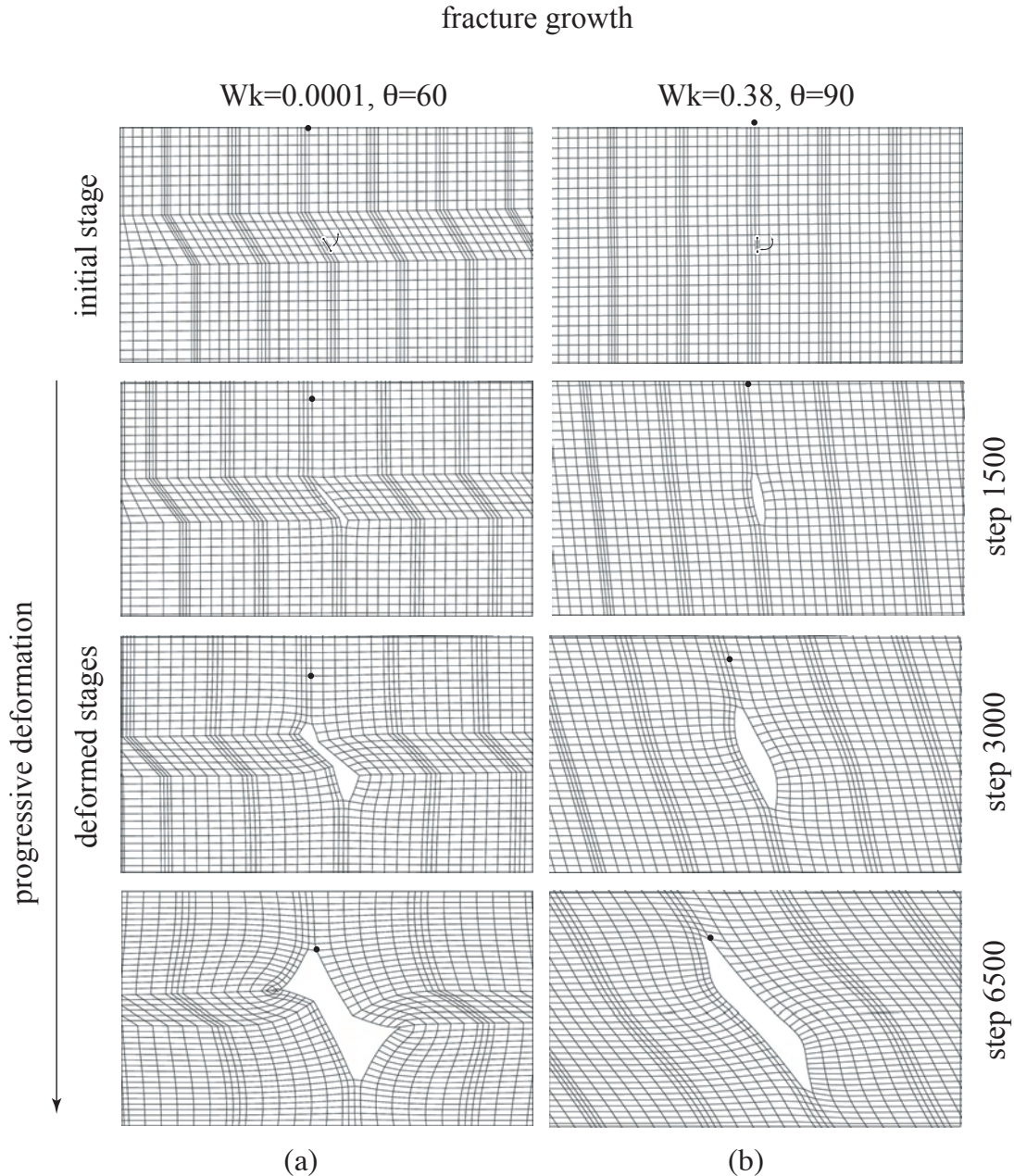


Fig. 1.12. Examples of FLAC experiments performed for asymmetric fracture geometry. The initial stages are shown in the first row. In the lower rows both example have fracture propagation during ductile flow. **(a)** Initial oblique fracture ($\theta = 60^\circ$) deformed in pure shear ($Wk = 0.0001$). **(b)** Initial orthogonal fracture deformed in simple shear ($Wk = 0.38$). Deformed stages in the lower rows show the development of asymmetric FBS, opening of a neck vein and asymmetric necking in the adjacent grid. Flanking structures form due to flow partitioning around fractures and opening veins. The geometry of the internal foliation is similar to that observed in field examples of X-type veins. See also the simulations in Appendix 1.

1.5. Development of foliation boudinage structures (FBSs)

Foliation boudinage structures form by a combination of ductile deformation (indicated by the deflection and folding of foliation in the rock), brittle fracturing and deposition of vein material. The large variety in vein shapes, from disc-shaped veins through massive lozenge-shaped veins containing cubic meters of quartz to fishmouth boudin structures, shows that vein filling from aqueous solution can happen at all stages of the formation process of FBS. We assume from field observations and FLAC experiments that the sequence disc-, lozenge- to fishmouth shapes represent a series of increasing deformation intensity, and that each category represents early stages of arrested deformation and vein deposition. Since quartz filling of boudin veins is rarely deformed or recrystallised, lozenge and fishmouth boudins must form before veins are filled, e.g. when the boudin veins were open, water-filled cavities. Since some of them contain cubic metres of quartz, cavities of this size can apparently open during ductile deformation of gneiss and micaschist at greenschist to amphibolite facies conditions. This may have interesting consequences for volumes of stored fluid and patterns of fluid migration in metamorphic rocks.

Completely closed fishmouth veins, as observed in the Furka area, probably also form by closure of open fluid-filled voids. The fact that these structures are more common in the Furka area than in the Çine Massif can be an effect of the higher ductile strain in the Furka area and the different rock types. Theoretically, closed fishmouth structures could also form by dissolution of material in more open lozenge-shaped veins. However, we did not find any evidence for such a mechanism such as deformation in the veins, stylolites or enrichment of insoluble material on vein edges or in the veins.

The presence of brittle fractures at low to medium metamorphic grade implies that fluid pressure must have been lithostatic. Although the name “foliation boudinage” implies that such structures can only form in foliated rock, e.g. due to its mechanical anisotropy, we find that the best foliation boudins are actually formed in weakly foliated gneiss rather than in strongly foliated micaschist or mylonite. Apparently, fluid pressure is more critical than fabric strength, although the fabric may play a role in determining the orientation of fractures. Therefore, the name “foliation boudin” is actually misleading.

1.5.1. Development of the main types of FBSs

Under pure shear condition layer normal shortening and foliation-parallel extension can cause the development of Mode I fractures if fluid pressure in the rock is high (Figs. 1.13 and 1.14). During further progressive deformation, the fractures can open and develop a lens or lozenge shape. If associated minor faults occur along the foliation planes, triangular veins can form in pure shear (Figs. 1.8e, f; 1.13 and 1.14). FLAC experiments indicate that lens shaped veins form in the case of non propagating fractures, while lozenge shaped ones form when Mode I fractures propagate. The reason is probably that propagating Mode I fractures cause the tip sections of the fracture walls to rotate outwards passively, remaining relatively straight and concentrating most ductile deformation in cusps in the centre of the fracture walls. If a fracture does not propagate, the walls deform more uniformly. This model seems to be supported by the observation that lens-shaped fractures in FBSs are narrow and have only been observed if FBSs are weakly developed. Wide-lens shaped veins do form in necks of boudinaged layers in other areas, but this may be due to lack of propagation of fractures beyond the affected layer.

Rotation of fracture walls leads to development of flanking structures around veins; since the fracture walls are bound by fluid on one side, they must be planes of zero shear stress, and can only support shortening or extension in that direction. In the far field, this does not apply and the resulting difference in the orientation of the stress field will lead to development of flanking folds in foliation boudins (Fig. 1.14).

Several types of symmetric and more or less closed lozenge-shaped FBSs can form depending on when vein filling occurs. If no vein filling occurs, closed fishmouth shapes form. Lozenge-shaped FBS veins only form in pure shear if both limbs of the former fracture bend outwards (Fig. 1.14). Crescent-type veins are interesting because they have two vein walls that curve in the same direction. They probably form if fractures are initially not straight, for example because the rock is inhomogeneous or because fracturing does not occur in tension, but in shear due to relatively high differential stress (Mode II fractures). If an initial fracture is curved, both fracture walls may curve out in the direction of the initial bend in the fracture. An alternative is that an initial Mode I fracture is folded into an open crescent shape before it starts opening. Theoretically, one would expect that such curved fractures could lead to triangular, arrow shaped veins like half lozenge shaped veins, with only one cusp (Fig. 1.13). In fact, the triangular veins that we found have other geometries and do not seem to form in this way (Fig. 1.14). Instead,

crescent-shaped veins form that have the smooth geometry of disc-shaped veins. The reason may be that if fracture walls bend out in two directions, the separating walls cause enhanced tension in the fracture tip and outward fracture propagation; if both walls curve in the same direction, such tension is less pronounced and fractures may not propagate outward at all, forming smooth curving veins instead (Fig. 1.13).

If a fracture forms in non-coaxial flow, it will rotate with progressive deformation and a slip component will develop along the open fracture; this will lead to asymmetric outward bulging on both sides of the fracture, and ultimately to X-shaped veins if the fracture continues to propagate (Fig. 1.14). Possibly, X-shaped veins can also form if the rock is heterogeneous and initial cusps do not develop opposite (Figs. 1.13, 1.14). If lozenge-shaped veins develop in non-coaxial flow, different types of flanking folds will develop on both sides, and asymmetric lozenge-shaped veins or asymmetric fishmouth FBSs can form. Double crescent veins may form as a special type of X-veins where the fault tips do not propagate; alternatively, they could form in coaxial flow if a fracture has originally a double curvature, or if it is folded into two opposite-facing folds before it starts opening.

Summarising, Fig. 1.13 shows the types of veins that could theoretically form out of straight or curved veins in pure shear and non-coaxial flow. Those in grey circles are the ones that we actually observed, while oval and arrow veins may not develop in natural FBSs for reasons given above. Fig. 1.14 shows the envisioned models for development of each of the observed types of FBSs.

1.5.2. Development of other varieties of structures in the Selimiye shear zone

Some types of mostly triangular FBSs are only found in the metasediments of the Çine Massif in the Selimiye shear zone and are not observed at all in the orthogneisses with coarser fabric. We suggest that they are restricted to micaschists in the shear zone and that strong anisotropy planes defined by micas, which provide easy slip planes, play an important role in their development (Fig. 1.14). After the development of a set of fractures at high fluid pressures in the shear zone, the stress field around the fractures changes. Combination of slip along the fractures and rotation leads to opening of the neck veins and development of various flanking structures around them (Fig. 1.14).

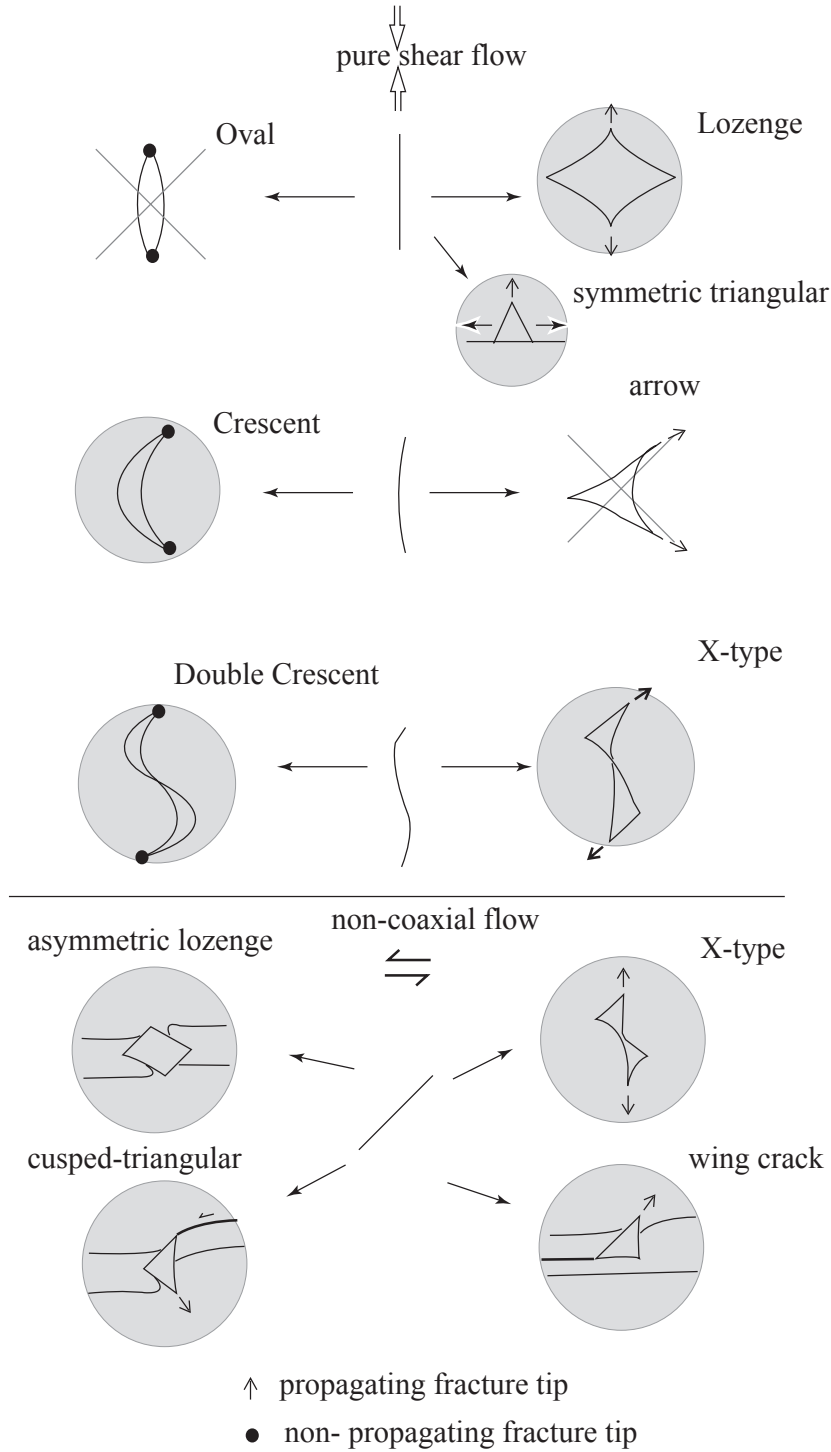


Fig. 1.13. Schematic presentation of the types of veins that can develop in FBSs depending on shape of the initial fracture, fracture propagation and bulk flow. Straight fractures will tend to propagate and form lozenge-, triangular- or X-type veins, while curved ones may fold and deform into crescent type veins. Shapes in grey circles occur in nature. Crossed out shapes have not been observed. See text for further explanation.

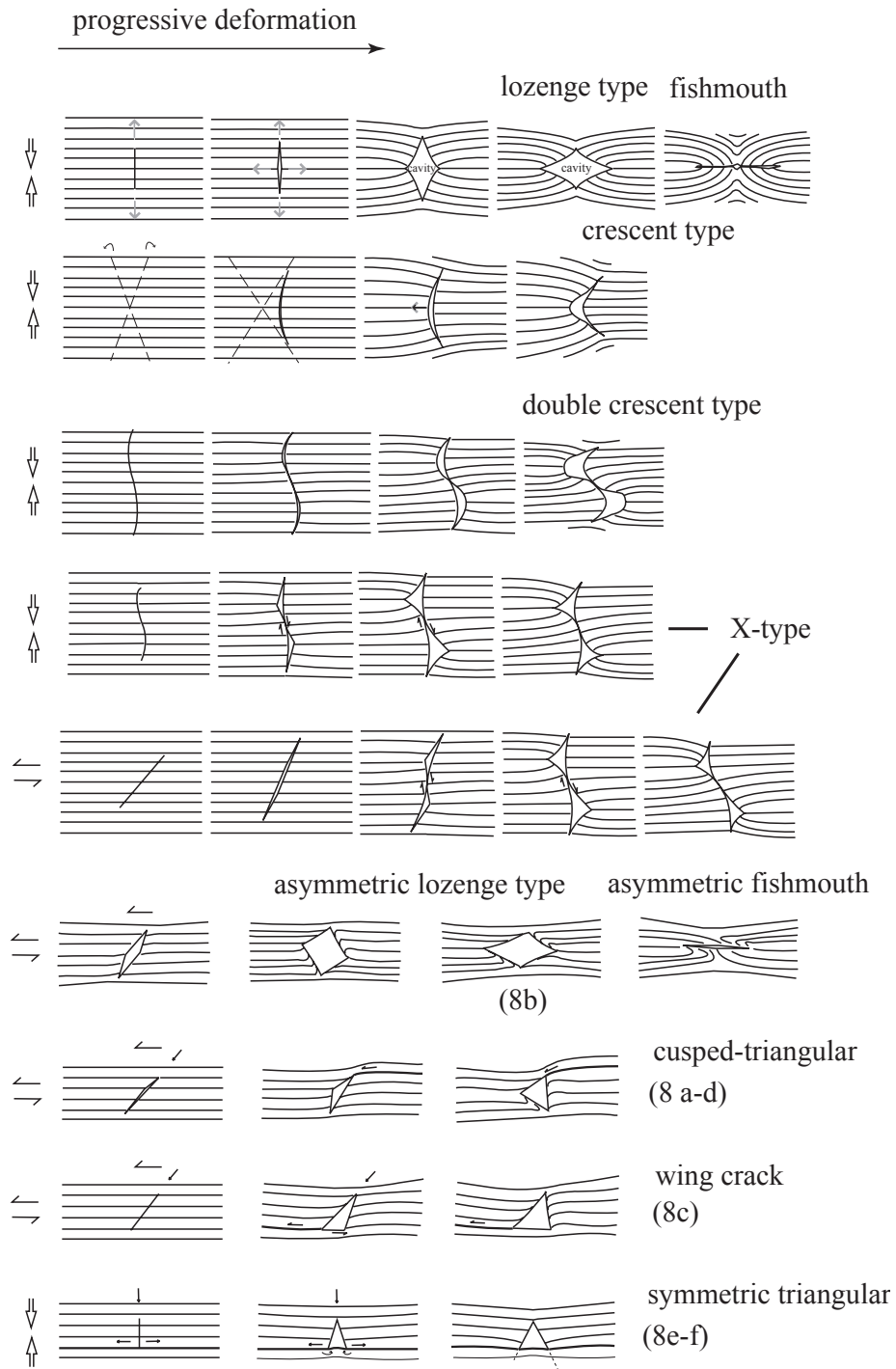


Fig. 1.14. Inferred development mechanisms of observed FBSs. Different vein geometries can form depending on flow type, fracture propagation, fracture rotation or folding, and combinations of these. See text for further explanation.

1.6. Conclusions

From our observations of natural examples in the studied areas four main types of foliation boudinage structures can be distinguished; lozenge-, crescent-, double-crescent- and X-type. All these types occur as open, vein filled structures but also show transition to a fishmouth geometry.

Foliation boudinage structures form by ductile deformation adjacent to brittle fractures and open fluid filled cavities in metamorphic rocks. Fluid pressure in the rock must be high in order to form foliation boudinage, and seems to be a more important factor to determine whether foliation boudinage will form than the actual presence of a strong planar anisotropy. As such, the term foliation boudinage may be misleading.

The geometry of foliation boudinage structures depends on the shape of the central vein and deflection of foliation close to this vein into flanking folds. The shape of the boudin neck veins in foliation boudinage depends on the initial orientation and shape of the fracture, the propagation behaviour of the fracture, the geometry of bulk flow, and the stage at which mineral filling takes place. FLAC experiments show that fracture propagation during ductile deformation strongly influences the geometry of developing veins. The cusps of the veins are better developed and more pronounced in the case of propagating fractures.

The geometry of deflected foliation in flanking folds is directly related to the shape of the veins, since the deflection is due to the fact that the veins are originally open fluid-filled cavities; as a result, principal stress axes must be parallel and orthogonal to vein walls and this defines the geometry of ductile flow close to the veins. Flanking folds will therefore develop during further progressive ductile deformation due to the difference in orientation of the stress field close to open veins and in the far field. The four main types of foliation boudinage described in this paper can be explained by an interplay of these factors. Complete collapse of non-mineral filled open cavities formed by foliation boudinage allows the formation of closed fishmouth structures.

Acknowledgements

Constructive reviews by Ben Goscombe and Paul F. Williams are gratefully acknowledged. We thank Talip Güngör and Hermann Lebit for their help and company in the study areas. This project was funded by the DFG-Graduiertenkolleg "Composition and Evolution of Crust and Mantle".

Chapter 2

Numerical modeling of foliation boudinage

Abstract

We used a two dimensional discrete element model to study the initiation and evolution of foliation boudinage structures and the behavior of anisotropic visco-elastic material deformed under pure shear conditions. We performed a number of simulations with different initial configurations to investigate the effects of material properties and anisotropy on the developing structures. The anisotropies are set by defining rheological heterogeneities in the models with single layer, multilayer with different elastic properties and a random distribution of “micas”, rows of horizontally aligned elements with the same elastic properties. The models show the development of boudinage in single layers, multilayers and in anisotropic materials with random mica distribution. We are specifically interested in the transition from layer boudinage to foliation boudinage. Pure shear deformation leads to complicated structures in the anisotropic random mica model. The types of structures that developed in the models are strongly influenced by changes in material properties. Strain localization is stronger in models with lower elastic constants and anisotropy. Asymmetric and complex geometries develop in models with higher elastic constants and anisotropy. During progressive deformation fractures of mode I, mode II and the combination of both were observed. Failure may occur at any time during progressive deformation depending on material properties. Slip along fractures and rotation together with flow and rotation of the foliation localize strain around developing dilation sites. Voids localize along extension fractures, at intersections of conjugate shear fractures and in small pull-apart structures along shear fractures. These voids or veins look identical to boudin necks and can also produce the typical spacing that leads to the actual “boudin” structure in layered rocks. The model produces structures very similar to the natural examples observed in studied field areas in Turkey and Switzerland.

2.1. Introduction

In nature many materials from micro to macro scale are anisotropic, i.e. a material property is not of equal magnitude in all directions. Rocks may be mechanically anisotropic due to shape and/or crystallographic preferred orientation of minerals or compositional layering that has different mechanical properties. Nature and degree of mechanical anisotropy of rocks from layering to strong shape fabric influence the rheological properties of such rocks and play an important role on the developing structures (Cobbold et al., 1971; Gottschalk et al., 1990; Ranalli and Yin, 1990; Shea and Kronenberg, 1992, 1993; Twiss and Moores, 1992; Weijermars, 1992; Cosgrove, 1997; Mandal et al., 2000; Ramsay and Lisle, 2000; Treagus, 2003; Fletcher, 2005; Passchier et al., 2005; Passchier and Trouw, 2005). Depending on the scale of observation anisotropic rocks can be considered statistically homogeneous when the anisotropy is penetrative and uniform within the rock.

Boudinage involves processes of fracturing and ductile deformation of a rock segment/mass subjected to higher strains than their surroundings. Boudinaged segments may be separated by discrete surfaces or by veins involving dilation of fractures, dissolution and precipitation of vein material. Boudinage structures are common in all scales in nature with various geometries in various lithologies and tectono-metamorphic conditions. They have been studied since they are important to understand rock deformation, rheology and strain localization and classified in different aspects such as boudin block geometry, material layeredness and boudin train obliquity (Goscombe et al., 2004 and references there in). Boudinage of layers is relatively well understood. However, formation of boudinage structures in homogeneous anisotropic rocks is still not fully understood.

Boudinage of layers (Fig. 2.1a) is thought to result from differences in rheology between a relatively stiff layer and a viscous matrix, where the stiff layer ruptures or necks normal to the extension direction in the rock (e.g. Ramberg, 1955; Strömgård, 1973; Lloyd and Ferguson, 1981; Lloyd et al., 1982; Ramsay and Huber, 1983, Ramsay and Lisle, 2000; Passchier and Druguet, 2002; Treagus and Lan, 2004; Koehn, in press; Koehn and Sachau, in press). The process is explained by stress transfer from the matrix to the layer and successive ‘mid-point’ fracturing (Lloyd et al., 1982). Layer normal compression induces flow of the matrix parallel to the layer, which builds up tensile stresses at the interface. When tensile stresses exceed the fracture strength of the stiff layer it fractures and boudins form. The geometry of boudins may be

modified by post-fracture ductile deformation into barrel or fishmouth shapes. It is suggested that successive fracturing will be influenced by material properties and pre-existing flaws and will continue until the boudins reach a critical length.

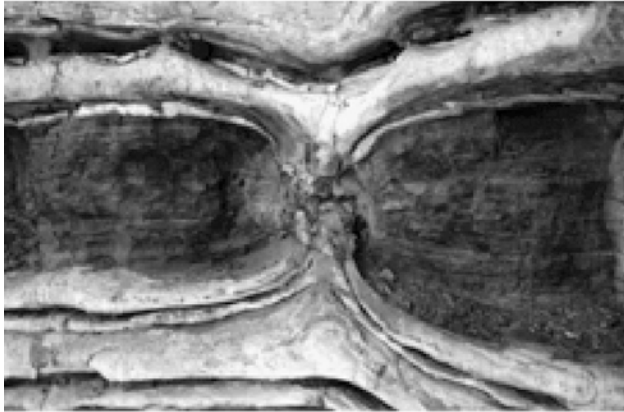
Multilayer boudinage (Figs. 2.1b and c) occurs in alternate layers of different competence (Strömgård, 1973; Mandal and Karmakar, 1989; Kidan and Cosgrove, 1996; Gosh and Sengupta, 1999; Mandal et al., 2000).

Foliation boudinage (Fig. 2.1d) forms in foliated rocks that are statistically homogeneous and do not involve layering (Hambrey and Milnes, 1975; Platt and Vissers, 1980; Lacassin, 1988; Swanson, 1992; Aerden, 1991; Druguet and Carreras, 2006).

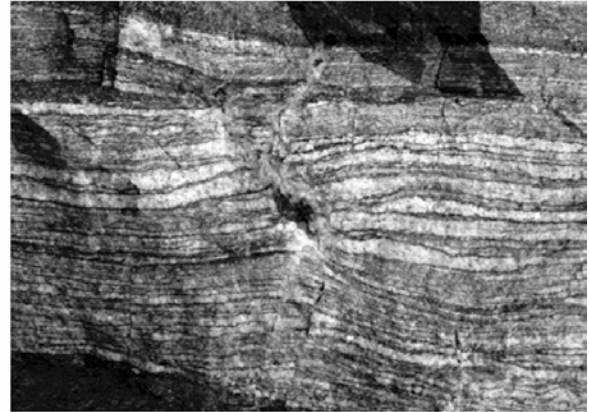
Transitions exist from single layer, multilayer to shape fabrics representing different degrees of anisotropy. The degree of anisotropy from multilayers to shape fabrics have been described by an anisotropy factor, the ratio between the viscosity under normal stress and the viscosity under shear stress (Cobbold, 1976; Honda, 1986; Weijermars, 1992; Mandal et al., 2000; Treagus, 2003). Weijermars (1992) suggested that this ratio expresses a measure for the potential misfit in the orientation of the principal axes of the bulk stress and strain-rate ellipsoid. He has shown that the resistance to normal compression is largely determined by the competent layers whereas resistance to shear is controlled by the soft layers.

In this paper we investigate boudinage of materials with different degrees of anisotropy. Numerical experiments were performed for layer, multilayer and foliation boudinage. The numerical model allows to study initiation and evolution of boudinage structures. We study visco-elastic deformation of materials with different anisotropy and the effect of material properties (e.g. Young's modulus, viscosity and breaking strength) on the developing structures. Further we discuss the role of anisotropy on the development of foliation boudinage structures.

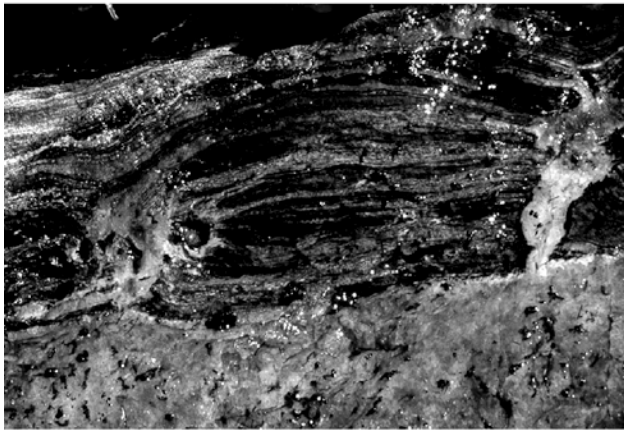
a) single-layer boudinage



b) multilayer boudinage with sublayers



c) multilayer boudinage



d) foliation boudinage



Figure 2.1. Natural boudinage structures in rocks with different degree of anisotropy. Boudinage of **(a)** a competent layer in a less competent host, Ugab River, Namibia, **(b)** multilayers with a pack of sub-layers, Sustenpass, Swiss Alps, **(c)** regularly alternating multilayers, Rwenzori Mountains, Uganda, **(d)** a foliated rock where anisotropy is defined by preferred orientation of micas, the Çine massif, SW Turkey.

2.2. The numerical model

The numerical model is based on a two-dimensional discrete element code (Koehn and Arnold, 2005; Koehn et al., 2006; Bons et al., in press). Discrete elements are defined by particles that are connected by a triangular network of visco-elastic springs. Spring constants of particles and breaking strength of springs are randomly distributed. This is defined by giving a mean value for the parameters and a distribution size to apply a statistical distribution around the mean value. Particles fill an area called a deformation box that has an initial width of 1.0 unit-length in the x- and y- direction. A triangular network is build by connecting particles that are shifted by a radius

in each second row in the x-direction. The radius of particles is scaled automatically in the program. Simulations presented here have resolutions of 50x57 –, 100x115 – and 200x230 – particles in x - and y - directions respectively.

A layer in the models is defined between maximum and minimum y-coordinates in the middle of the deformation box parallel to the x-direction and filled with stiffer particles than the surrounding matrix (Fig. 2.2a). In all models white and light gray particles are hard, dark colored particles are weak. Multilayers are set by alternation of even horizontal layers with different material properties (Fig. 2.2b). Young's modulus, viscosity, breaking strength and thickness of the layers are predefined in the models. Multilayers may be inhomogeneously distributed forming a pack of sub-layers (Fig. 2.2b) or alternate regularly. The layer number in the model is determined by dividing the y-size of the box with the sum of the thicknesses of two layers. If two neighbour particles have different constants, for example at a layer contact, an average of the two values is calculated. This becomes important when a layer has a thickness that is equal to the particle size. In a random-mica model the anisotropy in materials is set by a random distribution of “micas”, rows of horizontally aligned elements with the same elastic properties (Fig. 2.2c). An initial anisotropy is set by a function that redistributes the original values in the models. Initial set of material properties is also shifted by a function that changes elastic constant, viscosity and breaking strength of all particles in all models.

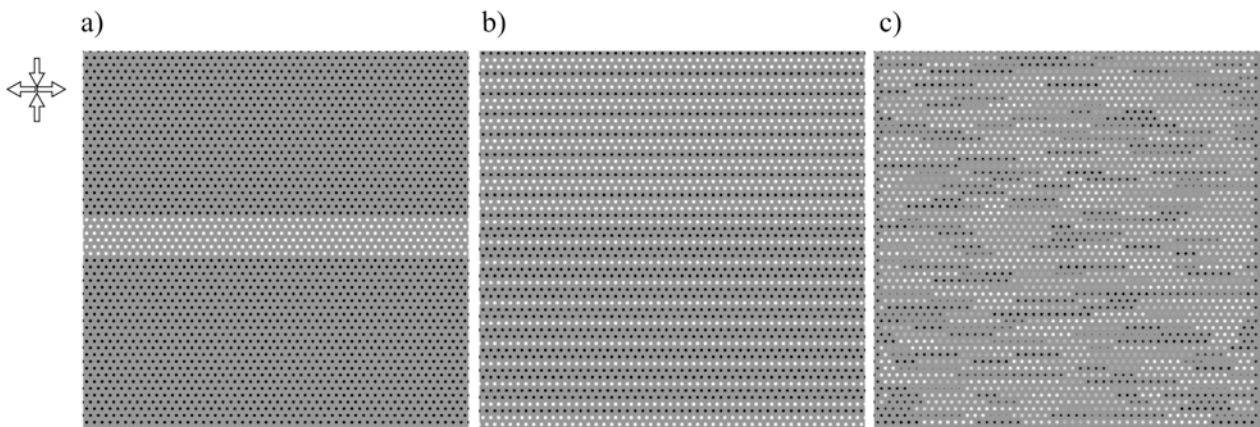


Figure 2.2. Initial configurations of the models with (a) a layer (b) multilayers, in this example they may form sublayers in which one of the lithologies dominates, and (c) randomly distributed micas. Pure shear deformation is applied with a layer normal compression and parallel extension. White particles are stiffer, dark particles are weak.

Particles that are fixed perpendicular to the boundary of the deformation box are defined as wall-particles and are moved parallel to the boundaries inwards or outwards to stress the system. In all simulations we applied pure shear deformation with layer normal compression and layer parallel extension. The lattice is strained at a constant rate with area conservation. When the upper boundary particles are pushed inwards, the movement in the x-direction is calculated for each deformation step in the program. After each deformation step a relaxation process starts in which particles in the model are moved in response to applied forces from the neighbour particles to find an equilibrium in the lattice. The force acting on the particle is determined by multiplying a spring constant by strain that is the difference between the spring length and the equilibrium length. The program repeats this relaxation process until each particle in the system is relaxed, i.e. they are not moving anymore, and then checks and calculates if critical tensile stress are reached for any spring to break. Springs will break once the local breaking strength is reached and will be removed from the system. The particles, which were connected with that spring, will still have repulsive forces. The relaxation routine will start again and continue until no more spring breaks before a new deformation step. After each change, stress is calculated again and updated in the system. Then viscous step starts with a Maxwell relaxation.

The model parameters are set as follows: The upper boundary is moved in the y-direction with a strain of 0.001 per deformation step and the time step for the viscous relaxation is set to 10^9 s. The strain rate is 10^{-12} s⁻¹. In the model the unscaled mean value of initial elastic constants is 1.0 and the breaking strength is 0.006. An initial elastic constant of 1.0 in the models refers to 10 GPa. Stresses and tensile strength of springs are scaled with the elastic constant. In the models the springs have a distribution of breaking strengths with a mean of 0.5 and a deviation of 1.2. In the scaled model these values will correspond to a distribution of breaking strengths of springs from 25 MPa to 100 MPa. But the real breaking strength of the aggregate is much lower, which is about 5 MPa, due to the distributions in the model. These values give initial model settings for all the following simulations unless stated otherwise.

Initial distributions of parameters in the model are additionally shifted by given factors in different simulations to investigate how a change in Young's Modulus, viscosity and breaking strength of particles influence behavior of the model.

2.3. Results

In the following the first examples illustrate progressive development of boudinage in single layers, multilayers and in anisotropic materials. The models show the initiation of different types of fractures and localization of flow around these discontinuities. Pure shear deformation of a material and anisotropy may lead to development of quite complicated structures. Further examples are given to discuss the effect of material properties; Young's modulus, viscosity and breaking strength on the developing structures.

2.3.1. Layer boudinage

Fig. 2.3 illustrates progressive development of single-layer boudinage and viscoelastic deformation of a layer. The initial configuration of the model is shown in Fig. 2.2a. Constants of the particles of the matrix are fixed to the initial set values. The particles in the layer have 10 times higher Young's modulus and viscosity than the particles of the surrounding matrix. Additionally the initial set values of Young's Modulus, viscosity and breaking strength of all particles in the model are shifted by factors of 0.1, 1×10^8 and 1.0 respectively.

All stresses are zero at the beginning, i.e. the lattice is in a relaxed state. Once deformation is applied stresses start to build up in the model. Tensile stresses are concentrated in the hard layer and shortening is mostly taken by the surrounding soft matrix. Figs. 2.3a and b show the fracture plots after 5 and 50 deformation steps. Several distinct fractures (dark particles) form within the layer and small mode I fractures at the boundary between the layer and matrix (Fig. 2.3a). Once the fractures form, stresses are relaxed around them except at the tip regions. Fractures propagate and conjugate sets develop in the following stages and localize within the hard layer (Fig. 2.3b). The layer segments are displaced (Fig. 2.3c) and start necking during subsequent viscous deformation since ductile flow is concentrated in the vicinity of these discrete structures and shear stresses are still strong between the layer and matrix boundary (Figs. 2.3c-f). Flanking structures and boudin gaps are well developed after stage 300. Further stretching of the layer leads to elongation, thinning and tapering of the boudins. Voids at boudin necks may be closed due to strong deflection of boudin edges and infolding of the fracture face. After stage 400 the model is shortened 58 % in the y-direction.

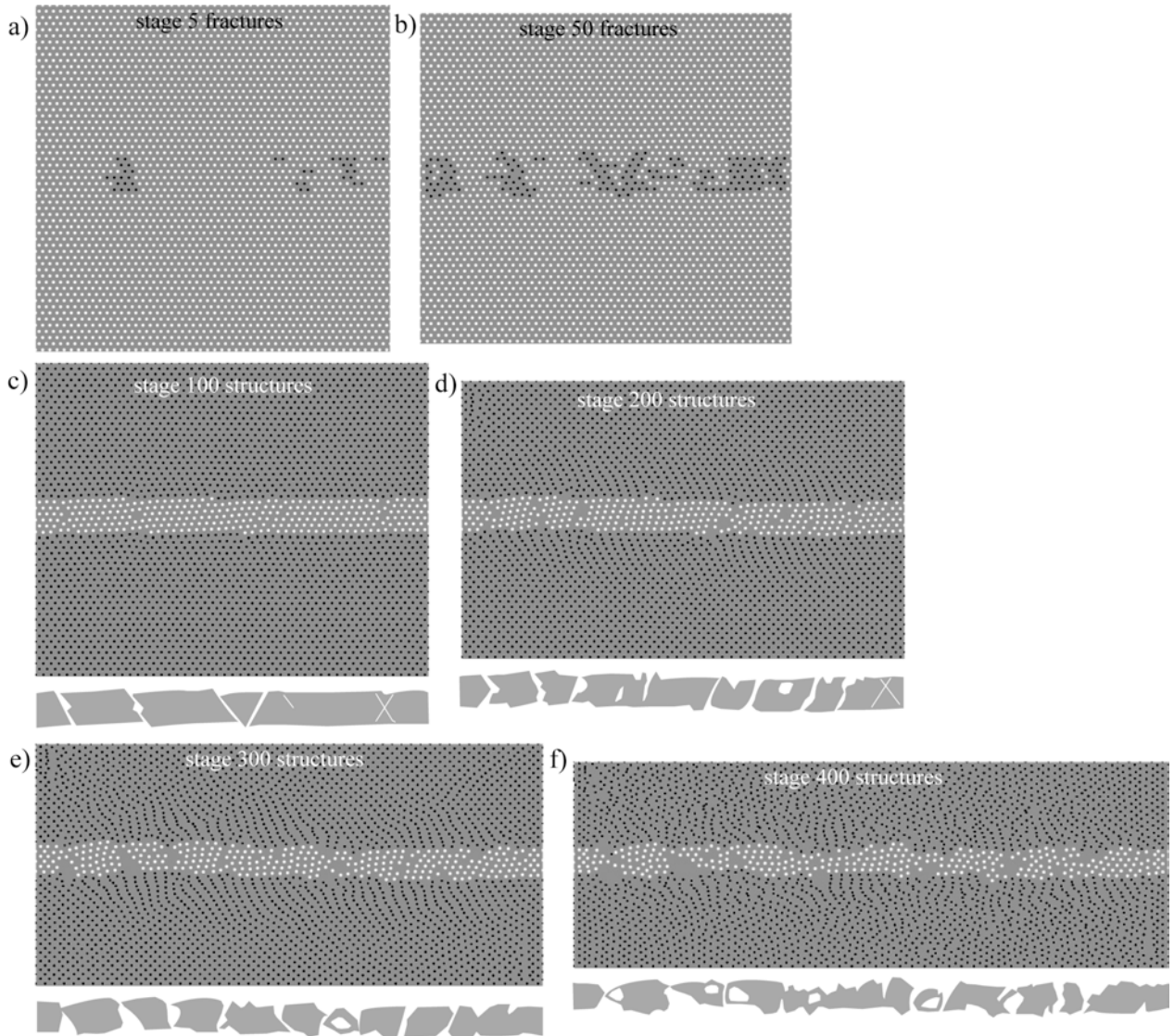
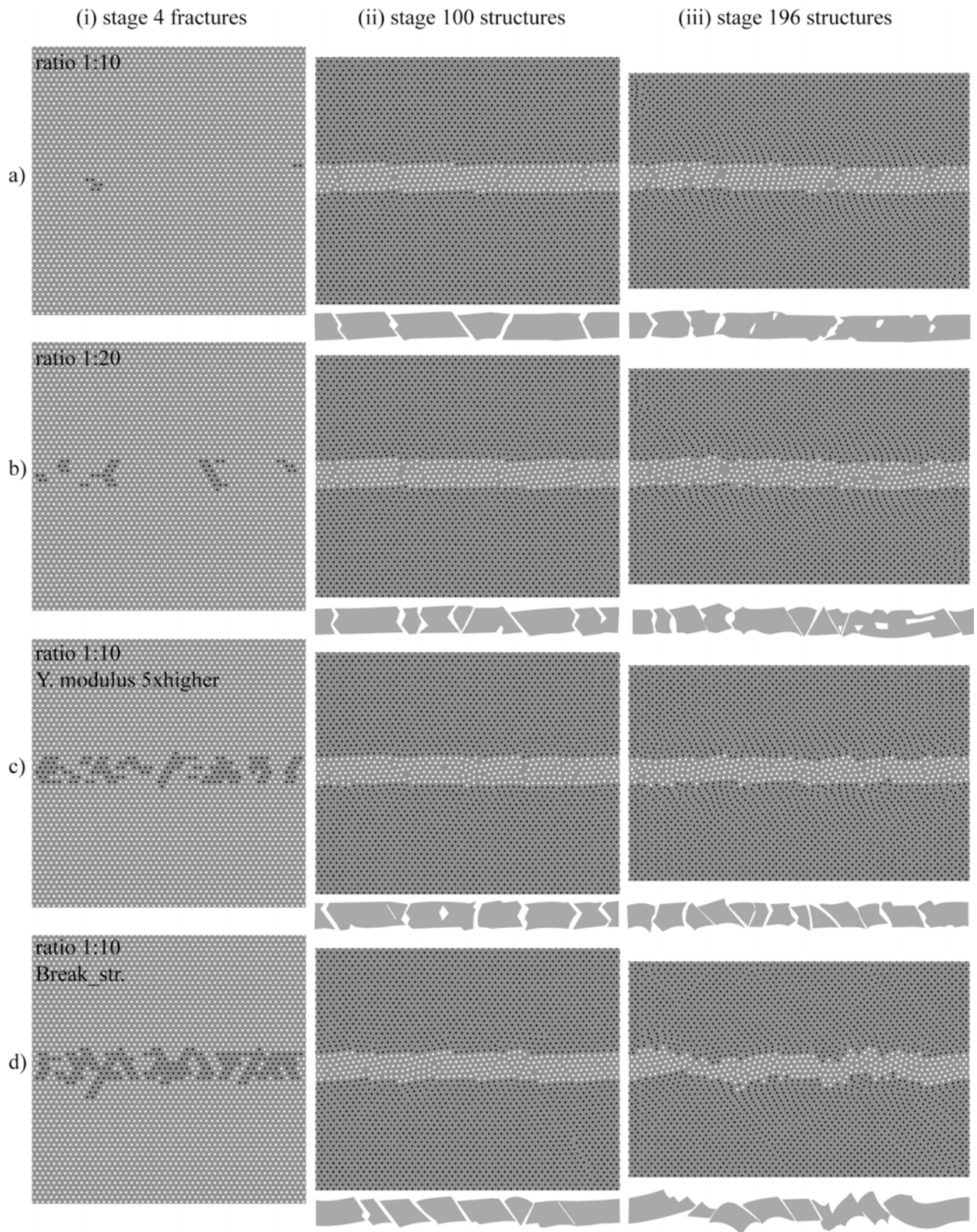


Figure 2.3. Simulation shows progressive development of layer boudinage. The initial lattice has a resolution of 50-particles in the x-direction. A layer has 10 times higher Young's modulus and viscosity than the matrix. The initial stage of the simulation is shown in Fig. 2a. **(a)** First fractures (dark particles) develop in the competent layer and some at the layer–matrix interface. **(b)** Fractures localize in the layer and some form conjugate pairs. The layer is segmented into several blocks by oblique fractures at early stages of boudinage. **(c)** Flow of the weaker matrix leads to displacement, rotation and separation of boudin blocks along the fractures. Simplified sketches of boudins in layers are given below. **(d)** Boudins that become more visible are separated by veins at stage 200. **(e)** Barrel shape boudins and fishmouth structures form with well developed spacing. **(f)** Further stretching, deflection, elongation, thinning and tapering of the boudins. Strong deformation leads to closure of some neck veins. *See movie on CD-ROM attached to the thesis.*

Fig. 2.4 shows four different simulations of layer boudinage with the same initial settings. Some of the material properties in the models are changed to study the influence of different parameters on material behavior and developing structures. The simulation in Fig. 2.4a has the same initial settings than the simulation in Fig. 2.3. For each simulation three stages at the same amount of strain are shown. The Young's modulus and viscosity of the particles in the central layer in Figs. 2.4a, c, d are 10 times higher than the matrix and in Fig. 2.4b 20 times higher, i.e. the competence contrast is higher. Particles in experiment 4c have an average Young's modulus that is 5 times higher than the other experiments. Breaking strength of springs in experiment 4d is set to be 10 times lower than that of the other experiments.

First column at stage 4 shows the fractures. In the models the intensity of fractures increase from (a) to (d) with an increase in Young's modulus and viscosity of the layer (Fig. 2.4i-b) and the whole model (Fig. 2.4i-c), and a decrease in breaking strength of springs (Fig. 2.4i-d). Fractures form earlier and a material behaves more brittle when the elastic constants of particles are relatively high (Figs. 2.4i-b, c) and the breaking strengths are low (Fig. 2.4i-d). In all models boudins and fracture spacing are well developed. However, spacing is larger in the models with lower elastic constants (Fig. 2.4i-a) and narrow with higher constants (Figs. 2.4i-b, c). Variation in rheological behavior and developing structures are represented on the second and third columns after stages 100 and 196. After stage 196 the shortening in the y-direction is 80%. A range of boudin block geometries similar to torn and domino boudins (Goscombe et al., 2004) develop in the simulations (Figs. 2.4ii, iii, a-d). Boudin blocks are separated by an extensional gap or a discrete surface (Fig. 2.4ii). Strain is accommodated by growth and progressive opening of the fractures into neck veins and by slip along shear fractures. Fractures and layer segments rotate. Compared to Fig. 2.4iii-a, the amount of rotation is higher in the models where competence contrast between the layer and matrix (Fig. 2.4iii-b) and an average Young's Modulus (Fig. 2.4iii-c) are relatively high, and where an average breaking strength is low (Fig. 2.4iii-d). Flow strength of material in Fig. 2.4d is lower than in the other experiments, which leads extreme folding of the layer segments.



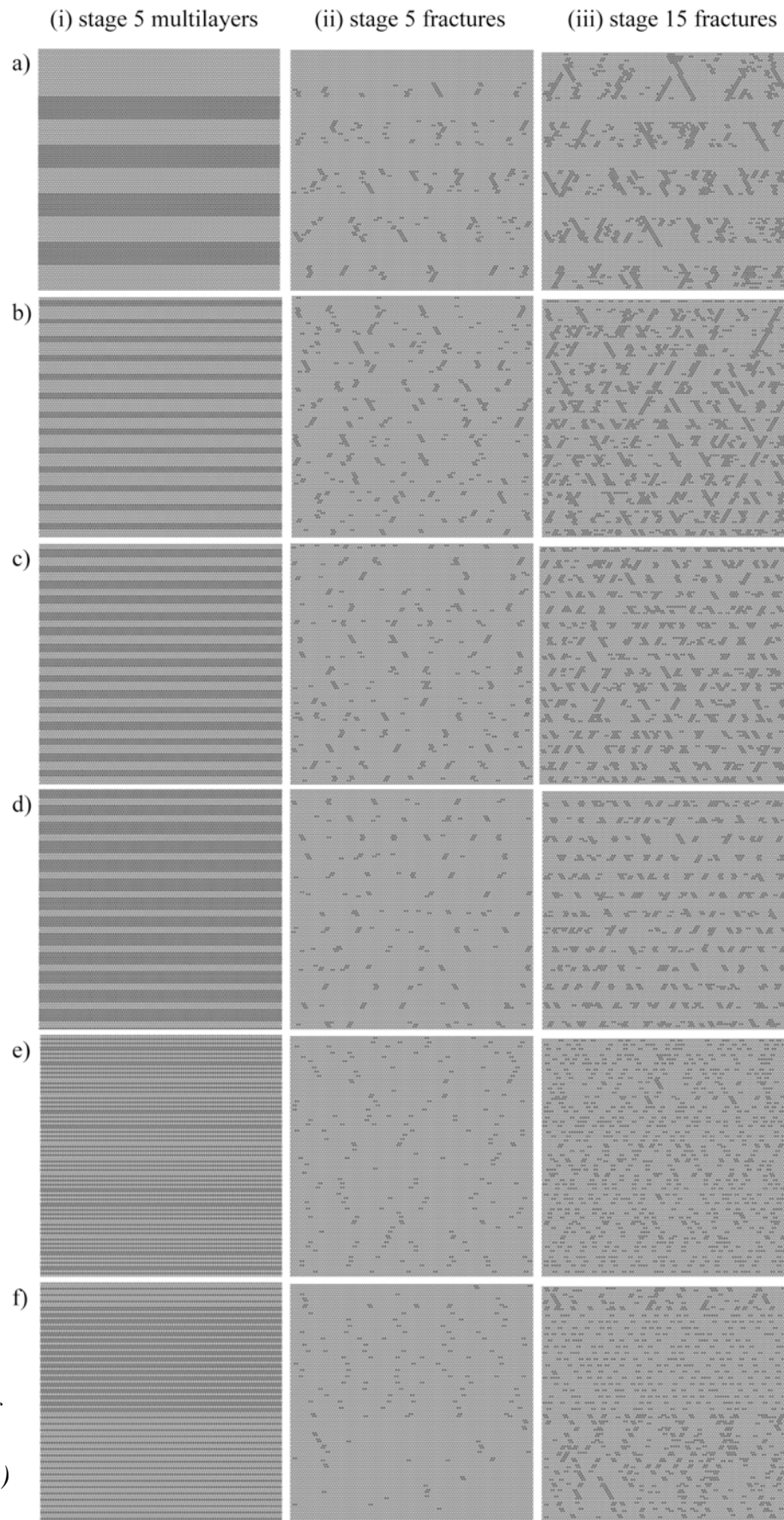
(caption of figure 2.4 on page 43)

2.3.2. Multilayer boudinage

Alternation of hard and soft layers may vary in multilayers (Fig. 2.5). They can alternate regularly (Figs. 2.5i, a-e) or irregularly forming sublayers, a pack of layers in which one of the lithologies dominates (Fig. 2.5i-f). The initial settings of all simulations are the same, only the layer thicknesses and arrangement of layers are modified. In all simulations the hard layers have properties that are fixed to the initial set values. The soft layers have a Young's modulus and viscosity that are 10 times lower than the hard layers. Additionally factors of 0.1, 1×10^8 and 0.1 shift the Young's modulus, viscosity and breaking strength of all particles in the model respectively. The lattice has a resolution of 100-particles in the x- direction. Variations in thickness and different arrangement of alternating layers may play an important role for the behavior of materials during progressive deformation. The fractures are shown after deformation stages 5 and 15 (Figs. 2.5ii-iii).

Figure 2.4. Four simulations with the same initial settings show examples of layer boudinage. Changes of parameters in the models are indicated at the upper left corner of the plots in the first column. Ratio is a competence contrast between a matrix and a layer. The initial lattice has a resolution of 50-particles in the x-direction. **(i)** Fractures at stage 4. Fractures are restricted to the layer but one shear fracture in (d) starts to propagate into the matrix. Number of fractures increase and spacing decreases, from (a) to (d), with an increase in elastic constants (b, c) and a decrease in breaking strength (d) of the material. **(ii)** At early stages of boudinage layers are segmented by fractures. Neck veins and flanking structures start to develop. Simplified sketches of boudins are given below. **(iii)** Different boudin block geometries form. Due to rotation and folding of boudins some veins are closed in (b, c, d). *See movies on CD-ROM attached to the thesis.*

Figure 2.5. Plots in **(i)** show variations in multilayers. The white-gray layers are more competent than the black layers. Layers with different thicknesses alternate regularly and the thickness of the hard layers decrease from (a) to (e). In (f) layers are distributed heterogeneously forming sublayers in which competent layers dominate in the lower sublayer and weak layers in the upper part. **(ii)** Fractures develop first in the competent layers in all simulations. **(iii)** They localize in competent layers but some start propagating into the matrix. In (b) where the weak layers are relatively thin, fractures propagate by jumping over weak layers and develop into shear fractures. In (f) mode I fractures dominate in the relatively weak sublayer and shear fractures in the hard sublayer.



*(caption of
figure 2.5
on page 43)*

The example in Fig. 2.6 shows progressive development of multilayer boudinage. The initial configuration of the model is shown in Fig. 2.2b. The lattice has a resolution of 50-particles in the x- direction. Competence contrast between the hard and soft layers is 10. The hard layers have a Young's modulus and viscosity that are 10 times lower than the initial set values. Therefore the material properties of the whole model become weaker than the main setting. Additionally factors of 0.1, 1×10^8 and 0.1 shift the Young's modulus, viscosity and breaking strength of all particles in the model respectively.

Alternating layers form sublayers. In the lower part of the model soft layers dominate (aligned dark particles) whereas in the upper part hard layers dominate (white particles). Sublayers behave as single layers where the lower sublayer behaves weaker and the upper sublayer behaves stronger. Mode I fractures form first in single hard layers in the lower part (Fig. 2.6a). This is due to higher stresses transferred to hard layers by strong flow of the surrounding matrix. In the following stages mode I and small shear fractures develop in hard layers in the upper part (Fig. 2.6b). Some propagate by jumping over the soft layers and tend to develop into larger shear fractures. In the next stages (Figs. 2.6c and d) conjugate pairs form. Layers are displaced and bent along the fractures like in a flanking shear band (Fig. 2.6d). Shear fractures localize in the upper sublayer where hard layers are dominant (Figs. 2.6c). In later stages they propagate into the soft sublayer (Fig. 2.6e). Voids open at the intersections of fractures (Fig. 2.6e). Flow localizes around the fractures and veins. Layers are folded at the tip of the fractures similar to pinch and swell structures (Fig. 2.6f).

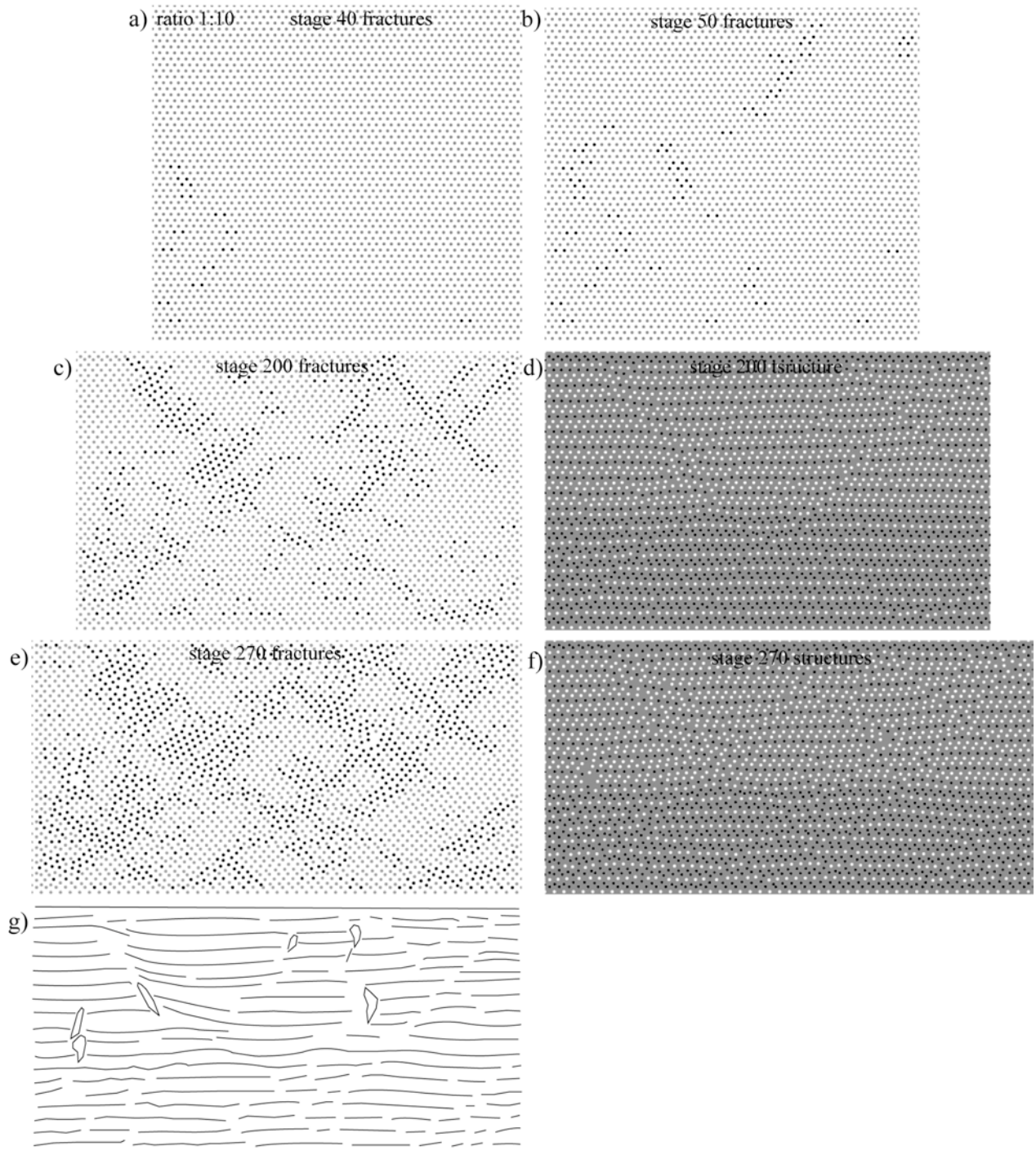
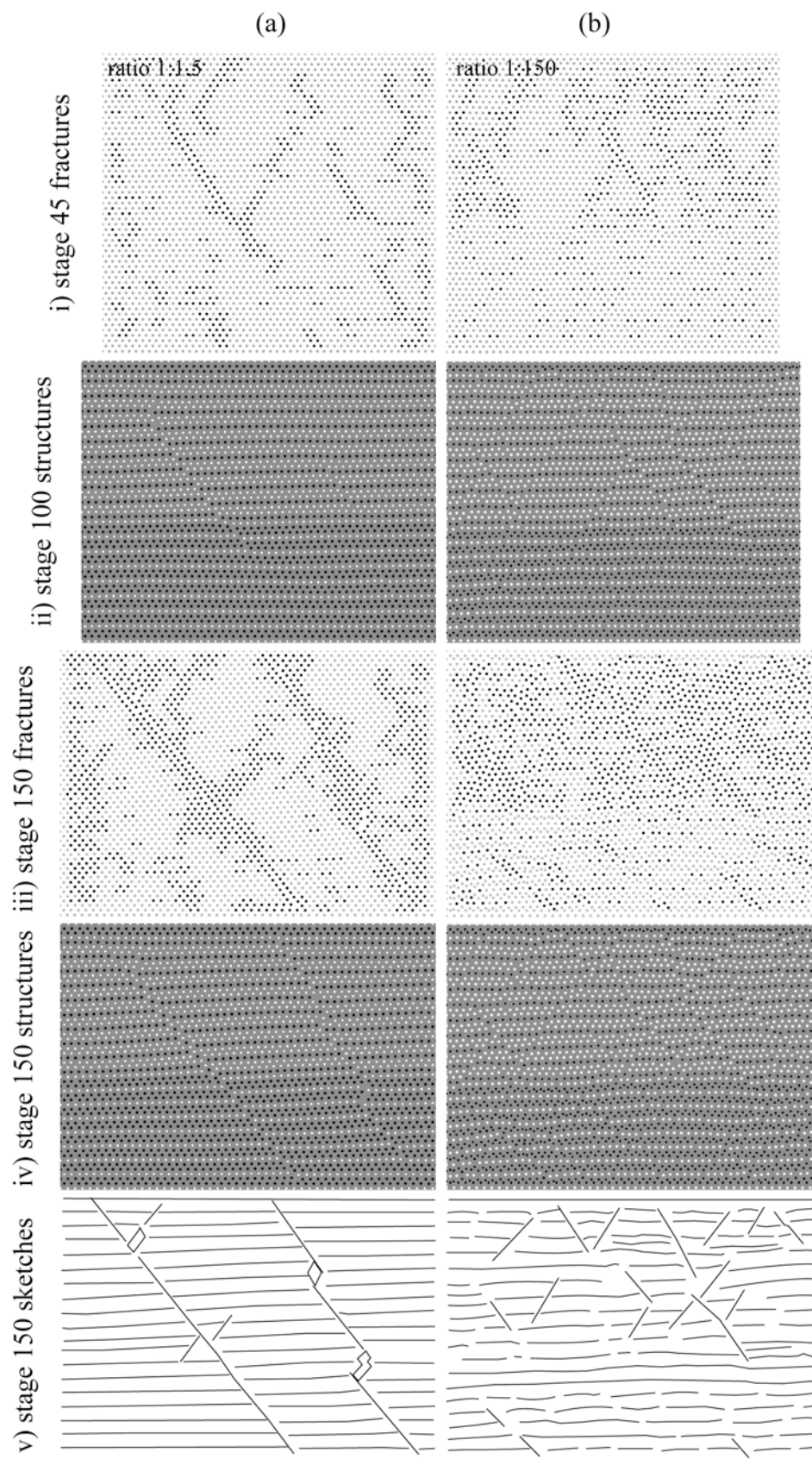


Figure 2.6. Simulation shows progressive development of multilayer boudinage. Alternation of multilayers form sublayers. Competence contrast between the layers is given as a ratio of the soft to hard layers at the upper left corner. **(a)** Mode I fractures develop first in single hard layers in the lower soft sublayer. **(b)** Mode I and small shear fractures develop in hard layers in the upper part. **(c)** Conjugate shear fractures develop and localize in the upper hard sublayer. **(d)** Flanking shear bands form. **(e)** Shear fractures rotate. Voids open at the intersections of fractures in the upper sublayer. **(f)** Shear bands and boudin like structures develop. **(g)** The sketch of the structures in (f). See movie on CD-ROM attached to the thesis.

Two simulations in Fig. 2.7 have the same initial settings but layers in Fig. 2.7a have a higher average Young's modulus and viscosity than the layers in Fig. 2.7b. The hard layers have the same properties in two simulations whereas the soft layers in Fig. 2.7a are 100 times stronger than the soft layers in Fig. 2.7b. The material properties of the soft layers in Fig. 2.7a have the initial model parameters. Competence contrast between the layers in Fig. 2.7a is 1.5 and in Fig. 2.7b 150.

Mode I fractures develop in single hard layers at early stages of deformation in both simulations. Shear fractures initiate later in hard sublayers where the material has higher average Young's modulus and viscosity (Figs. 2.7i-a, b). Size and spacing between shear fractures is larger in Fig. 2.7a. Layers are displaced and bent along the fractures (Figs. 2.7ii-a, b). In later stages of deformation shear fractures propagate through layers and develop into faults in Fig. 2.7iii-a because the competence contrast is relatively low in alternating layers. Strain accommodates more by slip along these large faults. Extensional veins develop at pull-aparts along the stair-stepping shear fractures. However in Fig. 2.7iii-b shear fractures localize within the upper hard sublayer while mode I fractures dominate in the lower soft sublayer where the competence contrast is higher between the layers. In the following stages fractures and layers rotate (Figs. 2.7iv-a, b) while rotation is more rigid in Fig. 2.7a, folding of layers is associated with rotation in Fig. 2.7b.

Figure 2.7. Two simulations with the same initial settings. The competence contrast in (a) is 1.5 and in (b) 150. Competent layers have the same properties in both models but soft layers in (a) are 100 times stronger than those in (b). **(i)** Mode I and shear fractures. **(ii)** Displacement and bending of layers along the shear fractures. **(iii)** (a) Propagation of shear fractures through layers and their development into large faults. Opening of extension veins at pull-aparts along the shear fractures. (b) Localization of shear fractures within the upper hard sublayer and mode I fractures in the lower soft sublayer. Competence contrast is high between the sublayers in (b). **(iv)** Rotation of fractures and layers. In (a) rigid block rotation, in (b) structures similar to pinch and swell, rotation associated with folding of layers. **(v)** Sketches of the last plots. *See movies on CD-ROM attached to the thesis.*



(caption of figure 2.7 on page 47)

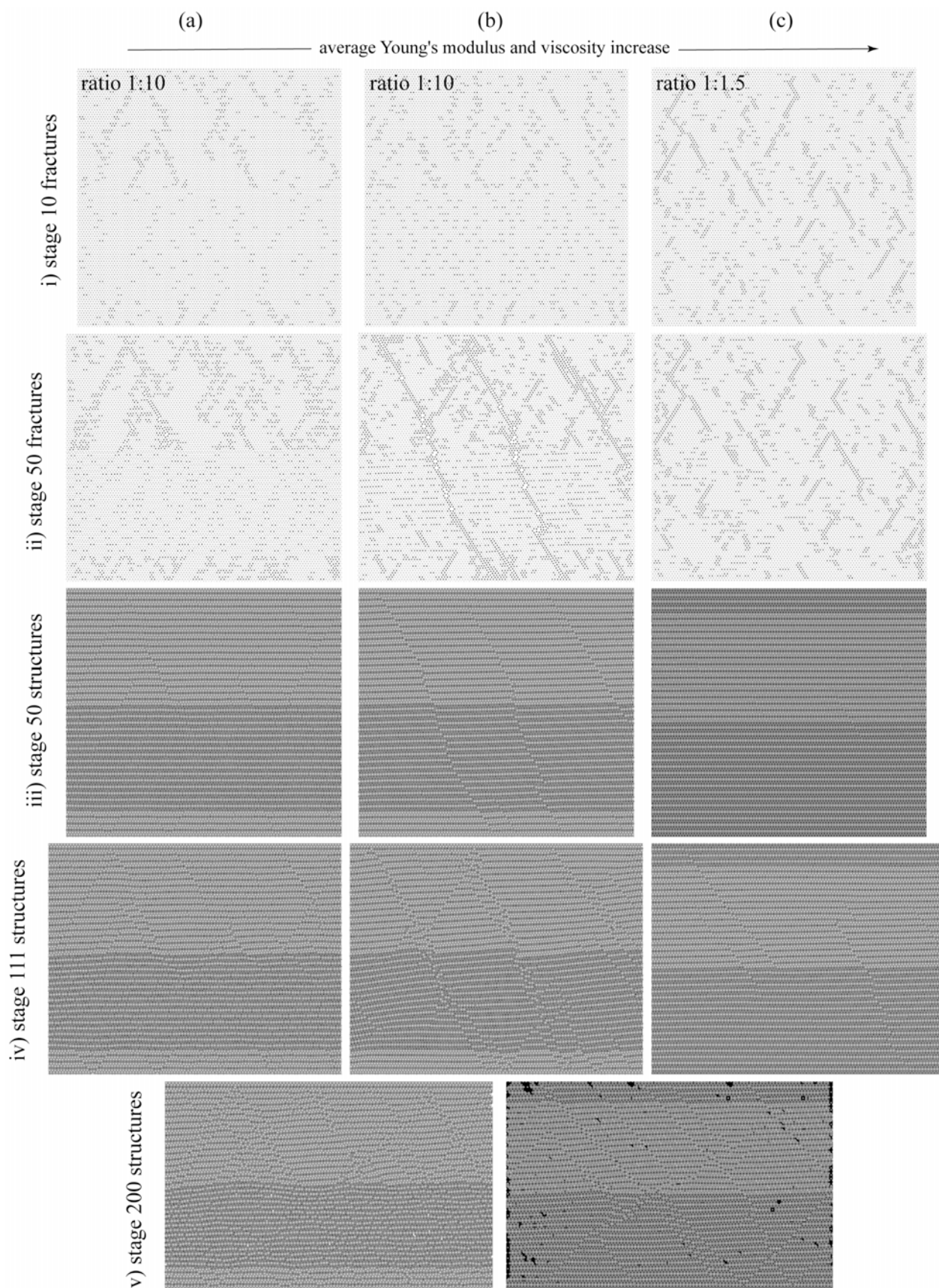
The following examples from Fig. 2.7A to 2.7D show a range of simulations in multilayers with various configurations of alternating layers. The initial lattice has a resolution of 100-particles in the x-direction in all models.

In three simulations in Fig. 2.7A alternating layers form sublayers. The average Young's modulus and viscosity of the layers increase from (a) to (c). The constants of the hard and soft layers are 10 times higher in (b) than in (a), and for the hard layers 15 times and for the soft layers 100 times higher in (c) than in (a). Competence contrast between the layers is 10 in (a, b) and 1.5 in (c). The initial settings of the model in (a) are the same than the simulation in Fig. 2.6 and the settings of the model in (c) identical to those shown in Fig. 2.7a. The first and second row show fracture plots after stages 10 and 50 in the figure 7A. Mode I fractures develop first in single hard layers embedded in the soft sublayers where weak layers dominate (Figs. 2.7A-i). Shear fractures develop in the hard sublayers. Shear fractures cut and propagate through layers in (b) and (c) where average elastic constants of the materials are relatively high and in (c) where competence contrast between the layers is relatively low. Fractures localize and extensional veins form at pull-aparts (Fig. 2.7A-ii). Layers are displaced and rotated along the fractures (Fig. 2.7A-iii). Slip and rotation is larger in Fig. 2.7A-iv,b compared to the other simulations due to large shear fractures or faults. In Fig. 2.7A-iv,a,c interacting smaller fractures prevent such large displacements and rotations. However they show differences in material behavior and structures (Fig. 2.7A-v). In Fig. 2.7A-v,a, block rotation and displacement of layers in the hard sublayer is accommodated by folding of the layers in the soft sublayer. They form structures similar to pinch and swell structures while in Fig. 2.7A-v,c they are rotated as rigid blocks.

Three simulations in Figure 2.7B show other examples of multilayer boudinage where several layers together behave like a single layer. Alternation of the layers is the same in all the models. The average material constants increase and the competence contrast decreases between the individual layers in the models from (a) to (c). The ratio is indicated in the upper left corners of the plots in the first row. The constant of hard layers in all models is fixed to the initial set values. The soft layers are 10000 times weaker than the hard layers in (a), 1000 and 100 times in (b) and (c). Fractures develop and localize in the layers where hard layers dominate in alternation (Fig. 2.7B-i). Fracture spacing decrease from (a) to (c). Boudins develop and rotate along the fractures. Mode I and shear fractures dilate and form neck veins (Fig. 2.7B-ii). Second order boudins develop by fracturing of the early boudins (Fig. 2.7B-iii). Displacement, dilation and rotation of boudins is larger in (a) where competence contrast is higher than in (b) and (c).

Fig. 2.7C shows three examples where layers alternate more regularly but still with some heterogeneity in distribution and thicknesses of alternating layers. The average Young's modulus and viscosity increase and the competence contrast decreases between individual layers from (a) to (c). The hard layers have the same initial constants. The soft layers in (a, b, c) are 1000, 100 and 10 times weaker than the hard layers. Fractures develop and propagate through the layers (Fig. 2.7C-i). Conjugate pairs and pull-aparts form. Size of fractures is smaller and similar in size in the models with a lower Young's modulus and viscosity (Fig. 2.7C-i, a). Size of fractures gets larger and more heterogeneous in the models with higher Young's modulus and viscosity (Figs. 2.7C-i, b, c). Fractures are more localized in the models where the elastic constants are low and the competence contrast is high between the layers (Fig. 2.7C-i, a) while they propagate through layers where the constants are high and the competence contrast is relatively low (Fig. 2.7C-i, c). In early stages of boudinage, layers are displaced along the fractures and flanking structures start to develop (Fig. 2.7C-ii). They fold and rotate in later stages (Fig. 2.7C-iii, iv).

Figure 2.7A. Three simulations showing developing structures during progressive deformation of multilayers. The average constants of the layers in the models increase from (a) to (c). Competence contrast between the soft and hard layers is indicated as a ratio on the upper left corner of the plots in the first row. **(i)** Mode I fractures develop in single hard layers in the soft sublayer while shear fractures develop in the hard sublayer in the models. Shear fractures are scattered in (c) where competence contrast between the layers is low and average constants are high. **(ii)** Mode I fractures localize in the soft sublayers and shear fractures in the hard sublayer in (a) that has lower average material constants compared to the other simulations. Shear fractures propagate and cut through the soft sublayer in (b). Extensional veins form at pull-aparts along the en-echelon shear fractures. Fracture propagation is slower in (c) where the material on average is stronger compared to the others. **(iii)** Layers are displaced by slip along the shear fractures. **(iv)** Fractures and layers rotate. **(v)** Structures after stage 200 in (a) and (c). Slip and rotation along the fractures in the hard sublayer is accommodated by folding of layers in the soft sublayer. Structures resemble pinch and swell structures. In (b) layers are displaced and rotated as rigid blocks. *See movies on CD-ROM attached to the thesis.*



(caption of figure 2.7A on page 50)

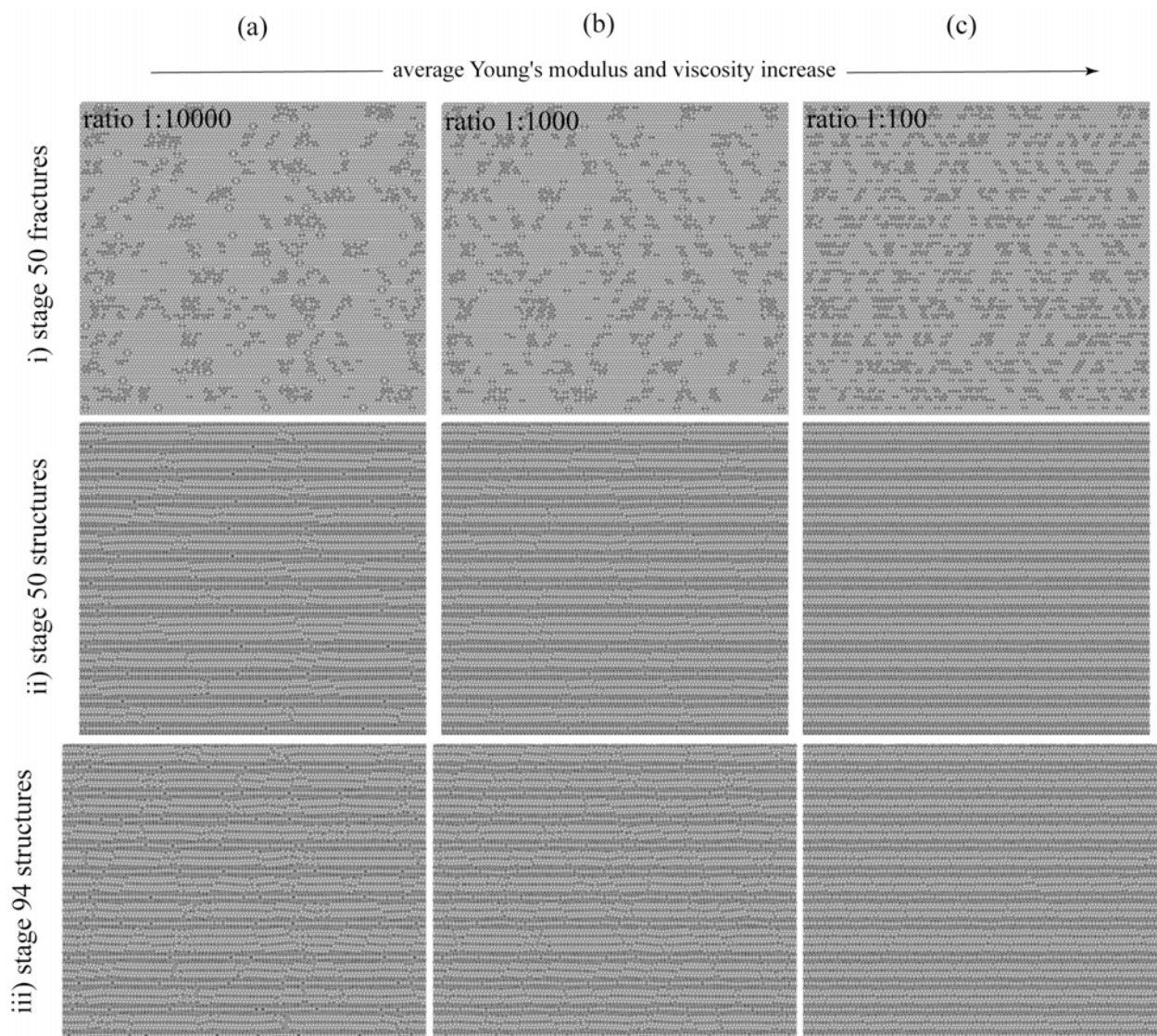


Figure 2.7B. Three simulations in multilayers. The average elastic constants of the materials in the models increase from (a) to (c). Competence contrast between the layers is indicated on the upper left corner of the plots in the first row. **(i)** Fractures in hard layers. **(ii)** Boudins and neck veins. **(iii)** Second order boudins by fracturing of the earlier boudins. *See movies on CD-ROM attached to the thesis.*

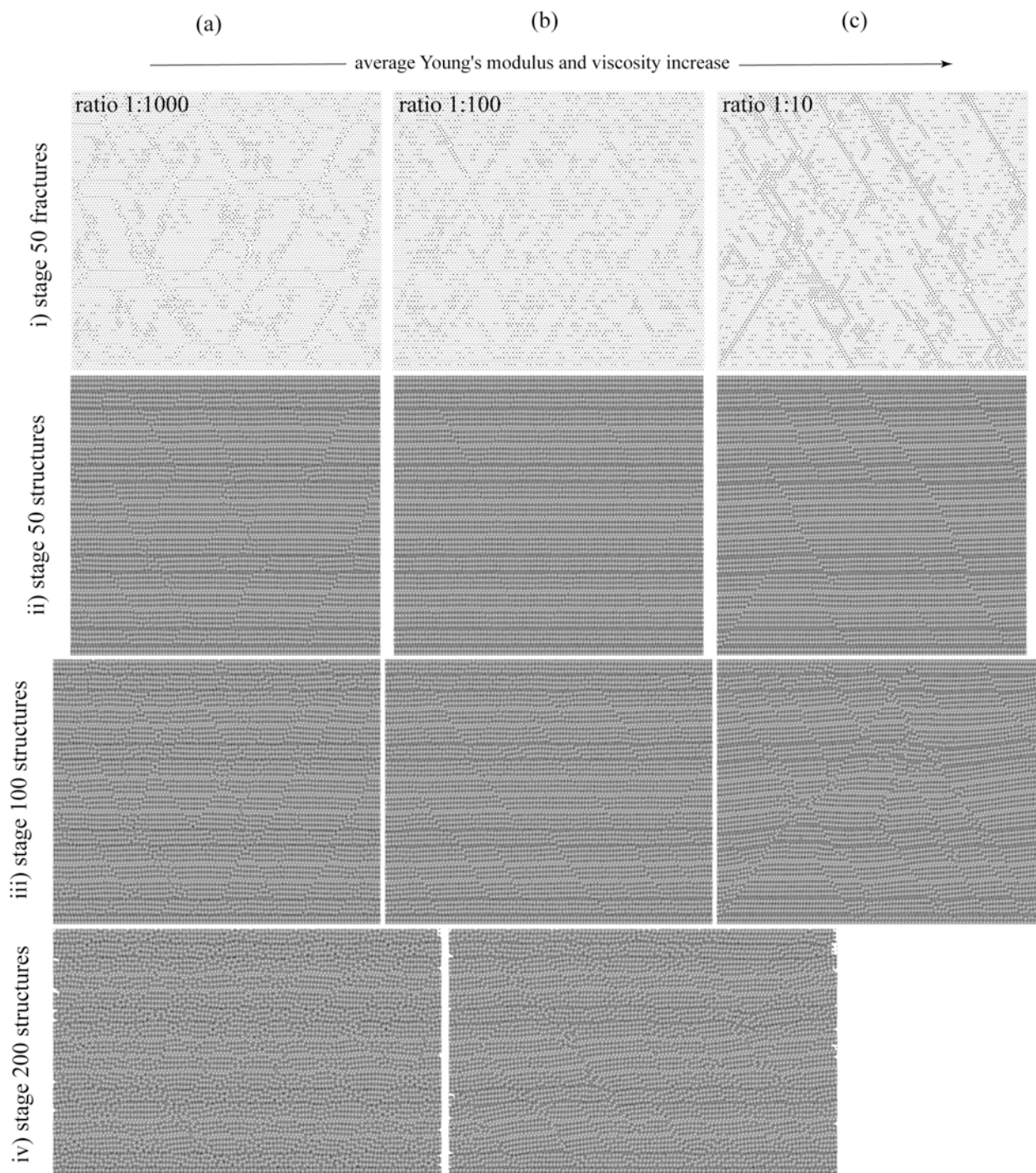


Figure 2.7C. Three simulations in multilayers where layers alternate more regularly. The average constants of the materials in the models increase from (a) to (c). Ratio between the layer constants is shown on the upper left corner of the plots in the first row. **(i)** Fractures after stage 50. Extensional veins develop at pull-aparts along en-echelon shear fractures. **(ii)** Layers are displaced, rotated and folded along the fractures. **(iii)** Boudins in multilayers. **(iv)** After stage 200 boudinage structures for (a, b). See movies on CD-ROM attached to the thesis.

Three simulations in Fig. 2.7D shown different arrangement of layers and its effects on the behavior of multilayers during progressive deformation. The weak layers in the models have same material properties. The hard layers in (c) 10 times weaker than the other simulations. Packs of layers in (a) behave like a single layer and deformation is more localized. In (c) layers alternate more regular and deformation becomes more penetrative through the layers. (b) represents the transition between the other two.

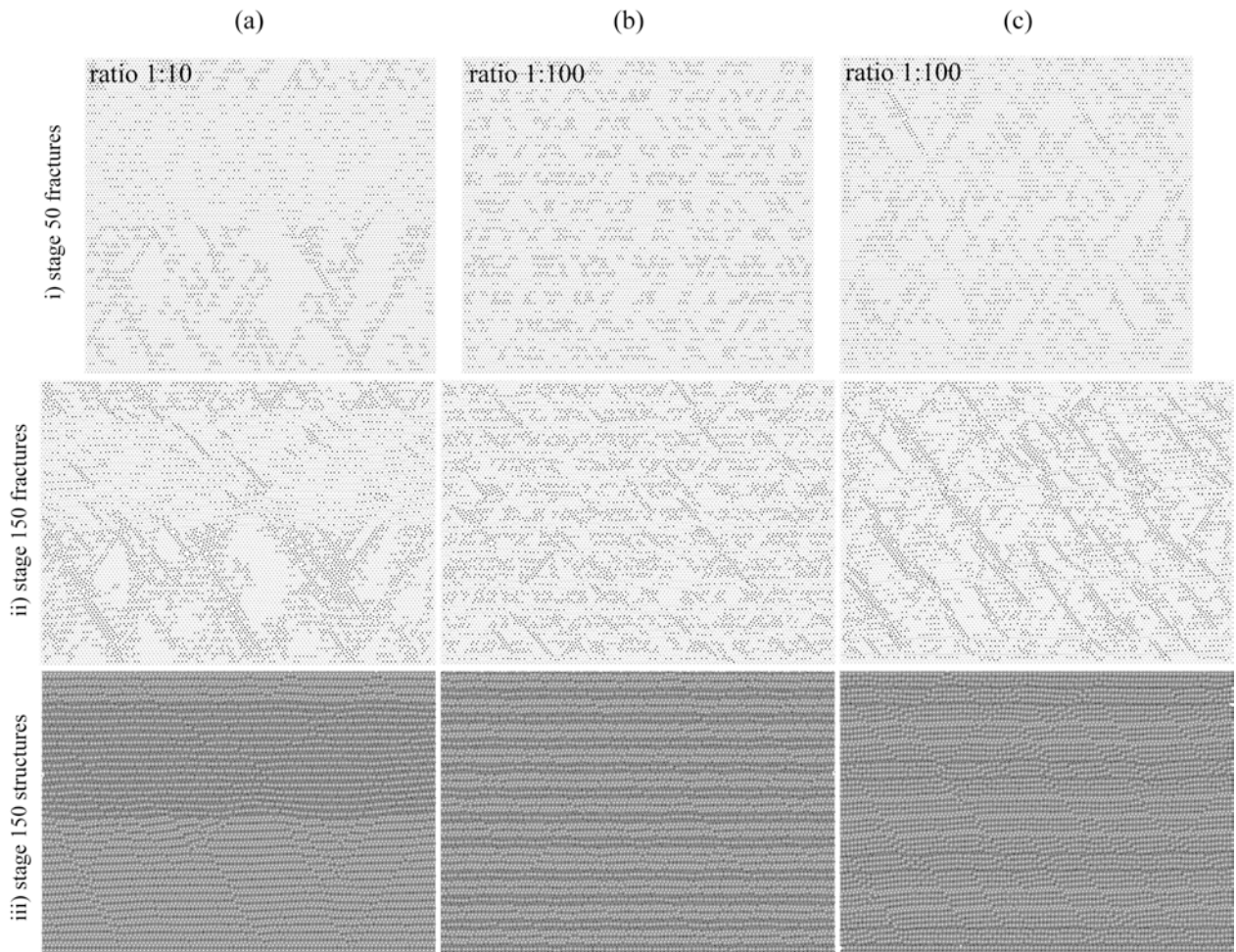


Figure 2.7D. Three simulations show boudinage in multilayers in which hard and soft layers are arranged with different alternation. The initial setting of the simulations is the same but the hard layers in (a) 10 times weaker than those in (b, c). **(i-ii)** Fracture patterns and localization. The arrangement of multilayers into sublayers in (a) results in their response to deformation as a single layer. Mode I fractures localize in the soft sublayer and shear fractures in the hard sublayer. Multilayers in (b) represent a transition between (a) and (c). Fractures propagate through layers in (c). **(iii)** Boudins in multilayers.

2.3.3. Foliation boudinage

Fig. 2.8 and Fig. 2.9 show examples of progressive development of foliation boudinage. The initial configurations of the models are shown in Fig. 2.2c. The initial lattice has a resolution of 50-particles in the x-direction. In Fig. 2.8 the springs have a distribution of breaking strengths with a mean of 0.4 and a deviation of 1.2. In the scaled model these values will refer to a distribution of breaking strengths of springs from 20 MPa to 80 MPa. In Fig. 2.9 the springs have a distribution of breaking strengths with a mean of 0.5 and a deviation of 1.2. In the scaled model these values will refer to a distribution of breaking strengths of springs from 25 MPa to 100 MPa. The Young's modulus, viscosity and breaking strength of all particles in both models are shifted by factors of 0.1, 1×10^8 and 1.0 respectively. In both models initial anisotropies are set to the same values. The initial anisotropy applies a pseudorandom distribution of parameters and adds more heterogeneity to the system. For example in these models it changes the Young's modulus of particles between 0.1-0.5.

Fig. 2.8 shows first the development of mode I (Fig. 2.8a) and then shear fractures (Fig. 2.8b) and then propagation, clustering and connection of fractures into large shear zones (Figs. 2.8c, e). Flow localizes around these discontinuities. Foliation starts bending and necking (Figs. 2.8d) and patterns similar to foliation boudinage structures develop (Figs. 2.8f, g, h).

In Fig. 2.9 similar to Fig. 2.8 mode I and shear fractures develop following each other (Fig. 2.9a-c). However, in the simulation in Fig. 2.9 number and size of fractures becomes smaller and the spacing is better developed. Foliation starts necking in the vicinity of opening small mode I and extensional shear fractures (Fig. 2.9d). Fractures localize (Fig. 2.9e) and foliation boudinage structures develop (Fig. 2.9f, g).

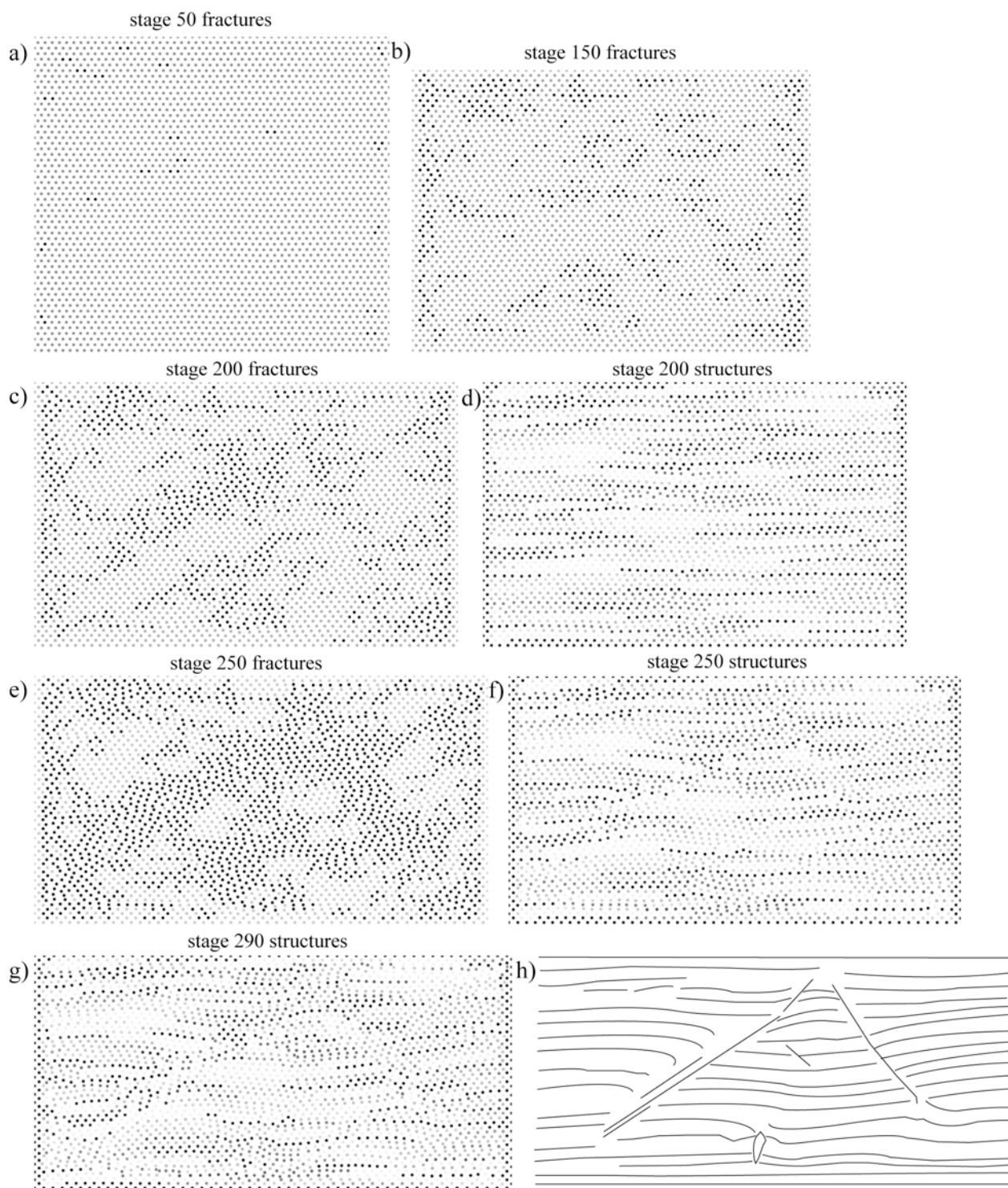


Figure 2.8. Simulation shows progressive development of foliation boudinage. **(a)** Small mode I fractures develop first. **(b)** Shear fractures develop later. **(c)** Fractures propagate and small voids open along developing large shear zones. **(d)** Foliation bends along the small fractures. **(e)** Fractures connect and develop into larger shear zones. Two connecting shear zones are oriented at different angles to model boundaries. **(f)** Slip and rotation adjacent to the fractures results in flanking structures. Voids open at the intersections. **(g)** Patterns are similar to foliation boudinage structures. Some voids are closed with further deformation. **(h)** Sketch of the structures after stage 290. See movie on CD-ROM attached to the thesis.

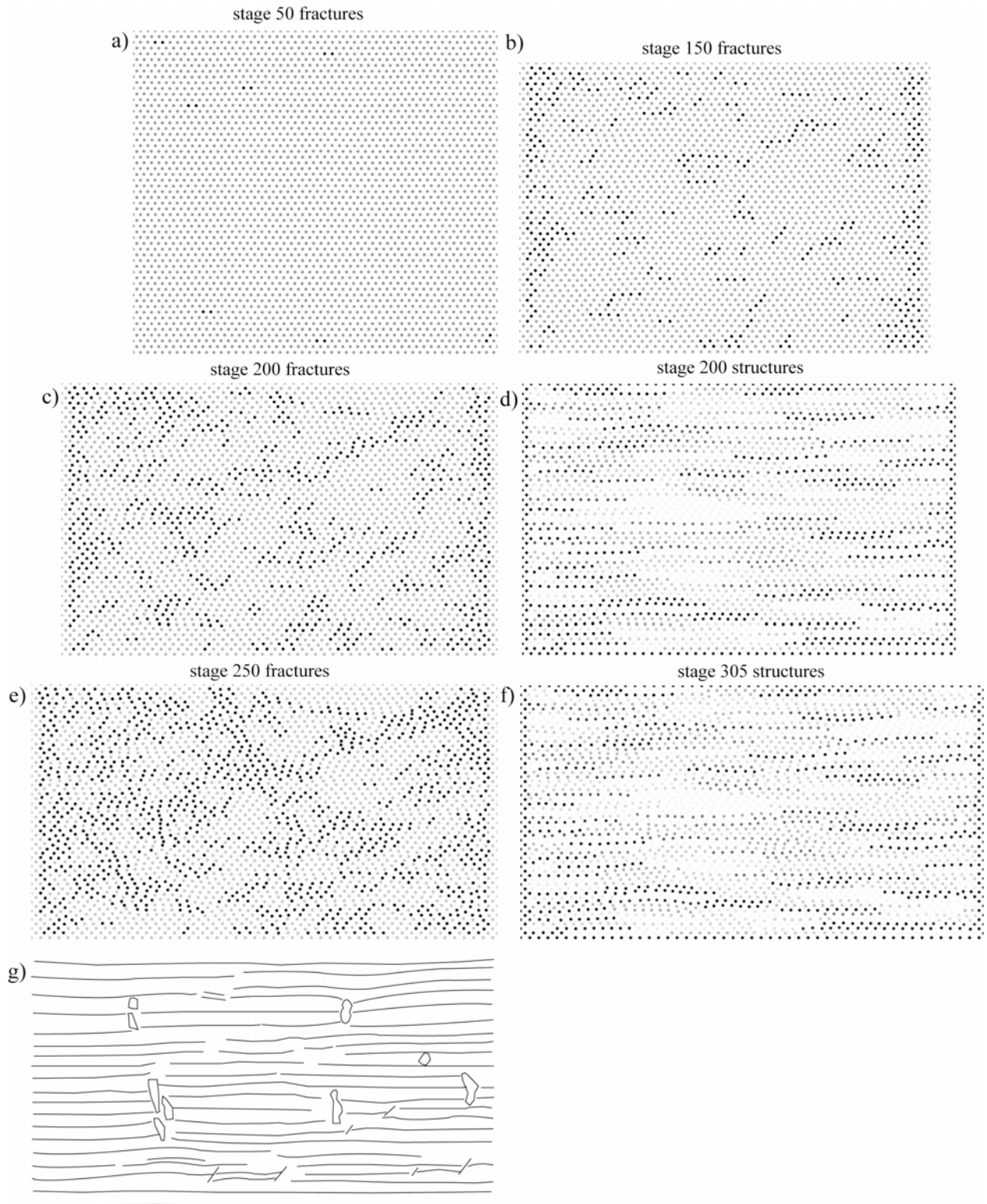


Figure 2.9. Progressive development of foliation boudinage. **(a)** Mode I fractures. **(b)** Shear fractures starts to connect with mode I fractures. **(c)** Voids along small extensional shear fractures. **(d)** Foliation bends around the fractures. **(e)** Voids at the intersections and fracture localization. **(f)** Foliation boudinage structures with better developed spacing. **(g)** Sketch of the structures after stage 305. *See movie on CD-ROM attached to the thesis.*

Fig. 2.10 shows another example of developing structures in a random mica model with the same settings in the Fig. 2.8. However, in this example the lattice has a resolution of 200-particles in the x- direction. Plots show deformation stage 266 where shear fractures that localize with a distinct spacing and form conjugate pairs (Fig. 10a) and shear bands (Fig. 2.10b).

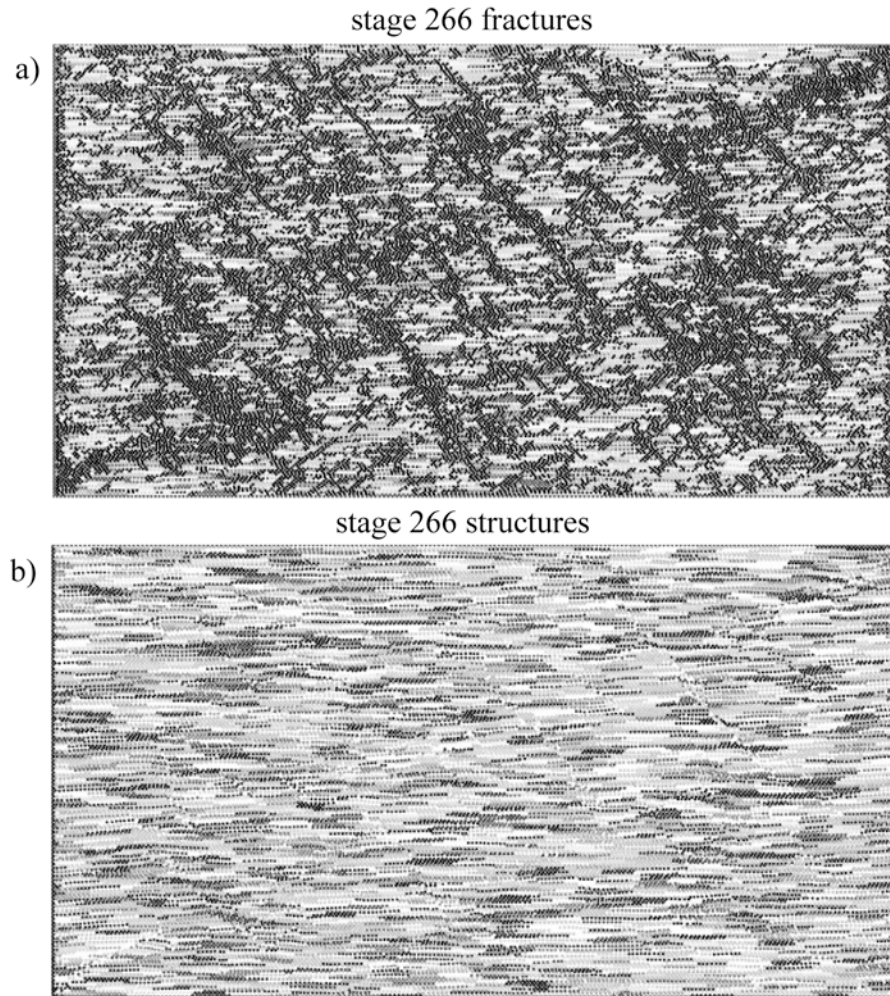


Figure 2.10. Examples of developing structures in random mica model. **(a)** Localized fractures and conjugate pairs. **(b)** Shear band structures. *See movie on CD-ROM attached to the thesis.*

In the following examples the individual effects of material properties in the random mica model are represent. In all simulations the initial lattice has a resolution of 100-particles in the x- direction.

Initial anisotropy: In the models initial anisotropy may be set different. This will change breaking strength, Young's modulus and viscosity of particles in the models. In Fig. 2.11 the initial anisotropy increases from (a) to (c). The initial configurations of the models are shown in

Fig. 2.2c. In all models the springs have a distribution of breaking strengths with a mean of 0.8 and a deviation of 1.2 representing a scaled distribution of breaking strengths of springs from 40 MPa to 160 MPa. The Young's modulus, viscosity and breaking strength of all particles in all models are shifted by factors of 0.1, 1×10^8 and 1.0 respectively. The fracture plots after stage 100 show that from (a) to (c) with an increase in initial anisotropy in the models fracture density increase and spacing decrease. Fractures are similar in size in (a) and become more heterogeneous in (c). Thus changes in initial anisotropy influence the developing patterns (Fig. 2.11).

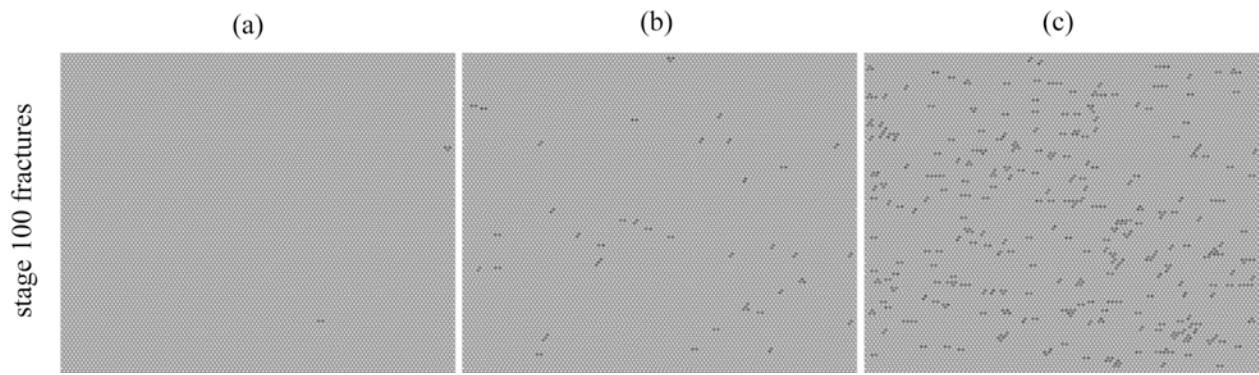
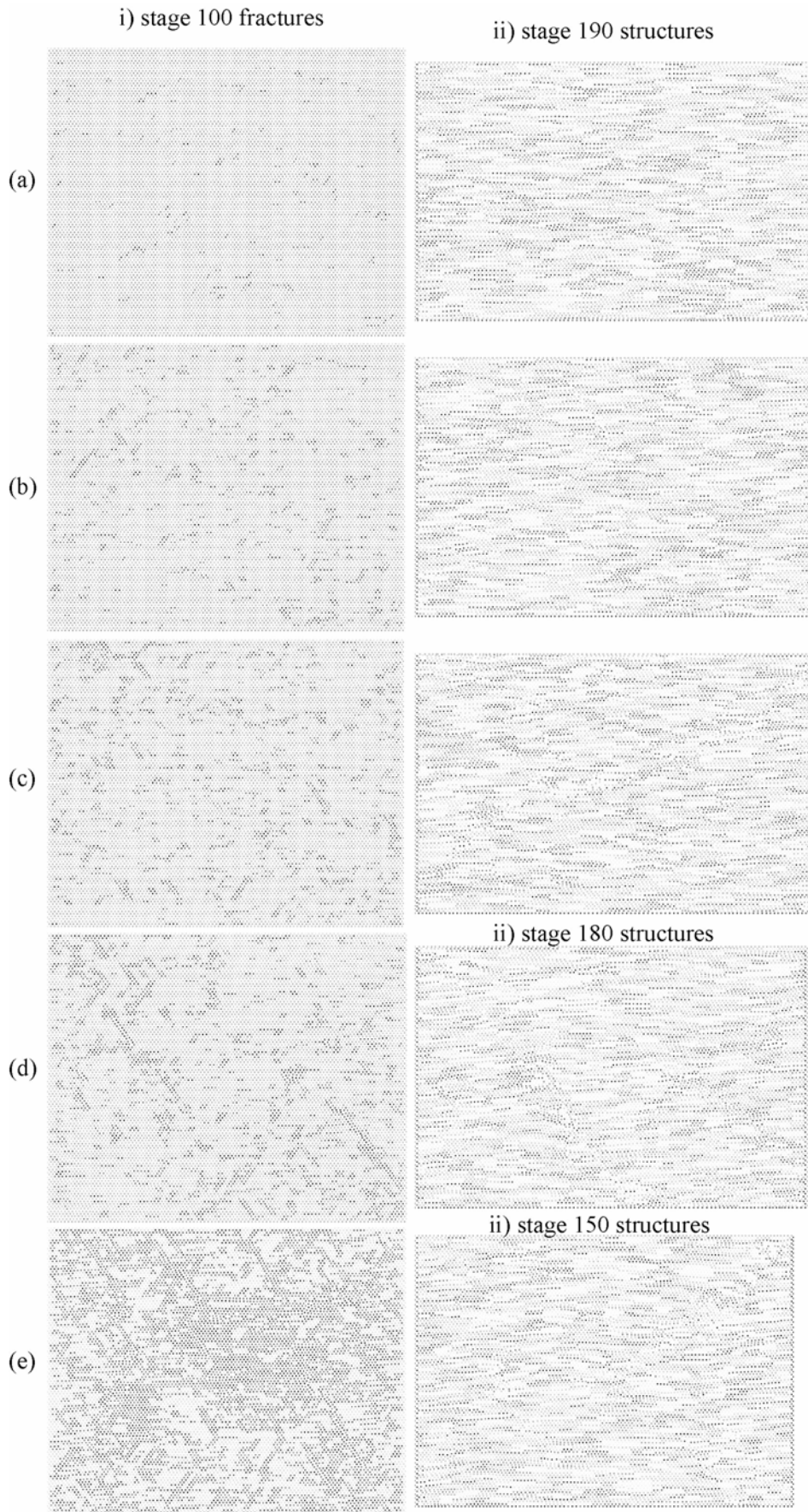


Figure 2.11. Fracture plots after stage 100 (89% shortening in the y-direction), are shown for three simulations with different initial anisotropy. From (a) to (c) with an increasing initial anisotropy in the models fracture density increase and spacing decrease.

Fracture toughness: In Fig. 2.12 the fracture toughness of materials decrease from Fig. 2.12a to Fig. 2.12e. In (a) it is set 5 times higher than in (e). In Fig. 2.12a the springs have a distribution of breaking strengths with a mean of 0.5 and a deviation of 1.2 (corresponding to a distribution of breaking strengths of springs from 25 MPa to 100 MPa in the scaled model). However in Fig. 2.12e the springs have a distribution of breaking strengths with a mean of 0.1 and a deviation of 1.2 (corresponding to a distribution of breaking strengths of springs from 5 MPa to 20 MPa in the scaled model), i.e. fracture toughness of the material is lower. The effects of these are obvious in developing structures (Fig. 2.12-i, ii). In the simulations heterogeneities, number and size of fractures increase and spacing decrease with a decreases in fracture toughness.

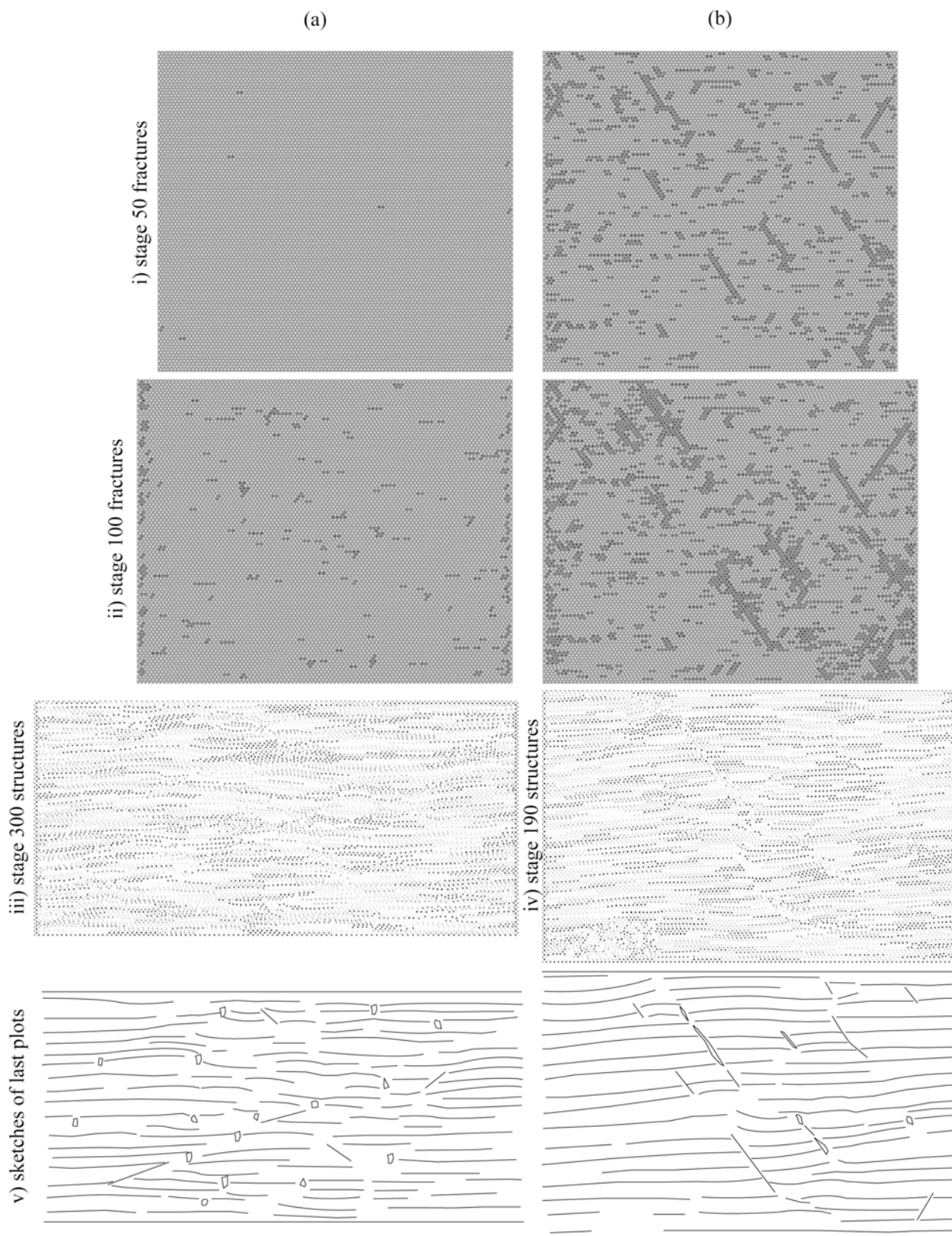


(caption of figure 2.12 on page 61)

Fig. 2.12A shows two other examples where the mean strength of the material is higher in (a) than in (b). In Fig. 2.12A-a the springs have a distribution of breaking strengths of springs between 25 MPa and 100 MPa in the scaled model while in Fig. 2.12A-b they are between 10 MPa to 40 MPa. Fractures develop earlier in Fig. 2.12A-i,b. after deformation stage 50 while small mode I fractures developed in (a), shear fractures developed already in (b). Fracture patterns in (b) with fork-end and intersecting shear fractures or fringes are similar to the geometries observed in the field (e.g. X- and double crescent-type boudinage structures). Small shear fractures start to develop during later stages of deformation in Fig. 2.12A-ii,a compared to the simulation in (b). Different types of foliation boudinage structures develop (Fig. 2.12A-iii,iv,v).

Figure 2.12. Five simulations show the change in structures with decreasing fracture toughness in the models from (a) to (e). **(i)** Fractures after stage 100. Number and size of fractures increase from (a) to (e). Fractures develop earlier in the models where breaking strength of springs has a larger distribution and localize more in the experiments with a narrow distribution. **(ii)** Structures after stages 190 for (a, b, c), 180 for (d) and 150 for (e). Necking starts around the opening small fractures in (a) while foliation bends and folds adjacent to the shear fractures in simulations with larger distribution due to flow perturbations. *See movies on CD-ROM attached to the thesis.*

Figure 2.12A. Two simulations with the same initial settings show progressive development of structures. The distribution of breaking strengths of springs is larger in (b). **(i)** (a) small mode I fractures, (b) mode I and shear fractures with different size. **(ii)** Small shear fractures in (a). Propagation and linking of fractures form fork-ends and fringes in (b). **(iii)** Foliation boudinage structures with well developed spacing and shear bands after stage 300 in (a). **(iv)** Foliation bends along the extensional shear fractures in (b). Flanking folds and shear bands develop. Foliation boudinage structures associated with large shear fractures. **(v)** Sketches of the structures in the last plots. *See movies on CD-ROM attached to the thesis.*



(caption of figure 2.12A on page 61)

Young's modulus: Two simulations in Fig. 2.13 show the influence of Young's modulus on the patterns. The simulation in (b) has an average Young's modulus that is 5 times higher than the simulation in (a). The material behaves more brittle when the Young's modulus is higher (Fig. 2.13b). Fracture density increases with increasing Young's modulus. Small fractures develop in Fig. 2.13a while larger fractures develop and localize into low angle shear zones in Fig. 2.13b.

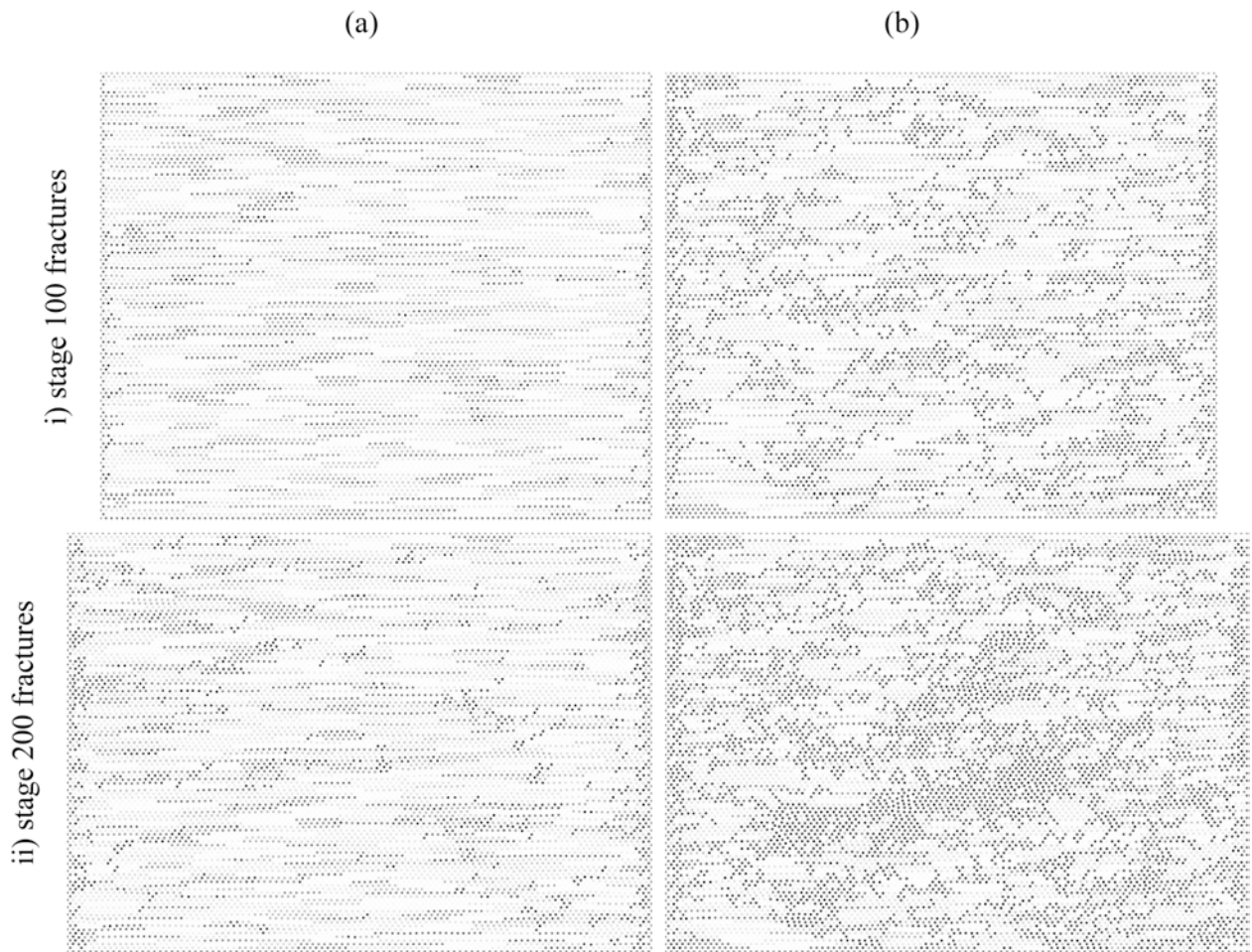
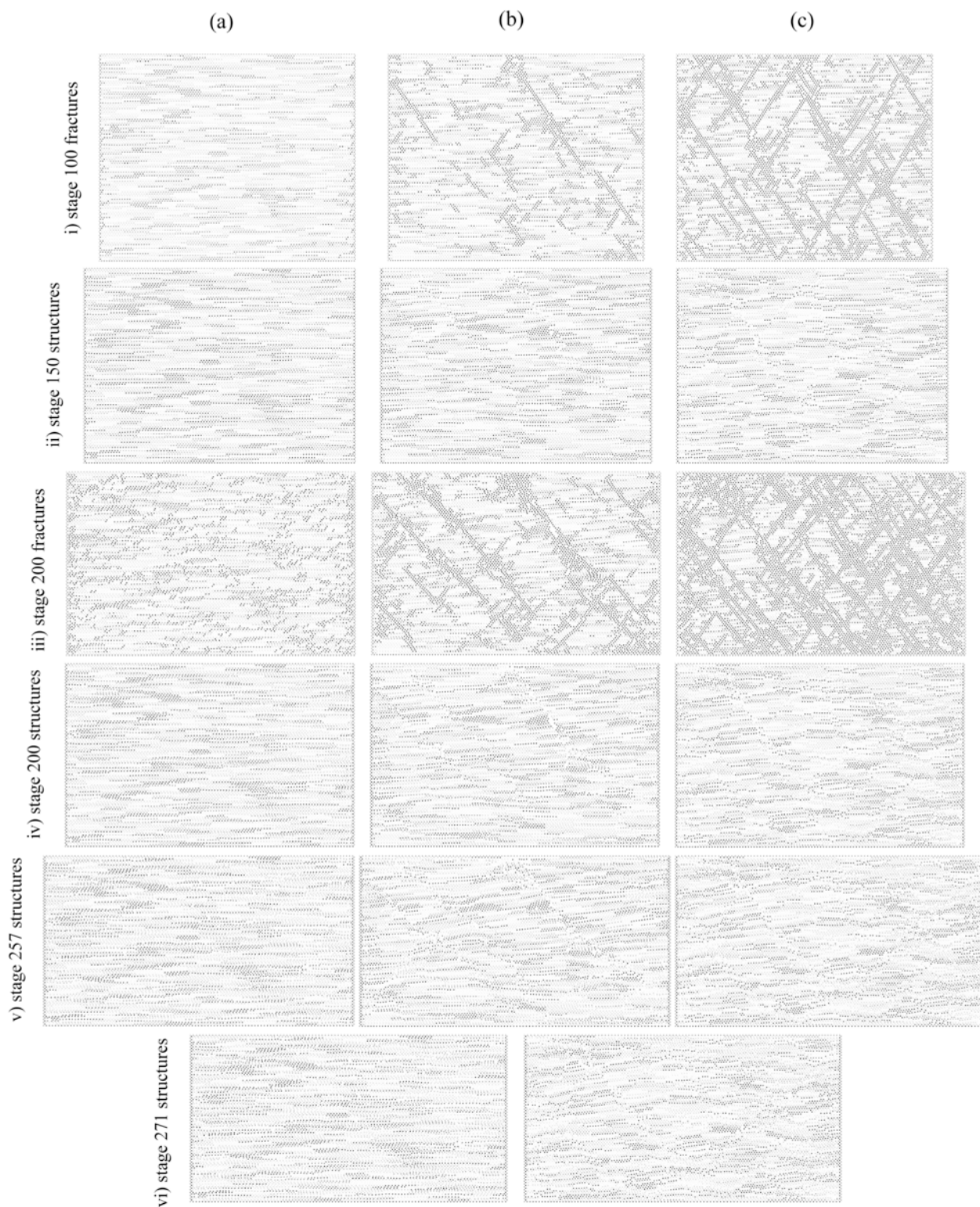


Figure 2.13. Two simulations with the same initial settings but the simulation in (a) has an average Young's Modulus of particles 5 times lower than in (b). **(i)** (a) mode I fractures, (b) mode I and shear fractures. **(ii)** (a) Small shear fractures, (b) large low angle shear zones.

Viscosity: Three simulations in Fig. 2.14 show changes in patterns with a change in viscosity. The viscosity of particles in the models increases from (a) to (c). In all models the springs have a distribution of breaking strengths with a mean of 0.8 and a deviation of 1.2 that represent a scaled distribution of breaking strengths of springs from 40 MPa to 160 MPa. The viscosity of particles in (b) is set 5 times higher and in (c) 10 times higher than the particles in (a). The changes in structures are represent in Fig. 2.14 from (i) to (ii). Viscosity has a similar effect on the behavior of the material than the Young's modulus. Fracture density and size increase with increasing viscosity of the material (Figs. 2.14i, iii).

Figure 2.14. Three simulations with the same initial settings but the average viscosity of the models increases from (a) to (c). **(i)** Transition from small mode I fractures (a) to shear fractures (b, c). Conjugate pairs develop. At pull-aparts along the stair-stepping shear fractures extension veins develop (b, c). Number and size of fractures increase from (a) to (c). **(ii)** Foliation bends and rotates along the fractures. **(iii)** Fractures after stage 200. Small extensional shear fractures open (a). Shear fractures propagate and connect (b, c) and extension veins get larger. **(iv)** Foliation pinches around the veins. Patterns are similar to foliation boudinage structures in nature. **(v)** Fractures and foliation rotate. Bending of foliation adjacent to the veins becomes stronger. Veins are rotated and shortened. Some are closed in (b, c). **(vi)** After stage 271 plots show the structures in (a and c). *See movie on CD-ROM attached to the thesis.*



(caption of figure 2.14 on page64)

2.4. Conclusions

The models produce a variety of single layer, multilayer and foliation boudinage structures. Numerical patterns are consistent with natural boudinage structures. Pure shear deformation alone can produce complex geometries in anisotropic materials. During progressive deformation fractures of mode I/II and combination of both develop in the models. However strain is more localized in the models with lower elastic constants and more dispersed in the models with higher elastic constants. Asymmetric structures do not necessarily form in simple shear. Anisotropy in the models leads to more heterogeneous structures. However, both symmetric and asymmetric structures are observed in the same models if small local variations in material properties exist. Early formed fractures change the stress fields in the models and may affect the orientation of forthcoming fractures. Voids open along extensional fractures, at intersections of shear fractures and pull-aparts along shear fractures.

The narrow distribution of breaking strength of springs, low Young's Modulus and viscosity of materials have similar effect on the behavior of materials. When the distribution is narrow and the Young's Modulus and viscosity are low, fractures localize and have distinct spacing.

Symmetric boudinage structures and extensional neck veins more commonly develop in the models with lower elastic constants and anisotropy. Asymmetric foliation boudinage structures (e.g. X-type) develop associated with shear fractures in the models where elastic constants and anisotropy of the materials are relatively high. In these models boudin neck veins form commonly at pull-aparts along the shear fractures and at the intersection of fractures.

Chapter 3

General conclusions

In this research, development of foliation boudinage structures during progressive deformation was studied using field observations and numerical simulations.

Foliation boudinage structures (FBSs) form by ductile deformation adjacent to brittle fractures and open fluid filled cavities in metamorphic rocks. In the first chapter we define a classification of foliation boudinage structures based on natural examples studied in the Çine Massif, SW Turkey and Furka Pass-Urseren Zone, Central Switzerland. The four main types of foliation boudinage structures have been distinguished: Lozenge-, crescent-, X- and double crescent- type. The names were given after the vein geometries in sections normal to the foliation and parallel to the lineation. All these types occur as open, vein filled structures but also show transitions to a fishmouth geometry. The shape of the central veins and the deflection pattern of the foliation in the vicinity of these veins define the typical shape of a foliation boudinage structure. Lozenge type FBSs are symmetric. Crescent-, X- and double crescent- type FBSs are asymmetric. The shape of the boudin neck veins in foliation boudinage depends on the initial orientation and shape of the fracture, the propagation behaviour of the fracture, the geometry of bulk flow, and the stage at which mineral filling takes place. FLAC experiments show that fracture propagation during ductile deformation strongly influences the geometry of developing veins. The cusps of the veins are well developed in the case of propagating fractures.

In the second chapter we investigate the initiation and evolution of foliation boudinage with a two dimensional discrete element model. We performed a number of simulations with different initial configurations to investigate the effects of material properties (Young's modulus, viscosity and breaking strength) and anisotropy on the developing structures during progressive pure shear deformation. The models produce similar patterns to the natural examples described in the first chapter. During progressive deformation fractures of mode I/II and combination of both develop in the models. Distinct and more localized fractures form in models with lower elastic constants. Extensional neck veins and symmetric boudinage

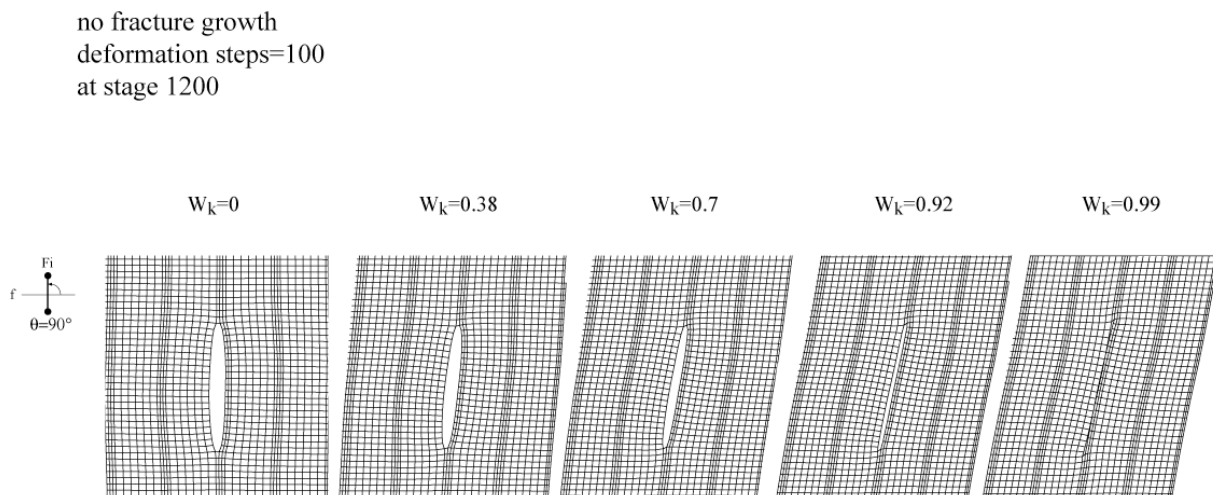
structures similar to the natural examples described in Chapter 1 commonly develop in these models. The narrow distribution of breaking strength of springs, low Young's Modulus and viscosity of materials have similar effect on the behavior of materials. The large distribution of breaking strength of springs, high Young's Modulus and viscosity of materials lead to more heterogeneous and dispersed fractures. Fracture patterns with fork-end or X-shape and Z- or S-shape are produced. The complex geometries described in the first chapter develop in these models with higher elastic constants and anisotropy. However, both symmetric and asymmetric structures are observed in the same models if small local variations in material properties exist.

Appendix

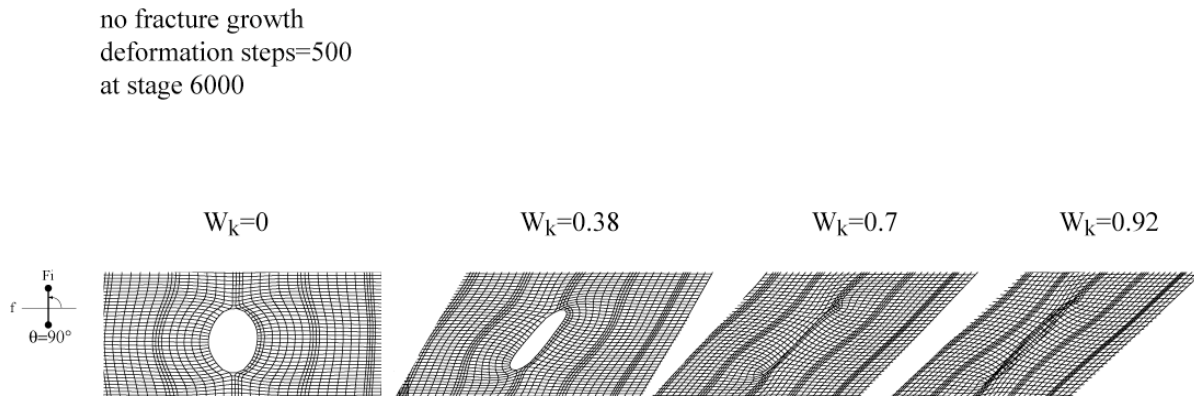
The appendix of this thesis consists of two sections. Section one shows the examples and variations in FLAC experiments mentioned in the first chapter and section two contains the movies belong to the figures in the second chapter on CD-ROM.

1. FLAC experiments

Five experiments in the following figure show veins developed in boudin necks during progressive deformation without fracture propagation. The effect of kinematic vorticity number from pure shear to simple shear is tested. The plots are at the same deformation stage. The initial fractures in all models are orthogonal. The initial stages of experiments before deformation are shown in Figs. 11 and 12 in Chapter 1. Symmetric and asymmetric lens shaped veins develop in the models.

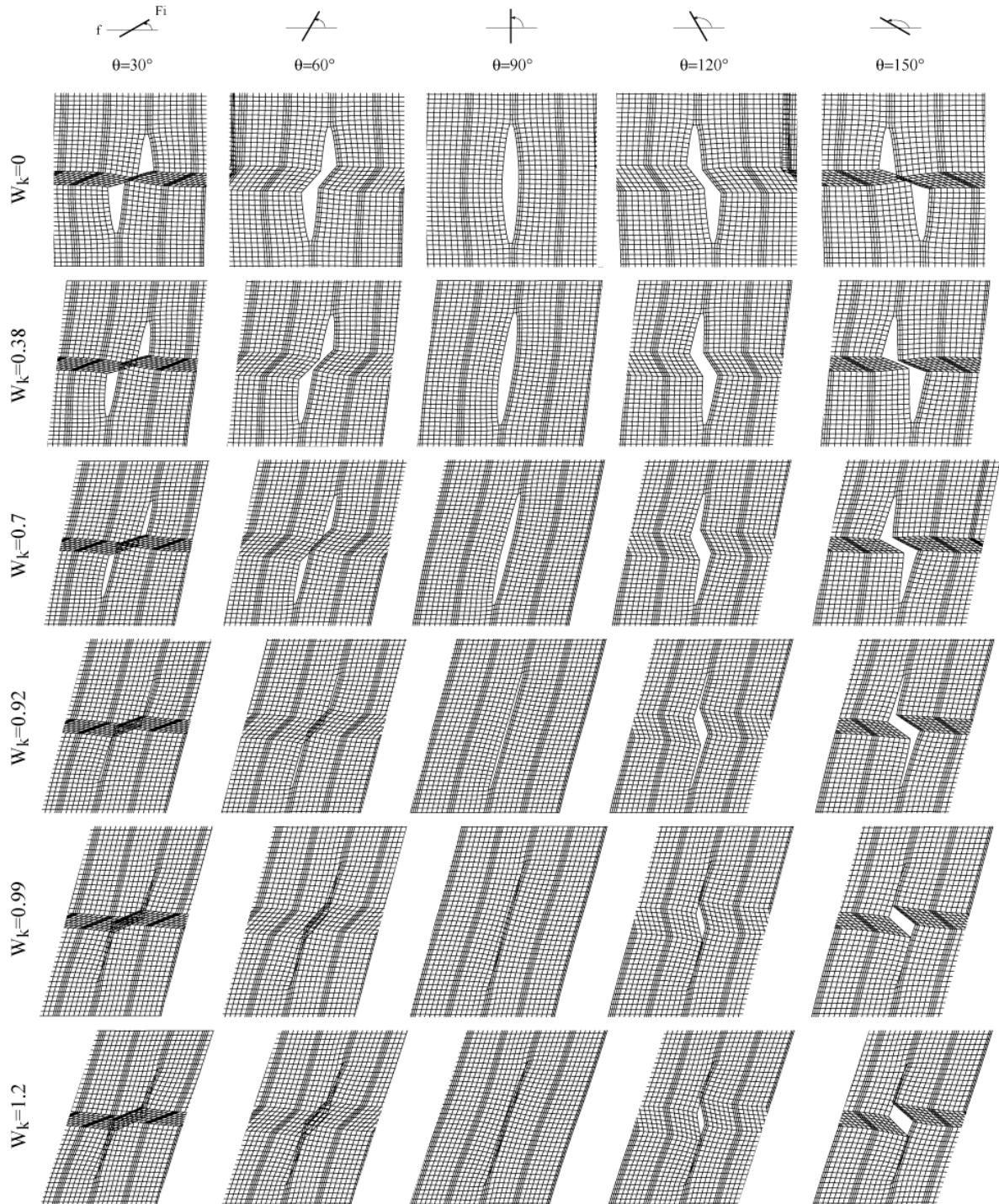


The following four experiments are similar to the experiments in the previous figure. However here deformation is larger. Round veins form under pure shear. Asymmetric lens shaped and closed veins develop in shear.

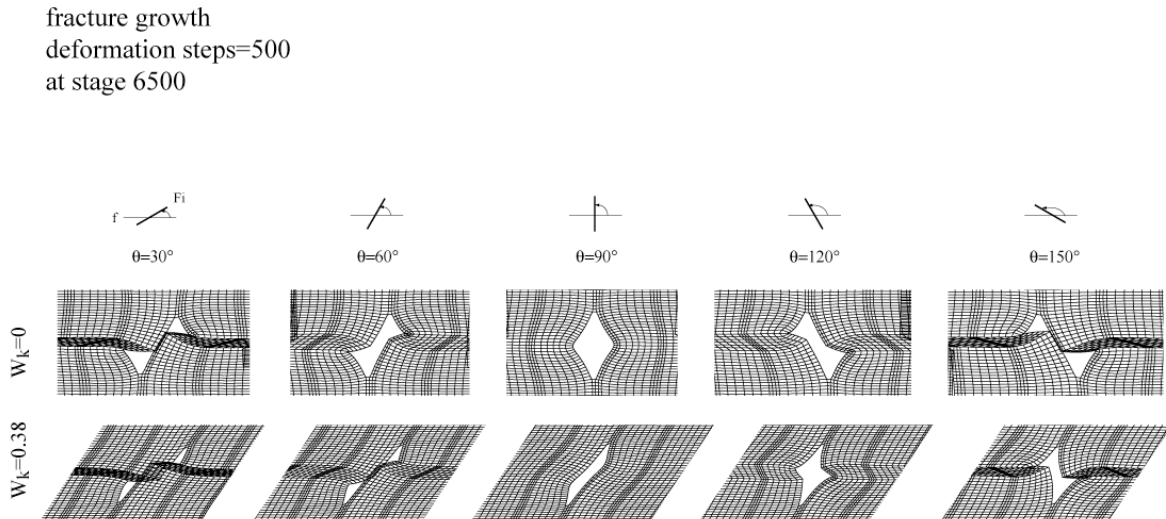


Fracture propagation during progressive deformation and the development of neck veins are shown with a series of experiments in the figure below. In the models the effects of different initial fracture orientations with a combination of kinematic vorticity numbers from pure shear to simple shear are tested. Various symmetric and asymmetric vein geometries develop.

fracture growth
deformation steps=100
plots at stage 1700



The experiments below are similar to the previous experiments with fracture growth. Here the ratio of deformation to fracture propagation rate is higher. In these models cusps are well develop both in symmetric and asymmetric veins.



2. Explanations for the movies

The movies on this CD-ROM show the examples of simulations that were run for the progressive development of boudinage structures. The letters ‘f, dif, mean’ after underscore refer to ‘fracture, differential stress, mean stress’. The names without extra letters show the Young’s modulus. In some of the movies fracture propagation, change in differential and mean stress are shown during progressive deformation. The red color in movies represents stiff particles and high stresses, the blue soft particles and low stresses.

The width of the pictures in the movies is not scaled. The applied deformation is pure shear with area conservation. In the movies however it looks like as if they are compressed only from the top. This is only due to the fact that the program fits the width of the pictures to the window size. Nonetheless they still show clearly the developing structures and the variations.

All movies belong to the figures in Chapter 2 and the numbers match the figure numbers as listed below.

-Layer boudinage

- movie3 (fig3 and fig4a)
- movie4b (fig4b), movie4c (fig4c), movie4d (fig4d)

-Multilayer boudinage

- movie6, (fig6)
- movie7a (fig7a), movie7b (fig7b)
- movie7Aa (fig7Aa), movie7Ab (fig7Ab), movie7Ac (fig7Ac)
- movie7Ba (fig7Ba), movie7Bb (fig7Bb), movie7Bc (fig7Bc)
- movie7Ca (fig7Ca), movie7Cb (fig7Cb), movie7Cc (fig7Cc)

-Foliation boudinage

- movie8 (fig8), movie9 (fig9), movie10 (fig10)
- movie12a (fig12a), movie12b (fig12b), movie12c (fig12c), movie12d (fig12d), movie12e (fig12e)
- movie12Aa (fig12Aa), movie12Ab (fig12Ab)
- movie14a (fig14a), movie14b (fig14b), movie14c (fig14c)

References

- Albrecht, J., Biino, G.G., Mercogli, I., Stille, P., 1991. Mafic-ultramafic rock associations in the Aar, Gotthard and Tavetsch massifs of the Helvetic domain in the Central Swiss Alps: markers of ophiolitic pre-Variscan sutures, reworked by polymetamorphic events? *Schweizerische Mineralogische und Petrographische Mitteilungen* 71, 295–300.
- Albrecht, J., 1994. Geologic units of the Aar massif and their pre-Alpine rock associations: a critical review. *Schweizerische Mineralogische und Petrographische Mitteilungen* 74, 5–27.
- Aerden, D.G.A.M., 1991. Foliation-boudinage control on the formation of the Rosebery Pb-Zn orebody, Tasmania. *Journal of Structural Geology* 13, 7, 759–775.
- Bernoulli, D., Graciansky, P.C.D., Monod, O., 1974. The extension of the Lycian nappes (SW Turkey) into the southeastern Aegean islands. *Eclogae Geologicae Helvetiae* 67, 39–90.
- Bons, P., 2001. Development of crystal morphology during unitaxial growth in a progressively widening vein: I. The numerical model. *Journal of Structural Geology* 23, 865–872.
- Bons, P., Koehn, D., Jessell, M.W., in press. *Microdynamic Simulation, from micro-processes to patterns in rocks*. Springer Lecture Series in Earth Sciences.
- Bozkurt, E., Satır, M., 2000. The southern Menderes Massif (western Turkey): geochronology and exhumation history. *Geological Journal* 35, 285–296.
- Bozkurt, E., 2004. Granitoid rocks of the southern Menderes massif (southwestern Turkey): field evidence for Tertiary magmatism in an extensional shear zone. *International Journal of Earth Sciences* 93, 52–71.
- Bozkurt, E., Winchester, J.A., Mittwede, S.K., Ottley, C.J., 2006. Geochemistry and tectonic implications of leucogranites and tourmalines of the southern Menderes Massif, Southwest Turkey. *Geodinamica Acta* 19, 363–390.
- Bozkurt, E., 2007. Extensional v. contractional origin for the southern Menderes shear zone, SW Turkey: tectonic and metamorphic implications. *Geological Magazine* 144, 191–210.
- Candan, O., Dora, O.Ö., 1997. The generalized map of the Menderes Massif. Department of Geological Engineering, Dokuz Eylül University, Izmir.
- Candan, O., Dora, O.Ö., Oberhänsli, R., Oelsner, F., Dürr, S., 1997. Blueschist relicts in the Mesozoic cover series of the Menderes massif and correlations with Samos Island, Cyclades. *Schweizerische Mineralogische und Petrographische Mitteilungen* 77, 95–99.
- Cobbold, P.R., Cosgrove, J.W., Summers, J.M., 1971. Development of internal structures in deformed anisotropic rocks. *Tectonophysics* 12, 23–53.

- Cobbold, P.R., 1976. Mechanical effects of anisotropy during large finite deformations. *Bulletin de la Société Géologique de France* 7, 1497–1510.
- Cosgrove, J.W., 1997. The influence of mechanical anisotropy on the behaviour of the lower crust. *Tectonophysics* 280, 1–14.
- Druguet, E., Carreras, J., 2006. Analogue modelling of syntectonic leucosomes in migmatitic schists. *Journal of Structural Geology* 28, 1734–1747.
- Erdogan, B., Güngör, T., 2004. The Problem of the Core-Cover Boundary of the Menderes Massif and an Emplacement Mechanism for Regionally Extensive Gneissic Granites, western Anatolia (Turkey). *Turkish Journal of Earth Sciences* 13, 15–36.
- Etheridge, M.A., Wall, V.J., Cox, S.F., 1984. High fluid pressures during regional metamorphism and deformation: implications for mass transport and deformation mechanism. *Journal of Geophysical Research* 89, B6, 4344–4358.
- Fletcher, R.C., 2005. Instability of an anisotropic power-law fluid in a basic state of plane flow. *Journal of Structural Geology* 27, 1155–1167.
- Frey, M., Mahlmann, R.F., 1999. The Alpine metamorphism of the central Alps. *Schweizerische Mineralogische und Petrographische Mitteilungen* 79, 135–154.
- Gessner, K., 2000. Eocene nappe tectonics and late-Alpine extension in the central Anatolide belt, western Turkey- structure, kinematics and deformation history. PhD thesis, Univ. Mainz, Germany.
- Gessner, K., Piazzolo, S., Güngör, T., Ring, U., Kröner, A., Passchier, C.W., 2001. Tectonic significance of deformation patterns in granitoid rocks of the Menderes nappes, Anatolide belt, southwest Turkey. *International Journal of Earth Sciences* 89, 766–780.
- Gessner, K., Collins, A.S., Ring, U., Güngör, T., 2004. Structural and thermal history of poly-orogenic basement: U-Pb geochronology of granitoid rocks in the southern Menderes Massif, Western Turkey. *Journal of the Geological Society, London*, 161, 93–101.
- Goscombe, B.D., Passchier, C.W., 2003. Asymmetric boudins as shear sense indicators-an assessment from field data. *Journal of Structural Geology* 25, 575–589.
- Goscombe, B.D., Passchier, C.W., Hand M., 2004. Boudinage classification: end-member boudin types and modified boudin structures. *Journal of Structural Geology* 26, 739–763.
- Gosh, S.K., Sengupta, S., 1999. Boudinage and composite boudinage in superposed deformations and syntectonic migmatization. *Journal of Structural Geology* 21, 97–110.
- Gottscahlk, R.R., Kronenberg, A.K., Russell, J.E., Handin, J., 1990. Mechanical Anisotropy of Gneiss: Failure Criterion and Textural Sources of Directional Behavior. *Journal of Geophysical Research* 95, 21613–21634.

- Graciansky, P.Ch.de, 1968. Teke Yarımadası (Likya) Toroslarının üst üste gelmiş ünitelerinin stratigrafisi ve Dinaro-Toroslar'daki yeri. MTA Dergisi 71, 73–93.
- Grasemann, B., Stüwe, K., 2001. The development of flanking folds during simple shear and their use as kinematic indicators. *Journal of Structural Geology* 23, 715–724.
- Grasemann, B., Stüwe, K., Vannay, J.C., 2003. Sense and non-sense of shear in flanking structures. *Journal of Structural Geology* 25, 19–34.
- Güngör, T., 1998. Stratigraphy and tectonic evolution of the Menderes Massif in the Söke-Selçuk Region. PhD thesis, Dokuz Eylül University, Izmir.
- Hambrey, M.J., Milnes, A.G., 1975. Boudinage in glacier ice-some examples. *Journal of Glaciology* 14, 383–393.
- Hanmer, S., 1986. Asymmetrical pull-aparts and foliation fish as kinematic indicators. *Journal of Structural Geology* 8, 111–122.
- Hetzel, R., Reischmann, T., 1996. Intrusion age of Pan-African augen gneisses in the southern Menderes Massif and the age of cooling after Alpine ductile extensional deformation. *Geological Magazine* 133, 565–572.
- Hilgers, C., Koehn, D., Bons, P.D., Urai, J.L., 2001. Development of crystal morphology during uniaxial growth in a progressively widening vein: II. Numerical simulations of the evolution of antitaxial fibrous veins. *Journal of Structural Geology* 23, 873–885.
- Honda, S., 1986. Strong anisotropic flow in a finely layered asthenosphere. *Geophysical Research Letters* 13, 1454–1457.
- Itasca Consulting Group, Inc., 1998. FLAC: Fast Lagrangian Analysis of Continua, Version 3.40. Itasca Consulting Group, Inc., Minneapolis.
- Kidan, T.W., Cosgrove, J.W., 1996. The deformation of multilayers by layer-normal compression; an experimental investigation. *Journal of Structural Geology* 18, 461–474.
- Koehn, D., *in press*. Fracturing (elle_latte). In: Bons, P., Koehn, D., Jessell, M.W., *Microdynamic Simulation, from micro-processes to patterns in rocks*. Springer Lecture Series in Earth Sciences.
- Koehn, D., Arnold, J., 2004. Fracturing in Polycrystalline Materials. *Journal of the Virtual Explorer* 15.
- Koehn, D., Arnold, J., Passchier, C.W., 2005. Fracture and vein patterns as indicators of deformation history: a numerical study. In: Gapais, D., Brun J.P., Cobbold, P.R. (eds). *Deformation Mechanisms, Rheology and Tectonics: from minerals to the lithosphere*. Geological Society, London, Special Publications, 243, 11–24.

- Koehn, D., Sachau, T., *in press*. Visco-elastic and brittle deformation. In: Bons, P., Koehn, D., Jessell, M.W. *Microdynamic Simulation, from micro-processes to patterns in rocks*. Springer Lecture Series in Earth Sciences.
- Kröner, A., Sengör, A.M.C., 1990. Archean and Proterozoic ancestry in late Precambrian to early Paleozoic crustal elements of southern Turkey as revealed by single-zircon dating. *Geology* 18, 1186–1190.
- Lacassin, R., 1988. Large-scale foliation boudinage in gneisses. *Journal of Structural Geology* 10, 643–647.
- Lebit, H., 1989. Die Urserenzone zwischen Realp und Tiefenbach (Kanton Uri/Schweiz). Unpublished Diplomarbeit, Freiburg.
- Lloyd, G.E., Ferguson, C.C., 1981. Boudinage structure: some new interpretations based on elastic-plastic finite element simulations. *Journal of Structural Geology* 3, 117–128.
- Lloyd, G.E., Ferguson, C.C., Reading, K., 1982. A stress-transfer model for the development of extension fracture boudinage. *Journal of Structural Geology* 4, 355–372.
- Loos, S., Reischmann, T., 1999. The evolution of the southern Menderes Massif in SW Turkey as revealed by zircon dating. *Journal of the Geological Society, London*, 156, 1021–1030.
- Mandal, N., Karmakar, S., 1989. Boudinage in homogeneous foliated rocks. *Tectonophysics* 170, 151–158.
- Mandal, N., Chakraborty, C., Samanta, S.K., 2000. Boudinage in multilayered rocks under layer-normal compression: a theoretical analysis. *Journal of Structural Geology* 22, 373–382.
- Mandal, N., Chakraborty, C., Samanta, S.K., 2000. An analysis of anisotropy of rocks containing shape fabrics of rigid inclusions. *Journal of Structural Geology* 22, 831–839.
- Marquer, D., Burkhard, M., 1992. Fluid circulation, progressive deformation and mass-transfer processes in the upper crust: the example of basement-cover relationships in the External Crystalline Massifs, Switzerland. *Journal of Structural Geology* 14, 1047–1057.
- Milnes, A.G., Pfiffner, O.A., 1977. Structural development of the Infrahelvetic complex, eastern Switzerland. *Eclogae Geologicae Helveticae* 70, 83–95.
- Platt, J.P., Vissers, R.L.M., 1980. Extensional structures in anisotropic rocks. *Journal of Structural Geology* 2, 397–410.
- Passchier, C.W., 2001. Flanking structures. *Journal of Structural Geology* 23, 951–962.
- Passchier, C.W., Druguet, E., 2002. Numerical modelling of asymmetric boudinage. *Journal of Structural Geology* 24, 1789–1803.

- Passchier, C.W., Mancktelow, N.S., Grasemann, B., 2005. Flow perturbations: a tool to study and characterize heterogeneous deformation. *Journal of Structural Geology* 27, 1011–1026.
- Passchier, C.W., Trouw, R.A.J. 2005. *Microtectonics*. 2nd edition, Springer–Verlag, Berlin, 366 pp.
- Ramberg, H., 1955. Natural and experimental boudinage and pinch- and –swell structures. *Journal of Geology* 63, 512–526.
- Ramsay, J.G., Huber, M.I., 1983. *The Techniques of Modern Structural Geology*. In: *Strain Analysis*, vol. 1. Academic Press, London, 307 pp.
- Ramsay, J.G., Lisle, R.J., 2000. *The Techniques of Modern Structural Geology*. In: *Applications of continuum mechanics in structural geology*, vol. 3. Academic Press, London.
- Ranalli, G., Yin, Z.M., 1990. Critical stress difference and orientation of faults in rocks with strength anisotropies: the two dimensional case. *Journal of Structural Geology* 12, 1067–1071.
- Régnier, J.L., Ring, U., Passchier, C.W., Gessner, K., Güngör, T., 2003. Contrasting metamorphic evolution of metasedimentary rocks from the Çine and Selimiye nappes in the Anatolide belt, western Turkey. *Journal of Metamorphic Geology* 21, 699–721.
- Régnier, J.L., Mezger, J.E., Passchier, C.W., 2007. Metamorphism of Precambrian-Palaeozoic schists of the Menderes core series and contact relationships with Proterozoic orthogneisses of the western Çine Massif, Anatolide belt, western Turkey. *Geological Magazine* 144, 67–104.
- Ring, U., Gessner, K., Güngör, T., Passchier, C.W., 1999. The Menderes Massif of western Turkey and the Cycladic Massif in the Aegean-do they really correlate? *Journal of Geological Society, London*, 156, 3–6.
- Schaltegger, U., 1994. Unravelling the pre-Mesozoic history of Aar and Gotthard massifs (Central Alps) by isotopic dating- a review. *Schweizerische Mineralogische und Petrographische Mitteilungen* 74, 41–51.
- Schaltegger, U., Gebauer, D., 1999. Pre-Alpine geochronology of the Central, Western and Southern Alps. *Schweizerische. Mineralogische und Petrographische Mitteilungen* 79, 79–87.
- Sengör, A.M.C., Yılmaz, Y., 1981. Tethyan evolution of Turkey: a plate tectonic approach. *Tectonophysics* 75, 181–241.
- Shea, W.T., Kronenberg, A.K., 1992. Rheology and Deformation Mechanisms of an Isotropic Mica Schist. *Journal of Geophysical Research* 97, 15201–15237.
- Shea, W.T., Kronenberg, A.K., 1993. Strength and anisotropy of foliated rocks with varied mica content. *Journal of Structural Geology* 15, 1097–1121.

-
- Spry, A., 1969. *Metamorphic Textures*. Pergamon Press, Oxford, 350 pp.
- Strömgård, K.E., 1973. Stress distribution during formation of boudinage and pressure shadows. *Tectonophysics* 16, 215–248.
- Swanson, M. T., 1992. Late Acadian-Alleghenian transpressional deformation: evidence from asymmetric boudinage in the Casco Bay area, coastal Maine. *Journal of Structural Geology* 14, 323–341.
- Treagus, S.H., Lan, L., 2004. Deformation of square objects and boudins. *Journal of Structural Geology* 26, 1361–1376.
- Twiss, R.J., Moores, E.M., 1992. *Structural Geology*. 1st edition, W.H. Freeman and Company, New York, 532 pp.
- von Raumer, J., Albrecht, J., Bussy, F., Lombardo, B., Ménot, R-P., Schaltegger, U., 1999. The Palaeozoic metamorphic evolution of the Alpine External Massifs. *Schweizerische mineralogische und Petrographische Mitteilungen* 79, 5–22.

Lebenslauf

- 16.04.1974 born in Salihli, Turkey
- 1991–1996 study of geology at Dokuz Eylül University, Izmir, Turkey
graduated in June 1996
- 1996–1997 study of language in English Preparatory School at the Foreign Languages
Department, Dokuz Eylül University, Izmir
graduated in June 1997
- 1997–1998 language course at Kingstreet College London, UK
Cambridge English Certificate in August 1998
- 1998–2001 MSc study in Geology at Graduate School of Natural and Applied Sciences,
Dokuz Eylül University, Izmir
graduated in August 2001
- 1999–2003 Teaching and Research Assistant at Dokuz Eylül University, Izmir
- 2003–2007 PhD study at Institute of Geosciences, Johannes Gutenberg University, Mainz,
Germany

